Vol. 72, No.3, September 2009
KDN PP5476/10/2009 (022607) ISSN 0126-513X

MAJLIS BAGI SESI 2009/2010 (IEM COUNCIL SESSION 2009/2010)

YANG DIPERTUA / PRESIDENT:
Y. Bhg. Dato' Engr. Prof. Dr Chuah Hean Teik

TIMBALAN YANG DIPERTUA / DEPUTY PRESIDENT:
Engr. Chen Kim Kieong, Vincent

NAIB YANG DIPERTUA / VICE PRESIDENTS:
Engr. P. E. Chong, Engr. Choo Kok Beng, Engr. Oon Chee Kheng, Ir. M. C. Hee, Engr. Lee Weng Onn,
Y. Bhg. Datuk Engr. Rosaline Ganendra, Engr. Yim Hon Wa

SETIAUSAHA KEHORMAT / HONORARY SECRETARY:
Engr. Assoc. Prof. Dr Chiang Choong Luin, Jeffrey

BENDAHARI KEHORMAT / HONORARY TREASURER:
Engr. Tan Yean Chin

WAKIL AWAM / CIVIL REPRESENTATIVE:
Engr. Dr Mohd. Zamin bin Jumaat

WAKIL MEKANIKAL / MECHANICAL REPRESENTATIVE:
Engr. Tan Chee Lin @ Tan Ah Kow, Philip

WAKIL ELEKTRIK / ELECTRICAL REPRESENTATIVE:
Engr. Yusouf bin Ahmad

WAKIL STRUKTUR / STRUCTURAL REPRESENTATIVE:
Engr. Tu Yong Eng

WAKIL KIMIA DAN DISIPLIN LAIN / CHEMICAL AND OTHERS REPRESENTATIVE:
Engr. Razmahwata bin Mohamad Razalli

AHLI MAJLIS / COUNCIL MEMBERS:
Engr. Haji Tunai Shamsidi bin Ahmad, Engr. Dr Chung Boon Kuan, Engr. Gunasagaran a/l Kristnan, Engr. Khor Hock Keat, Engr. Mohd. Aman bin Haji Idris, Engr. Ng Yong Kong, Engr. Ong Ching Loon, Engr. Dr Tan Kuang Leong, Engr. Toh Ai Ching, Engr. Ishak bin Abdul Rahman, Engr. Ivan Tan Chee Yen, Engr. S. Kukanesan, Engr. Lai Sze Ching, Engr. Manogaran a/l K. Raman, Engr. Dr Lee Teang Shui, Engr. Li Thang Fai, Engr. Assoc. Prof. Dr Mohd. Saleh bin Jaafar, Engr. Noor Hisham bin Yahaya, Engr. Prof. Dr Lee Sze Wei, Engr. Prof. Dr Ruslan bin Hassan, Engr. Yee Yew Weng, Engr. Mah Soo, Engr. Dr Ahmad Anuar bin Othman, Y. Bhg. Dato Engr. Haji Abdul Rashid bin Maidin, Engr. Yau Chau Fong, Engr. Wong Chee Fui, Engr. Mohd. Khir bin Muhammad, Y. Bhg. Dato' Engr. Haji Mohd. Isa bin Haji Sarman

AHLI MAJLIS (DILANTIK) / COUNCIL MEMBERS (BY APPOINTMENT):
Y. Bhg. Dato Engr. Hj. Ahmad Husaini bin Sulaiman, Y. Bhg. Dato Engr. (Dr) Seo Kian Haw

BEKAS YANG DIPERTUA TERAKHIR / IMMEDIATE PAST PRESIDENT:
Y. Bhg. Dato' Paduka Engr. Prof. (Dr) Haji Keizrul bin Abdullah

BEKAS YANG DIPERTUA / PAST PRESIDENTS:
Y. Bhg. Dato' Engr. Pang Leong Hoon, Y. Bhg. Academician Dato' Engr. Lee Yee Cheong, Y. Bhg. Dato' Engr. (Dr) Hj. Ahmad Zaidee bin Laidin, Y. Bhg. Datuk Engr. Prof. Dr Ow Chee Sheng, Engr. Dr Gue See Sew

PENGERUSI CAWANGAN / BRANCH CHAIRMAN:
1. Pulau Pinang – Engr. Dr Lim Kok Khong
2. Selatan – Engr. Sim Tian Liang
3. Perak – Engr. Angus Ang Mei Yu
4. Kedah-Perlis – Engr. Hj. Abdullah bin Othman
5. Negeri Sembilan – Engr. Hj. Baharuddin bin Ahmad Nasir
6. Timur – Engr. Hj. Nik Mohd. Amin bin Nik Taib
7. Terengganu – Engr. Hj. Rusli bin Embok
8. Melaka – Engr. Mohammad Ariff bin Hj. A. Karim
9. Sarawak – Engr. Dr John Panil
10. Sabah – Y. Bhg. Dato' Engr. Chee Shi Tong, John
11. Miri – Engr. Teo Chok Teck, Richard

AHLI JAWATANKUASA INFORMASI DAN PENERBITAN / STANDING COMMITTEE ON INFORMATION AND PUBLICATIONS 2009/2010:
Pengerusi/Chairman: Engr. Oon Chee Kheng
Naib Pengerusi/Vice Chairman: Engr. Mohd. Khir bin Muhammad
Setiausaha/Secretary: Engr. Lau Tai Onn
Ketua Pengarang / Chief Editor: Engr. Oon Chee Kheng
Pengarang Buletin / Bulletin Editor: Engr. Dr Yeoh Hak Koon, Grad. IEM
Pengarang Jurnal/Journal Editor: Engr. Assoc. Prof. Dr Muhammad Azmi bin Ayub
Pengerusi Perpustakaan/Library Chairman: Engr. C.M.M. Aboobucker
Ahli-Ahli/Committee Members: Engr. Chin Mee Poon, Engr. Hj. Look Keman bin Sahari, Engr. Assoc. Prof. Dr Mohd. Saleh bin Jaafar, Engr. Yee Thien Seng, Engr. Dr Arazi bin Idrus, Engr. Yee Yew Weng, Engr. Tu Yong Eng, Engr. Prof. Dr Mohd. Zamin bin Jumaat, Engr. Prof. Dr Siti Hawa binti Hamzah, Engr. Dr Chong Chien Fatt, Engr. Mohd. Aman bin Hj. Idris, Engr. Khairur Rijal bin Jamaludin, Grad. IEM

LEMBAGA PENGARANG /EDITORIAL BOARD 2009/2010:
Ketua Pengarang / Chief Editor: Engr. Oon Chee Kheng
Pengarang Buletin / Bulletin Editor: Engr. Dr Yeoh Hak Koon, Grad. IEM
Pengarang (Jurnal)/Journal Editor: Engr. Assoc. Prof. Dr Muhammad Azmi bin Ayub
Ahli-Ahli/Committee Members: Engr. Lau Tai Onn, Engr. Hj. Look Keman bin Sahari, Engr. Chin Mee Poon, Engr. Yee Thien Seng, Engr. Assoc. Prof. Dr Mohd. Saleh bin Jaafar, Engr. Yee. Yew Weng, Engr. Dr Arazi bin Idrus, Engr. Tu Yong Eng,

AHLI JAWATANKUASA JURNAL / SUB-COMMITTEE ON JOURNAL 2009/2010:
Pengerusi/Chairman: Engr. Assoc. Prof. Dr Muhammad Azmi bin Ayub
Setiausaha/Secretary: Engr. Khairur Rijal bin Jamaludin, Grad. IEM
Penasihat/Advisor: Engr. Assoc. Prof. Dr Aminuddin bin Mohd. Baki
Ahli-Ahli/Committee Member: Engr. Dr Nor Hayati binti Abdul Hamid, Assoc. Prof. Dr Zubaidah binti Ismail, Engr. Dr Ramlee bin Karim, Dr Saad Mekhilef, Engr. Assoc. Prof. Dr Luqman Chuah bin Abdullah, Grad. IEM, Dr Raja Syamsul Azmir bin Raja Abdullah, Engr. Prof. Dr Junaidah binti Ariffin, Engr. Ahmad Rasdan bin Ismail, Engr. Assoc. Prof. Dr Mohd. Saleh bin Jaafar, Engr. Dr Arazi bin Idrus

IEM Secretariat: Nor Aziah Budin, Nurul Aida Mustafa

THE INSTITUTION OF ENGINEERS, MALAYSIA
Bangunan Ingenieur, Lots 60 & 62, Jalan 52/4, P.O.Box 223 (Jalan Sultan),
46720 Petaling Jaya, Selangor Darul Ehsan.
Tel: 03-7968 4001/4002 Fax: 03-7957 7678
E-mail: sec@iem.org.my Homepage: http://www.iem.org.my

Printed by: SETIAKAWAN PRINTERS SDN. BHD. (42662U)
NO. 5 & 7, Jalan Industri PBP 11,Taman Industri Pusat Bandar Puchong,
47100 Selangor Darul Ehsan.
Tel: 603-5891 7363 Fax: 603-5891 7232/33 E-mail: skpsb@tm.net.my

CONTENTS

1 Golden Anniversary Event 18th Professor Chin Fung Kee Memorial Lecture
Mr. Lee Ek Tieng Chairman GIC Asset Management Pte Ltd

9 Experimental Investigation of an Air Enhancement Device on the Performance of a Spark Ignition Engine
by Mior Azman Meor Said, Shaharin Anwar Sulaiman and Rahmat Iskandar Shazi

15 Role of Senior Managment in TQM Implementation in Malaysian Small and Medium Enterprises
by Baba Md. Deros, Mohd Nizam Ab. Rahman, Jaharah A. Ghani, Dzuraidah Abd. Wahab, Mohd. Hazri Hashim and Nor Kamaliana Khamis

21 Effect of Ship Size, Forward Speed and Wave Direction on Relative Wave Height of Container Ships in Rough Seas
by N. M. Golam Zakaria

35 Numerical Study of an An isotropically Supported Rotor with Parametric Excitation
by Chih Feng Lee, Yee Wei Tan and Janusz M. Krodkiewski

46 Derivation of Switching Angles of the Cascaded Multilevel Voltage Source Inverter Subjected to a New Pulse Width Modulation Scheme
by Zainal Salam and Junaidi Abdul Aziz

56 Hybrid Input Shaping and Pid Control of a Flexible Robot Manipulator
by M. A. Ahmad, Z. Mohamed and Z. H. Ismail

ADVISORY PANELS

a) Professor Laurence Frederick Boswell (City University, London) - Structural
b) Professor Dr Mike Jackson (Loughborough University, UK) - Mechatronics
c) Professor Jim Baird (Glasgow Caledonian University, Uk) - Waste Management/Environmental
d) Professor Jae-eung Oh, (Hanyang University (HYU), Korea - Mechanical
e) Professor Zekai Sen, (Istanbul Technical University, Turkey) - Hydrology
f) Professor Eddy Soedjono, (Kampus ITS, Sukolilo, Surabaya, Indonesia)- Environmental
g) Professor Emeritus William J.Chancellor, (University of California, Davis) - Biological/Agricultural
h) Assoc. Prof. Margaret Jollands, (RMIT University, Australia) - Environmental/Engineering Education
i) Professor Dr Richard Felder (North Carolina State University, USA) - Chemical
j) Dr Nutthita Chuankrerkkul (Metallurgy and Materials Science Research Institute, Bangkok, Thailand) - Metallurgy/Materials
k) Professor Seung Rae Lee, (KAIST, Korea) - Civil and Environment

IEM BRANCHES

HEADQUARTERS	**THE INSTITUTION OF ENGINEERS, MALAYSIA** Bangunan Ingenieur, Lot 60/62, Jalan 52/4, P.O.Box 223, (Jalan Sultan), 46720 Petaling Jaya, Selangor	Tel: 03-7968 4001 / 4002 Fax: 03-7957 7678 sec@iem.org.my www.iem.org.my
NORTHERN (Penang)	**IEM PENANG BRANCH SECRETARIAT** Level 5, 5-A Northam Venture, 37, Jalan Sultan Ahmad Shah, 10050 Penang	Tel: 04-818 2045 / 04-818 2046 Fax: 04-226 4490 iempenangbranch@gmail.com
SOUTHERN (Johor Bahru)	**IEM SOUTHERN BRANCH SECRETARIAT** No. 24-B, Jalan Abiad, Taman Tebrau Jaya, 80400 Johor Bahru, Johor	Tel: 07-331 9705 Fax: 07-331 9710 iemsouthern@gmail.com www.iemsb.org.my
PERAK	**IEM PENANG BRANCH SECRETARIAT** No. 8-10, Jalan Tokong, 31650 Ipoh, Perak	Tel: 05-254 5962 Fax: 05-253 4362 meiyu@streamyx.com
EASTERN (Kelantan)	**IEM EASTERN BRANCH SECRETARIAT** KMS Ingenieur Sdn Bhd, Unit 1-11 & 1-12, Wisma Ingenieur, Jalan Raja Perempuan Zainab II, 16150 Kubang Kerian, Kota Bahru, Kelantan	Tel: 09-764 3791 Fax: 09-765 1058 ayahmin@gmail.com kmsingenieur@gmail.com
TERENGGANU	**C/O THE CHIEF EXECUTIVE OFFICER** Syarikat Air Terengganu Berhad (SATU), Jalan Sultan Ismail, 20200 Kuala Terengganu, Terengganu	Tel: 09-620 1103 Fax: 09-620 1104 juliana@satuwater.com.my
NEGERI SEMBILAN	**ENGR. MOHD. NOR** C/O Prodesign Engineers S/B, No. 28-1, Jalan Durian Emas 4, Betaria Business Centre, Off Jalan Dato' Siamang Gagap, 70100 Seremban, Negeri Sembilan	Tel: 06-767 7333 Fax: 06-767 7000 prodesignsb@gmail.com
MELAKA	**IEM MELAKA BRANCH SECRETARIAT** C/O Sri Perunding Consulting Engineers, 2, Jalan Malinja 2, Taman Malinja, Bukit Baru, 75150 Melaka	Tel: 06-284 8028 Fax: 06-283 8919 spcesb@gmail.com
SARAWAK	**IEM SARAWAK BRANCH SECRETARIAT** Ultimate Professional Centre, No.16, 2nd Floor, Jalan Bukit Mata Kuching, 93100 Kuching, Sarawak	Tel: 082-428 506 Fax: 082-243 718 iemsarawak@gmail.com
SABAH	**IEM SABAH BRANCH SECRETARIAT** Lot 25, 3rd Floor, Block C, Damai Pointcommercial Centre, Lorong Damai Point, Off Jalan Damai, 88100 Kota Kinabalu, Sabah	Tel: 088-259 122 Fax: 088-236 749 iemsabah@sabah.org.my
MIRI	**IEM MIRI BRANCH SECRETARIAT** Lot 2935, 2nd Floor, Faradale Commercial Centre, Jalan Bulan Sabit, 98000 Miri, Sarawak.	Tel: 085-423 718 Fax:085-424 718 iem-miri@org.my
KEDAH/PERLIS	**IEM KEDAH/PERLIS BRANCH SECRETARIAT** 135-C, Tingkat 2, Kompleks Alor Setar, Lebuhraya Darul Aman, 05100 Alor Setar, Kedah	Tel: 04-734 3420 Fax:04-733 3962 ijmcxp@yahoo.my

EFFECT OF SHIP SIZE, FORWARD SPEED AND WAVE DIRECTION ON RELATIVE WAVE HEIGHT OF CONTAINER SHIPS IN ROUGH SEAS

(Date received: 19.11.2007)

N.M.G. Zakaria
Department of Naval Architecture and Marine Engineering
Bangladesh University of Engineering and Technology (BUET),
Dhaka-1000, Bangladesh
Email: gzakaria@name.buet.ac.bd

ABSTRACT

This paper deals with the numerical calculations of relative wave height of ships in the rough seas. Linear potential theory has been applied for describing fluid motion and 3-D sink-source technique has been used to determine hydrodynamic forces for surface ship advancing in waves at constant forward speed. The numerical results are compared not only with some experimental results but also with some other contemporary methods in frequency domain analysis used by others researchers. The numerical results of 3-D Green Function which has been solved by the method of singularities distributed over the hull surface is then used to analysis the results in time domain. For the simulation of the random sea, a fully probabilistic technique with unequal frequency spacing has been applied. Empirical non-linear roll damping has been incorporated to predict motion response in rough sea and time domain simulation of relative wave height of typical ship like container ships of different size and speed in short crested irregular waves have been carried out with different sea states. The numerical results of the maximum and significant values of irregular relative wave heights for different sea states have been discussed by comparing with some requirements by a Classification Society of shipping in order to assess if its rule consider enough allowance of deck load issue in case of severe sea states and it is evident from the numerical simulation that irrespective of the size of the ships, there is more prone to bow slamming or propeller emergence for the case of most severe sea state considered in this paper.

Keywords: *Container Ship, Relative Wave Height, Rough Sea, Source-sink Method*

1.0 INTRODUCTION

The prediction of seakeeping parameters like ship response, wave load, deck wetness, slamming (sudden impact on the bottom of the ship) *etc*. in a realistic seaway is some of the most important aspects of ship design. Wave induced motions are capable of making the ship's intended roles impossible, whilst extreme wave loadings on deck may have catastrophic consequences during her voyage to ocean route and this issue of wave load on deck is getting more and more importance by the designers of ocean going vessel specially after the tragic accident of the Derbyshire in the year 1980. For determination of deck load and designing of out fittings such as hatch cover / fore deck fittings, relative wave height has been considered as an essential parameter and this has been further emphasized by the IACS [1] and Classification societies of shipping for improving the safety of ship considering the wave load issue for the design of the outfittings on deck and hull structure itself. Previously simple 2-D Strip Method, 2.5–D Slender ship theory and 3-D method without forward speed had been used more frequently for the seakeeping problems of ship. But due to neglect of 3-D and forward speed effects on hydrodynamic forces of the ship, these methods do not necessarily give good estimation of seakeeping performance. On the other hand, 3-D Source–sink method is expected to provide better estimation of all relevant responses, so 3-D Source-sink method is becoming very useful and popular day by day. Also the modern developments in computer performance and numerical technique have made it possible to solve 3-D problem with forward speed more easily than in the past.

The 3-D Green function method is the most popular among 3-D seakeeping methods striving to overcome insufficiencies of strip methods. For the problems without forward speed, the Green function is easy to compute. In this case of forward speed, many numerical and theoretical difficulties appear. Despite the numerical difficulties involved in its computations, the advantage of this Green function are an automatic fulfillment of the linearised free-surface and radiation conditions, the absence of mesh on the free surface avoiding reflection on the boundary and the filtering of smaller wave lengths. Development of a practical scheme requires an efficient from of the functions. Two main types based on alternative representations are available, Noblesse and Yang[2]. First one is defined by Simple Fourier Integrals that involve relatively complicated special functions applied which has been applied in this paper and second one is the expression by single Fourier Integrals along the Steepest descent integration path in the complex Fourier Plane(namely Bessho's method) applied, for example, by Maury *et al* [3]. Another increasingly popular approach is Rankine panel methods which could in principle capture all steady-flow effects. Although, Rankine panel method uses simple Rankine singularities but it deserves special attention in satisfying the radiation condition when the speed

frequency parameter is less than 0.25 and the number of unknown is much higher in the Rankine panel method than in the Green function method [4], as the free surface should also be discretised. Also the size of the free surface domain should be carefully chosen, specially when the solutions in the low-frequency range are of interest. That is why, among the state-of-the-art seakeeping tools linked to the finite element structural analysis packages, in practice, the computer codes developed based on the Green function method are dominant in the shipbuilding industries [4].

In this paper, Kelvin singularity with translating and pulsating Green function in the form presented by Inglis and Price [5] has been used. The problem is solved by the method of singularities distributed over the hull surface. Hess and Smith method [6] is used to obtain the density of these singularities. The numerical solution for the case of surface ship is approximately obtained by considering the hull as a position of plane polygonal elements, bearing a constant singularity distribution. Velocity potential at any particular point in the free surface is determined by using 3-D Green function with forward speed which satisfies the boundary conditions for a pulsating source in the fluid and a computer code has been developed. The accuracy of the present computer code has been tested in an extensive manner. Firstly, the calculation of Green function has been tested for a point source moving along a radial distance with forward speed and then the present numerical code has been applied for a more realistic ship form of Series60 ship of C_B=0.7. A comparative study has been shown with the numerical results of present 3-D source-sink method with some available experiment data as well as some contemporary analytical techniques used by many researchers in this field. After satisfying the capability of the present coding, a detailed calculation has been performed for some Container vessels. Hydrodynamic co-efficient such as added mass, damping and exciting forces of different direction have been calculated at first and then these numerical results have been used for simulation of short crested irregular waves. To get longer simulation time, unequal frequency spacing method has been used for the simulation of random sea. The result of the maximum and significant values of irregular relative wave heights for various sea conditions has been calculated. The effect of speed and wave direction on irregular relative wave height has been considered and finally some conclusions have been drawn based on the numerical calculations which may provide some valuable information for the design of ocean going vessel.

2.0 MOTION RESPONSES OF SHIP

A right-hand Cartesian coordinate system (x, y, z) has been considered with Z directed vertically upwards and origin at the water line of the center plane of the ship. Let the ship is moving in the X direction with forward speed U and oscillating with encountering frequency ω_e in wave with frequency of ω. Let us assume that fluid is inviscid and incompressible and the free surface extends to infinity. If both incoming wave elevation and body oscillation are small, then a harmonically oscillating flow field containing such fluid is described by the velocity potential and total velocity potential can be written as

$$\phi = \phi_w + \phi_7 + \sum_{j=1}^{6} - i\omega_e \overline{X}_j \phi_j \tag{1}$$

Where, the cases j = 1, 2, 3, 4, 5 and correspond to surge, sway, heave, roll, pitch, and yaw, respectively.

The singularity distribution over the hull boundary surface can be expressed by Green function of the translating and pulsating source and can be written as [7]:

$$G(x_p, y_p, z_p; x_Q, y_Q z_Q) = \left(\frac{1}{R} - \frac{1}{R_1}\right) + \frac{2g}{\pi}\left\{\int_0^{\gamma}\int_0^{\alpha} + \int_{\gamma}^{\pi/2}\int_{L_1} + \int_{\pi/2}^{\pi}\int_{L_2}\right\} f(\theta, k)\, d\theta\, dk \tag{2}$$

where,

$$f(\theta,k) = \frac{ke^{k\lfloor(z_p+z_Q)+i(x_p-x_Q)\cos\theta\rfloor}\cos[k(y_p-y_Q)\sin\theta]}{gk-(\omega+kU\cos\theta)^2} \tag{3}$$

$$\beta = U\omega/g, \quad \gamma = 0, \text{ if } \beta, < 0.25 \text{ and}$$
$$\gamma = \arccos(1/4\beta), \text{ if } \beta \geq 0.25 \tag{4}$$

$$R^2 = (x_p-x_Q)^2 + (y_p-y_Q)^2 + (z_p-z_Q)^2 \quad \text{and}$$
$$R_1^2 = (x_p-x_Q)^2 + (y_p-y_Q)^2 + (z_p+z_Q)^2 \tag{5}$$

The fundamental singularity G defined by Equation (2) is a function of parameter $\beta=U\omega_e/g$ and $k=\omega_e^2/g$. The behaviour of this function is similar to the kelvin singularity (1960) but produces four free waves associated with the singularities k_1, k_2, k_3 and k_4 which can be expressed as Inglis and Price [5].

$$\sqrt{gk_1}, \sqrt{gk_3} = \frac{1-\sqrt{1-4\beta\cos\theta}}{2\beta\cos\theta}\,\omega_e \quad \text{and}$$

$$\sqrt{gk_2}, -\sqrt{gk_4} = \frac{1-\sqrt{1+4\beta\cos\theta}}{2\beta\cos\theta}\,\omega_e \tag{6}$$

If $\sigma_j(Q)$ is considered as the strength of source distributed over the hull boundary surface at point Q then the potential at any point P inside the fluid can be expressed by the singularity distribution over the hull boundary surface (x_Q, y_Q, z_Q) and Green function as:

$$\phi_j(P) = -\frac{1}{4\pi}\left[\iint_{S_H} G(P,Q)\sigma_j(Q)ds + \frac{U^2}{g}\oint_{C_H} G(P,Q)\sigma_j(Q)n_1 dl\right] \tag{7}$$

Where, contour integral is over the intersection of the hull surface S_H and the free surface and derivations are given in Inoue and Makino [8].

After getting the velocity potentials with the help of numerical calculation, the radiation forces (i = 1, 2, 3) and moments (i = 4, 5, 6) caused by the dynamic fluid pressure acting on the body due to the *j-th* mode can be obtained by :

$$Fij = \rho\iint_s\left(\omega_e^2\overline{X}j\phi j + i\omega_e U\overline{X}j\frac{\partial\phi_j}{\partial x}\right)n_i\, ds \tag{8}$$

From radiation forces and moments added mass and damping coefficients are obtained by:

$$a_{ij} = -\rho\, Re\iint_s\left(\phi_j + i\frac{U}{\omega_e}\frac{\partial\phi_j}{\partial x}\right)n_i\, ds \tag{9}$$

$$b_{ij} = -\rho\omega\, e\, Im\iint_s\left(\phi_j + \frac{U}{\omega_e}\frac{\partial\phi_j}{\partial x}\right)n_i\, ds \tag{10}$$

Wave exciting forces and moments can be obtained by.

$$Fi = i\rho\omega_e e^{-i\omega_e t}\iint_s\left\{(\phi_w+\phi_7) + i\frac{U}{\omega_e}\frac{\partial(\phi_w+\phi_7)}{\partial x}\right\}n_i\, ds \tag{11}$$

3.0 MOTION EQUATION IN TIME DOMAIN

The motion of a floating body in time domain under an arbitrary external force can be expressed by

$$\sum_{j=1}^{6}(M_{ij}+m_{ij})\ddot{X}_j+\int_{-\infty}^{t}R_{ij}(t-\tau)\ddot{X}\,jd\tau+B_n|x|x+C_{ij}X_j=F_i(t) \quad (12)$$

for i = 1, 2, …, 6 and where

Frequency independent added mass matrix and retardation function have the following form:

$$m_{ij}=a_{ij}(\omega)+\frac{1}{\omega}\int_0^{\infty}R_{ij}(t)\sin(\omega t)\,dt \quad (13)$$

$$R_{ij}=\frac{2}{\pi}\int_0^{\infty}b_{ij}(\omega)\cos(\omega t)\,d\omega \quad (14)$$

The wave exciting force in short crested waves in time domain is written as follows:

$$F_i(t)=\sum_m\sum_n T^i_{mn}a_{mn}(\omega_m,\beta_n)\cos(\omega_m t-k_m x\cos\beta n-k_m y\sin\beta_n+\varepsilon_{mn}) \quad (15)$$

Where, T^i_{mn} is complex transfer function of wave exciting force with frequency ω_m and direction of propagation β_n, ε_{mn} is random phase, a_{mn} is the amplitude of component wave with frequency ω_m and direction of propagation β_n and is calculated by using the wave spectrum $S(\omega_m, \beta_n)$ as follows:

$$a_{mn}(\omega_m,\beta_n)=\sqrt{2S(\omega_m,\beta_n)\,\Delta\omega\,\Delta\beta} \quad (16)$$

The incident wave elevation at a point (x, y) can be written by:

$$\zeta_w(t)=\sum_m\sum_n a_{mn}(\omega_m,\beta_n)\cos(\omega_m t-k_m x\cos\beta_n-k_m y\sin\beta_n+\varepsilon_{mn}) \quad (17)$$

The relative wave height at arbitrary point of ship is calculated as follows:

$$z_r(x_r,y_r)=\zeta_w(x_r,y_r)-\zeta(x_r,y_r) \quad (18)$$

where, the vertical displacement at arbitrary point of the ship can be obtained by:

$$\zeta(x_r,y_r)=X_3-(x_r,y_G)X_5+y_rX_4 \quad (19)$$

4.0 VALIDATION STUDY

It is very important to verify and validate the numerical code before using it for practical purpose. That is why emphasis is put on the verification against results not only from other codes, but also validation against model tests is made. A very precise verification which would require an exact match of the results, could have been made with a program using the same theory and the same algorithms. But such results are not always available and even if the type of theory was the same, the method for determining hydrodynamic coefficient such as added mass and damping could be different. In this paper, the accuracy of the present numerical coding has been tested at first by using point source moving along some radial distance and then numerical

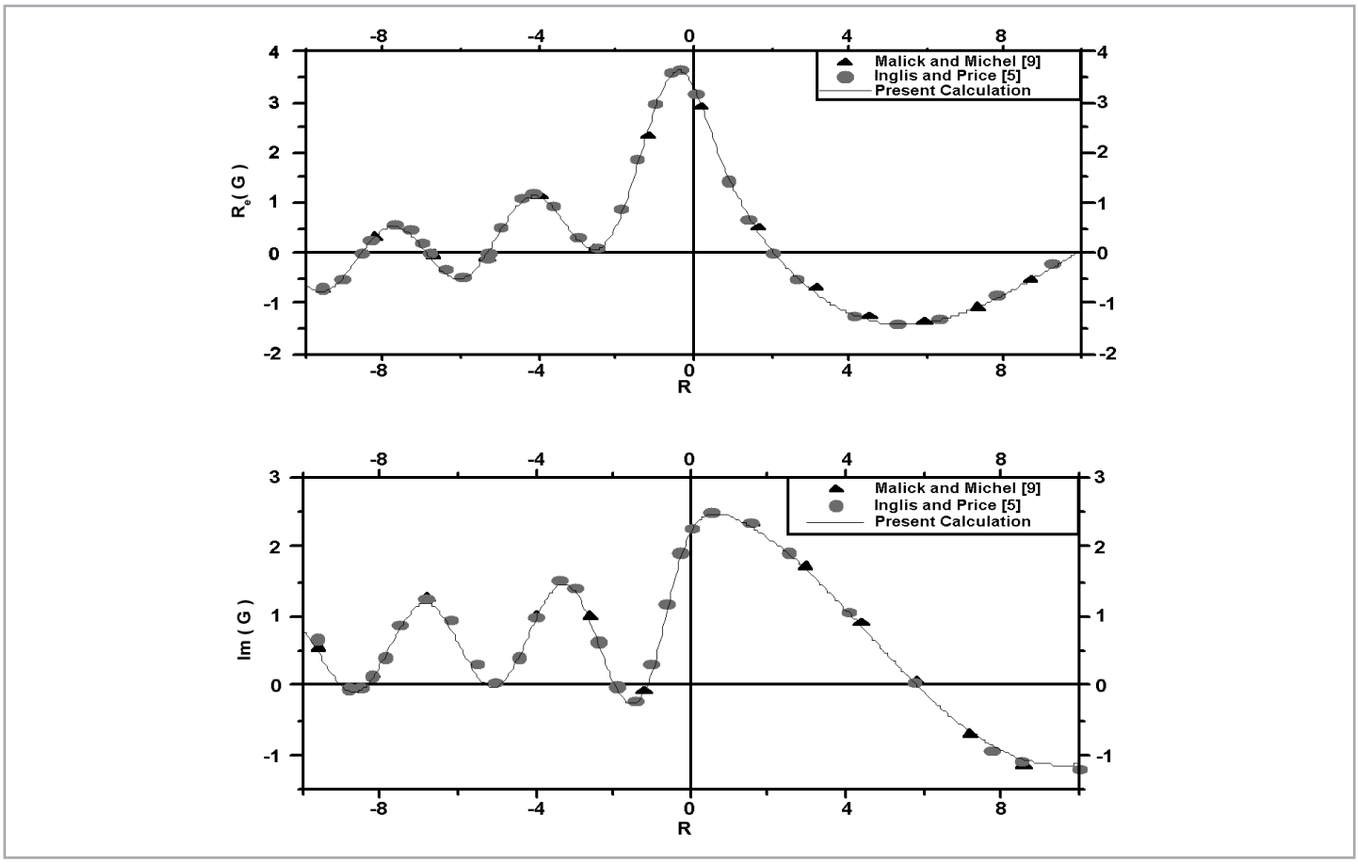

Figure 1: Real and imaginary part of the Green's function for U=2m/s, ω=1.4, β=0.29, F_n=0.64, z'=-1.0

result of the Green function and its derivatives have been examined comparing some published results such as Ba and Guilbaud [9]. Figure 1 shows the real and imaginary part of the Green function with forward speed U=2 m/s and ω=1.4 rad/s for the point source located at (0,0,-1) and here very good convergence has been found among the numerical methods. Next, Series60 ship (L/B=7.0, B/d=2.5, C_B=0.70) has been used for numerical calculations which would enable to judge the effectiveness of the present numerical calculation for the case of more realistic ship form rather than any mathematical ship form. Numerical results from other codes as well as experimental data have been taken from Baiely *et al*.[10] for the comparison.

For the heave responses, as shown in Figure 2, the present numerical computation along with other theoretical methods are in close agreement with each other and agreement with the experimental data is also close. The three different theoretical

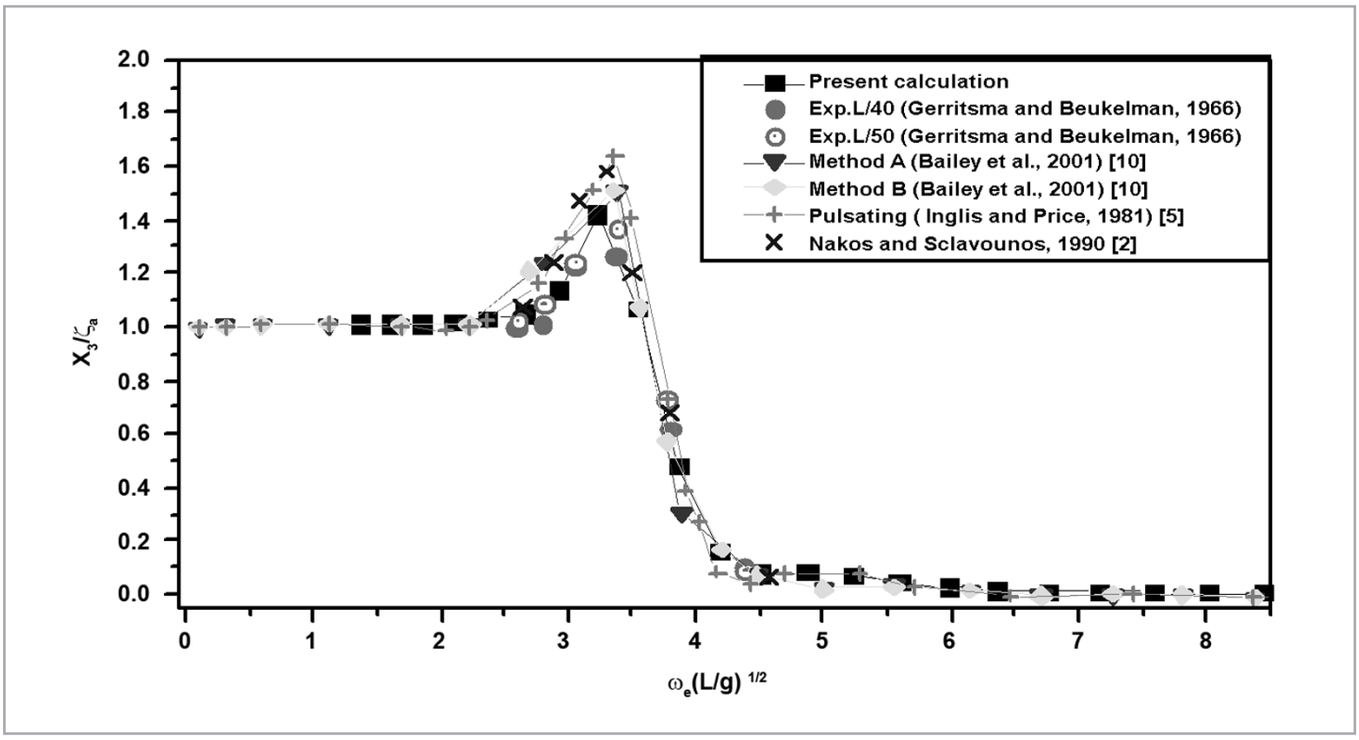

Figure 2: Heave motion for Series60 ship of C_B=0.7 at F_n=0.2 in head sea

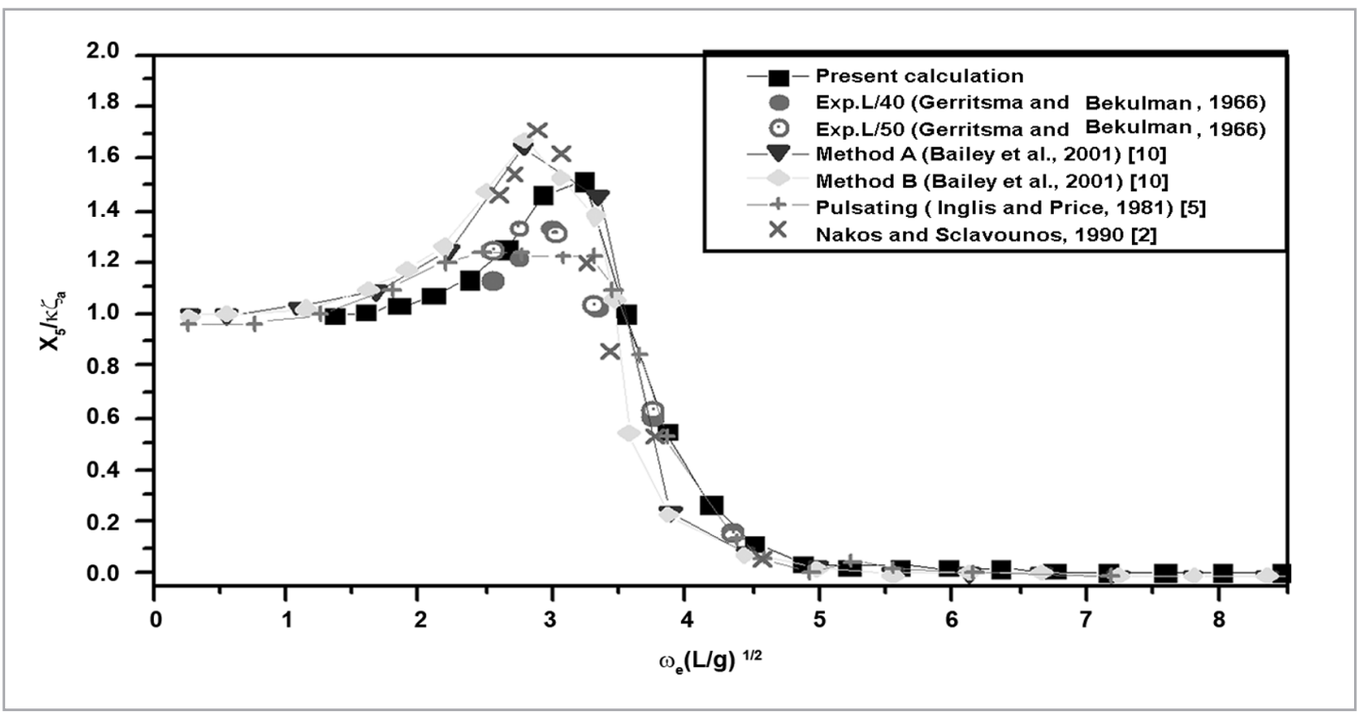

Figure 3: Pitch motion for Series60 ship of C_B=0.7 at F_n=0.2 in head sea

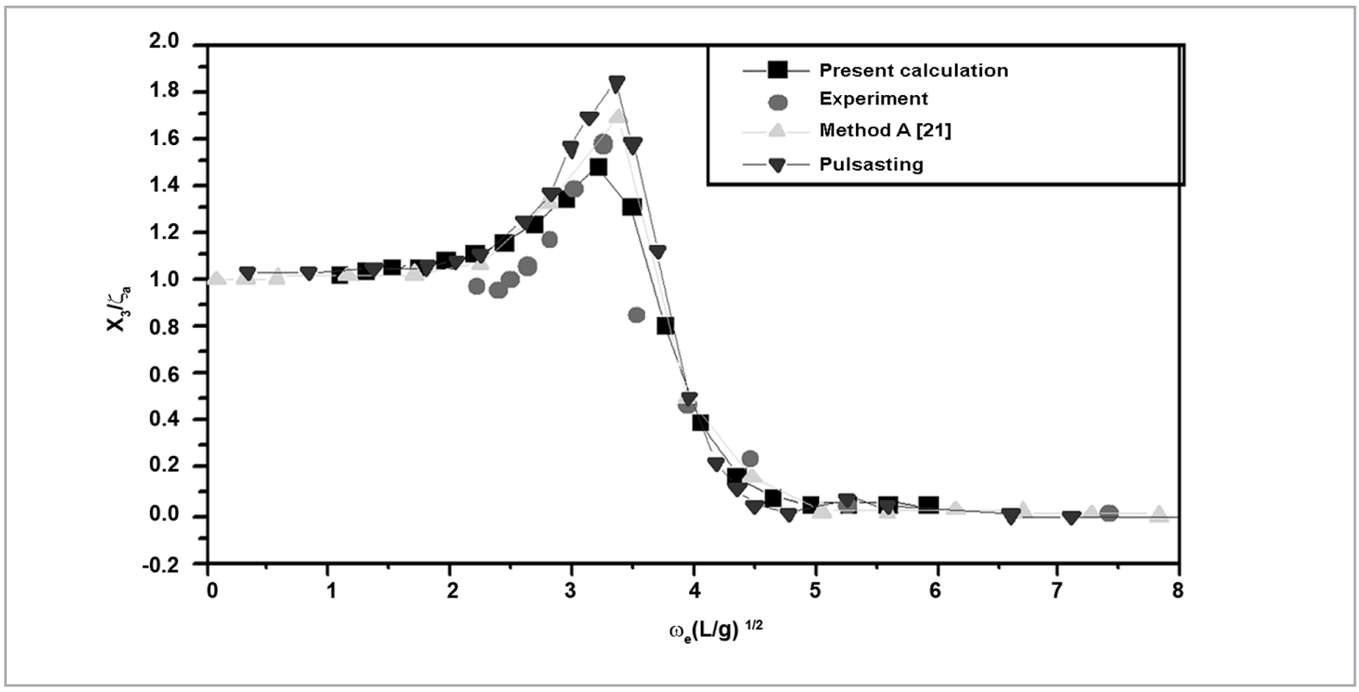

Figure 4: Heave responses for the series 60 ship of C_B=0.7 at F_n=0.2 in oblique waves with heading angle, x = 135°

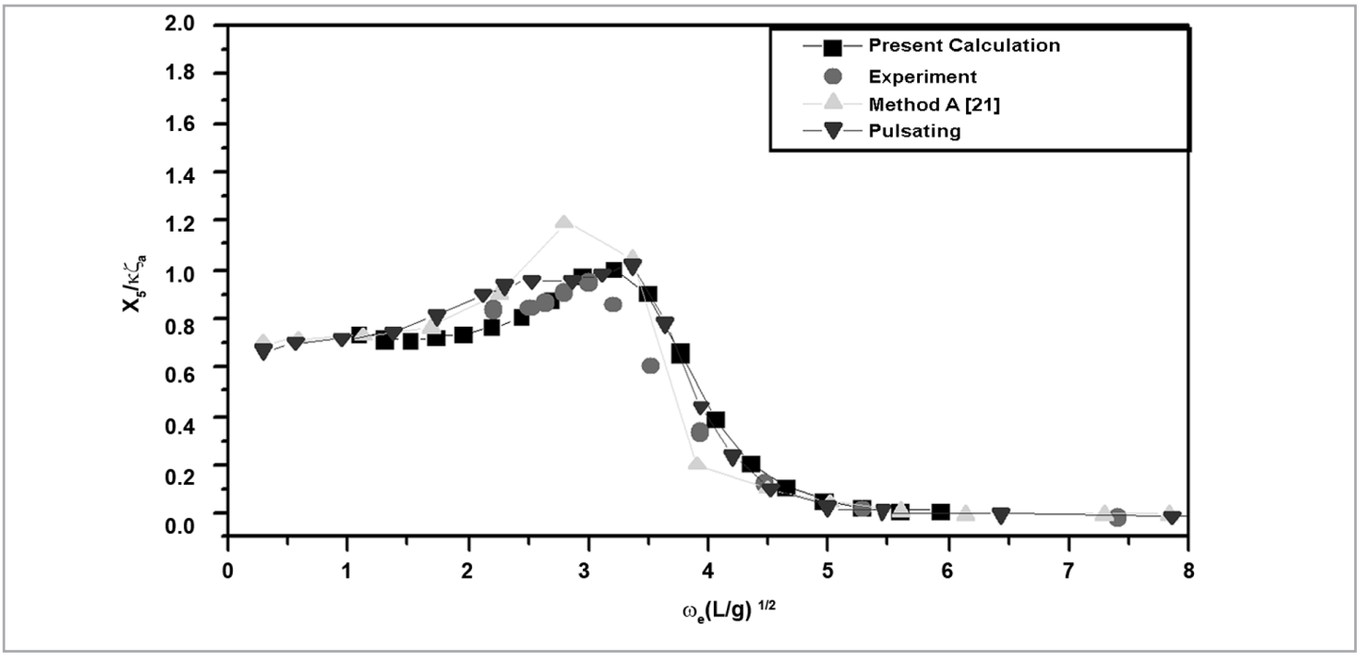

Figure 5: Pitch responses for the series 60 ship of C_B=0.7 at F_n=0.2 in oblique waves with heading angle, x = 135°

methods accurately predicts the resonant response although over-estimated by them all, but the present method gives the more closer one. For pitch response, as shown in Figure 3, the present computation as well as methods A and B, together with the Rankine panel methods of Makos and Sclavounos [11] exhibit the correct trends with frequency with accurately predict the resonance frequency when compared to experimental data. As it with the heave response the pitch resonance responses over predicted, in this case by a greater amount. The pulsating source method provides predictions in closer agreement to the experimental data in the region of resonance, if anything under-estimating the magnitude of the resonant response. The experimental data indicate a sharper resonant response than is predicted by the pulsating source method. This is reflected in the predictions of methods and those of Makos and Sclavounos[11]. It has been appeared that pitch resonance move to an marginally higher frequency with the increase of the wave height, something the linear methods are unable to demonstrate.

Heave and pitch responses for the series 60 travelling in oblique regular waves with heading angle, X = 135°are shown in the Figures 4 and 5. Present numerical computation has been compared with the pulsating source method together with those form of method A and with experimental measurements. Once

again the present calculation gives overall good prediction of heave response well across the whole frequency range, providing a good estimate of the resonance frequency, although, the magnitude is slightly under-predicted. The heave amplitude at resonance is greater in oblique waves than in head waves. This is the case both in the theoretical predictions and the experimental measurements, although the experimental measurements show a greater increase. The pitch resonant frequency is also well predicted and also good prediction than the head wave case. Both the pulsating source and the present computation give a much less sharp resonance response with the prediction of magnitude is better than method A. Both experiments and theoretical predictions show a decrease in the pitch response compared to head sea.

5.0 NUMERICAL RESULT AND DISCUSSION

As for numerical examples, container ships of different sizes have been chosen. The principal particulars of these ships are summarised in Tables 1. The numerical simulations have been performed for three different sea states which are moderate gale, strong gale and hurricane and the significant wave height and mean wave period of these three sea states are listed in Table 2. For container ship-I, the calculation has been performed for Froude number 0.18 with the main direction of angle of attack 180 deg (head sea) and for container ship-II and III, the calculations have been done for Froude number 0.20 with the same sea conditions. The principal particulars and other data, used in table1, are determined base on actual ships in the paper of Inoue *et al*. [12]. Figure 6 shows the typical mesh arrangement of container ship for the numerical calculation in frequency domain analysis where the wetted surface of the vessel is discretised by quadrilateral panels.

Table 1: Principal particulars of container ships

Items	Container-I	Container-II	Container-III
LBP	160.0 m	218.0 m	270.0 m
B	25.70 m	32.10 m	32.20 m
D	8.24m	13.67m	24.71m
d	9.01 m	10.0 m	10.85 m
Δ	56097 m^3	41147 m^3	56097 m^3
U	13.9kts	18.0kts	20.0kts
C_b	0.6328	0.588	0.598
C_w	0.757	0.757	0.757
C_m	0.950	0.950	0.950
KG	10.04m	13.42m	10.12 m
L.C.G.	-1.43 m	-3.85 m	-3.49 m
GM	1.03 m	0.64m	1.15 m
K_{xx}	37.5 % B	37.5 % B	37.5 % B
K_{yy}	24.8 % LBP	24.8 % LBP	24.8 % LBP
K_{zz}	24.8 % LBP	24.8 % LBP	24.8 % LBP

Table 2: Sea state for numerical simulation

Sea state	Mean period	Significant wave height
Moderate gale	T=6 Sec	H = 5 m
Strong gale	T=10 Sec	H=10m
Hurricane	T=10 Sec	H=15m

Using the numerical results given by frequency domain analysis, the motion Equation(12) has been solved using Newmark [13] generalised acceleration method. Non – linear roll damping has been incorporated which is based on the experimental works of Watanabe [14]. As for wave spectrum, ISSC spectrum has been used in this paper.

Figure 7 shows an example of wave profile for strong gale condition in short crested irregular waves using unequal frequency spacing technique. Figures 8 to 10 show the motion responses of heave, roll and pitch with respect to center of gravity of ship in this condition solving Equation (12) for container ship-II at crusing speed of 18 knots. Roll motion is induced even in head seas because of directional component of short crested irregular waves. Using Equation (18), the relative wave height at different positions of ship, such as Midship position, F. P. Position and A.P. position, have been shown in Figures 11 to 13.

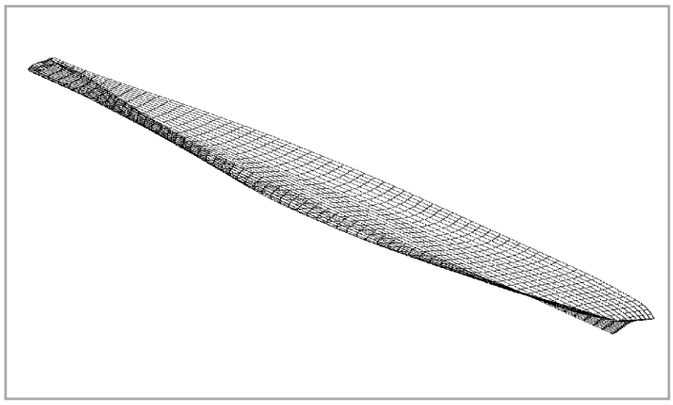

Figure 6: Grid modeling of body surface of container vessel

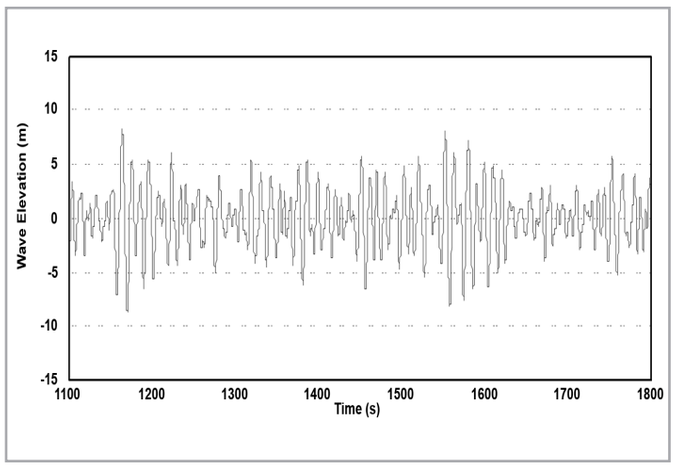

Figure 7: Wave profile of short crested irregular wave in strong gale (H=10m, T=10sec)

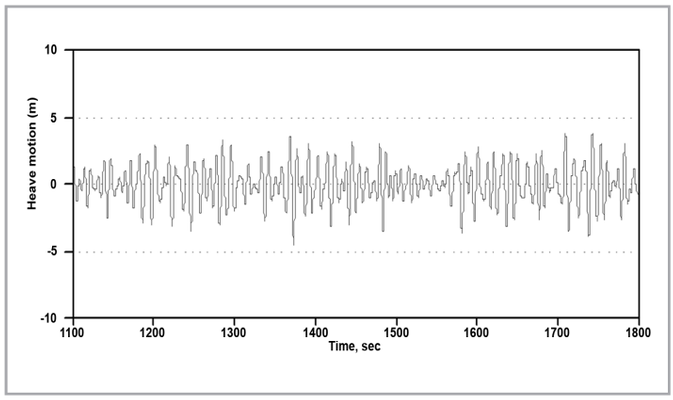

Figure 8: Heave motion of container ship-II in strong gale

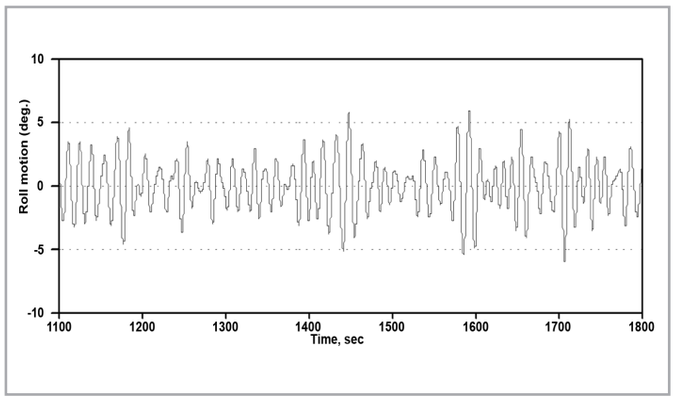

Figure 9: Roll motion of container ship-II in strong gale

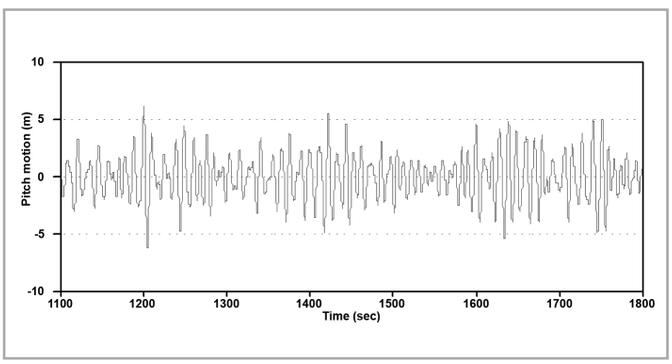

Figure 10: Pitch motion of Container ship-II in strong gale

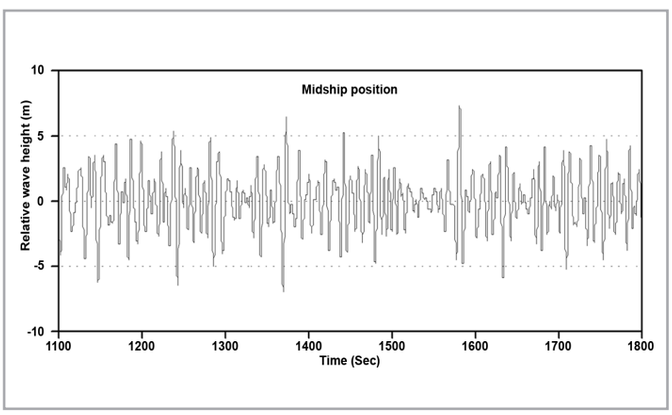

Figure 11: Relative wave height of container ship-II in strong gale at midship position

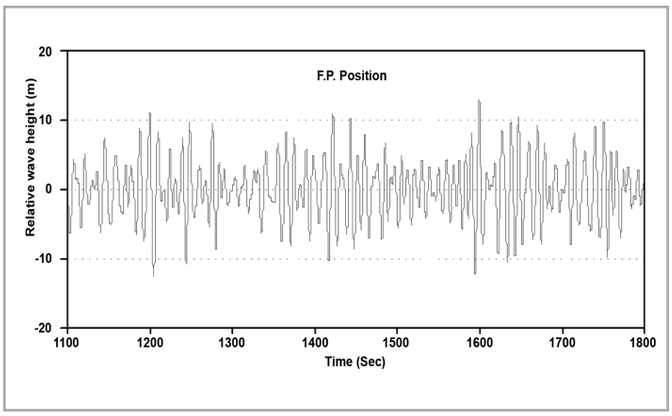

Figure 12: Relative wave height of container ship-II in strong gale at midship position

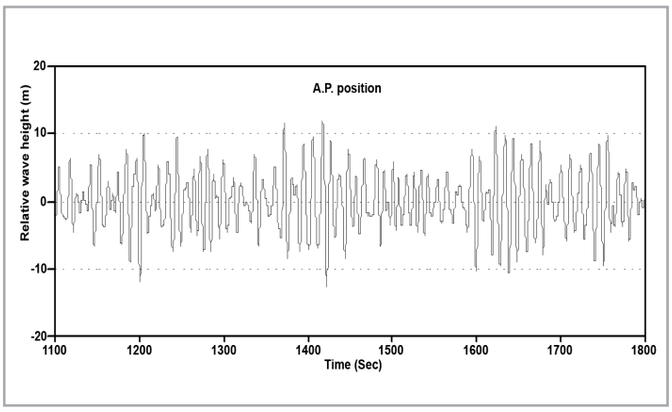

Figure 13: Relative wave height of Container ship-II in strong gale at midship position

From this computation of relative wave height at side wall of main hull from the load water line in short crested irregular waves, the maximum and the 1/3 highest mean values of time domain simulations have been calculated along the ship length. The deck load for weather deck given as a function of vertical distance from the designed maximum load line to the weather deck at side is not to be less than the value required by *NK* rules and guidance [15] and this is referred as the minimum deck load for weather deck. From this requirement, we can determine the corresponding height at where the weather deck load becomes zero and this corresponding height of deck load has been assumed as above the height of the maximum relative wave height. The rule also requires closing appliances for the openings of outfitting on deck and also it may be omitted where some height of openings exceeds the decks. The height at where closing appliances may be omitted has been considered as the value above the 1/3 highest mean values of relative wave height. These two kinds of heights are referred to the relative wave heights in various sea states.

Figures 14-16 show the results of the maximum and the 1/3 highest mean of relative wave heights along the ship length of container ship-II for 3 different sea states mentioned above. For moderate gale, relative wave heights are below the corresponding height of deck and the height of closing appliances omission. But in hurricane, the relative wave heights are over the reference heights and bottom slamming may be occurred. In strong gale the maximum values does not exceed the corresponding height of deck at fore and aft but bow slamming is appeared sometimes.

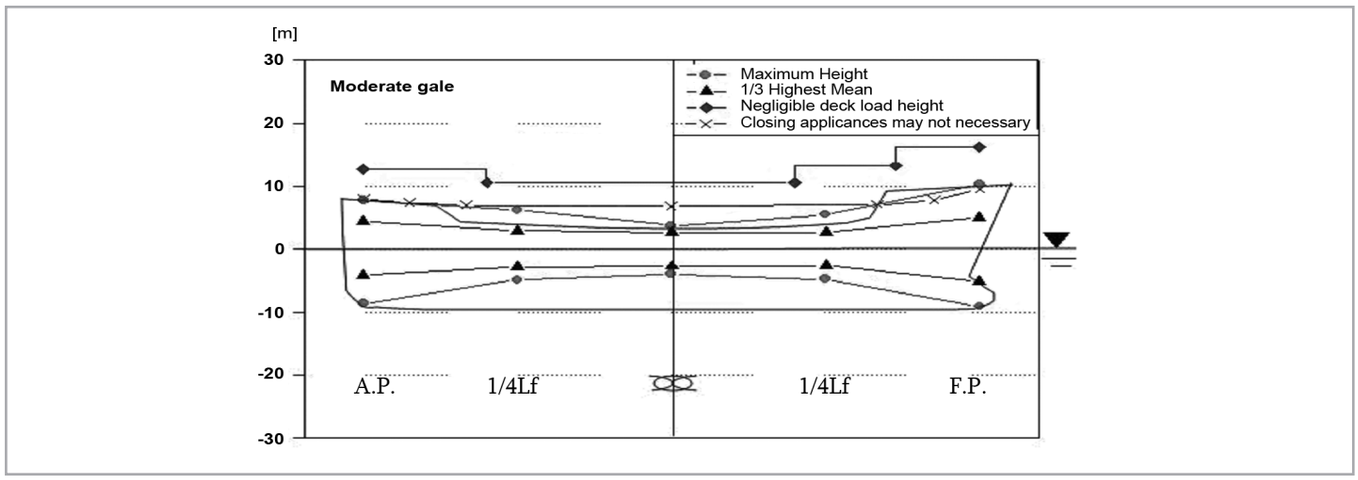

Figure 14: Relative wave height of container ship-II in moderate gale

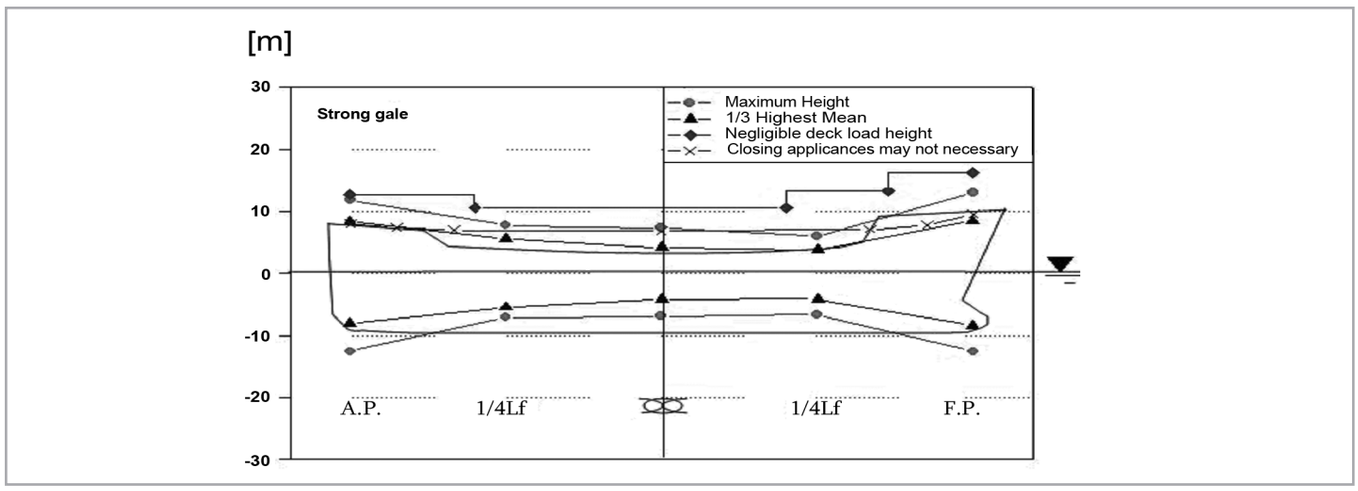

Figure 15: Relative wave height of container ship-II in strong gale

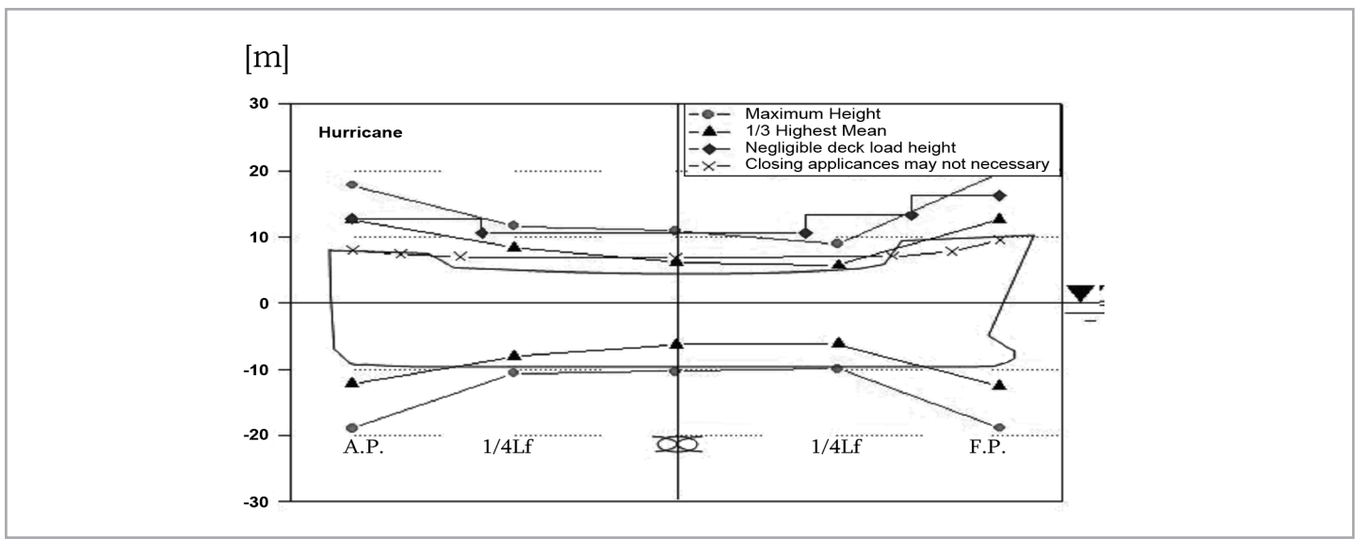

Figure 16: Relative wave height of container ship-II in hurricane

Figures 17-19 show the results of smallest container ship (Container ship-I) for 3 different states. Bottom slamming and propeller racing are more evident for the case of hurricane. Figures 20-22 show the results of Panamax container ship (Container ship-III) for 3 different states; the maximum and the 1/3 height mean values both exceed the corresponding reference height in fore and aft positions and also bottom slamming seems to be very severe for hurricane condition.

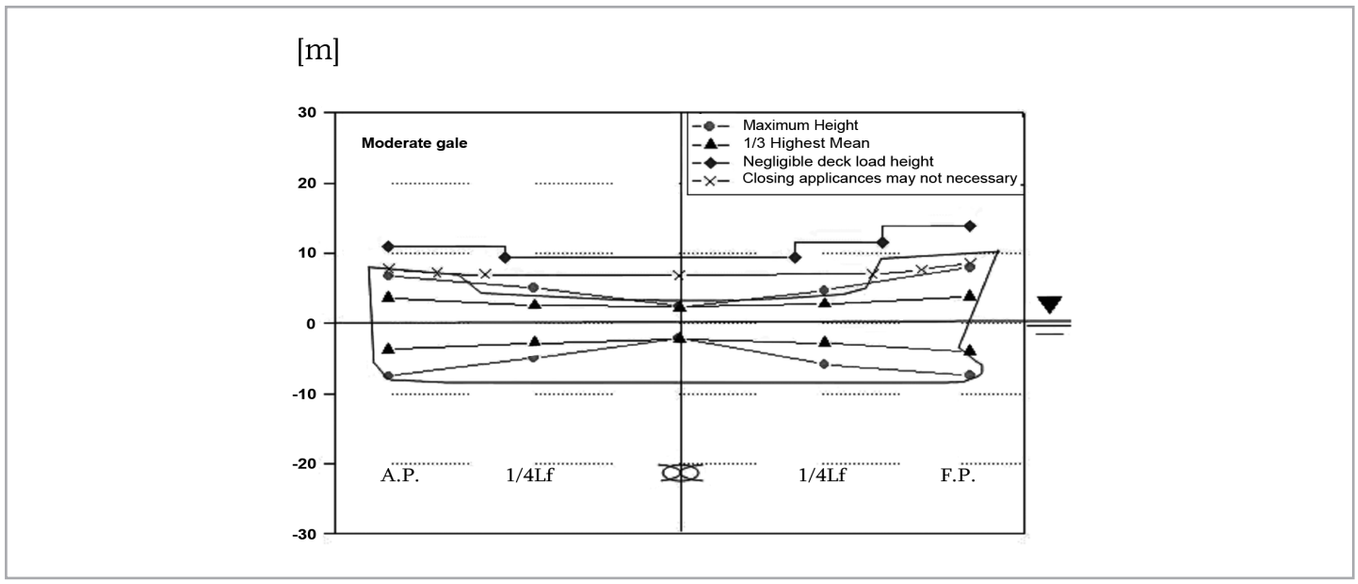

Figure 17: Relative wave height of Container Ship-I in moderate gale

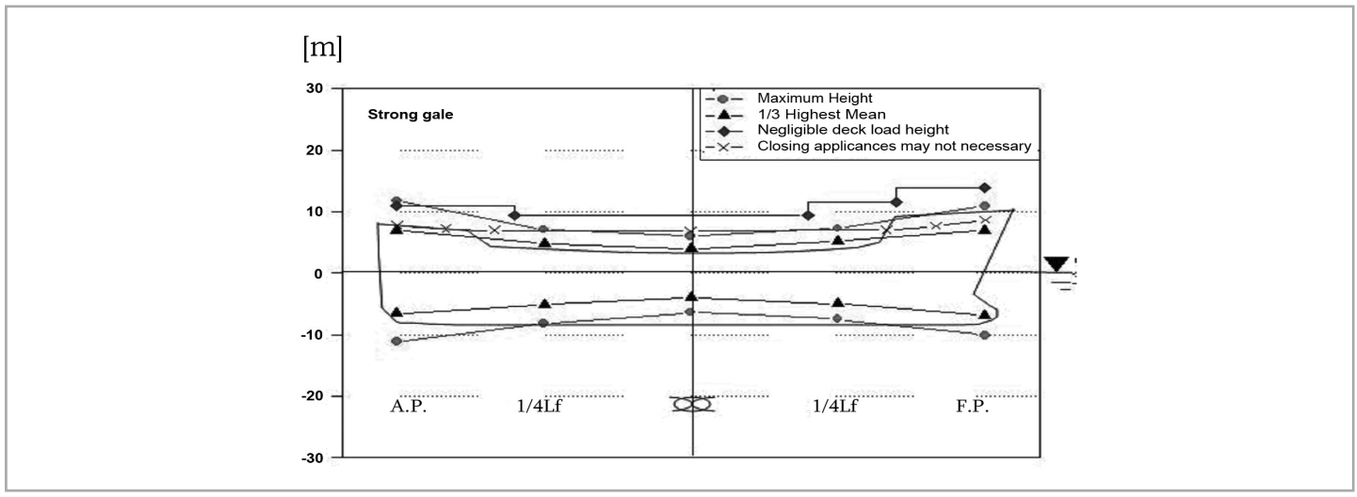

Figure 18: Relative wave height of container ship-I in strong gale

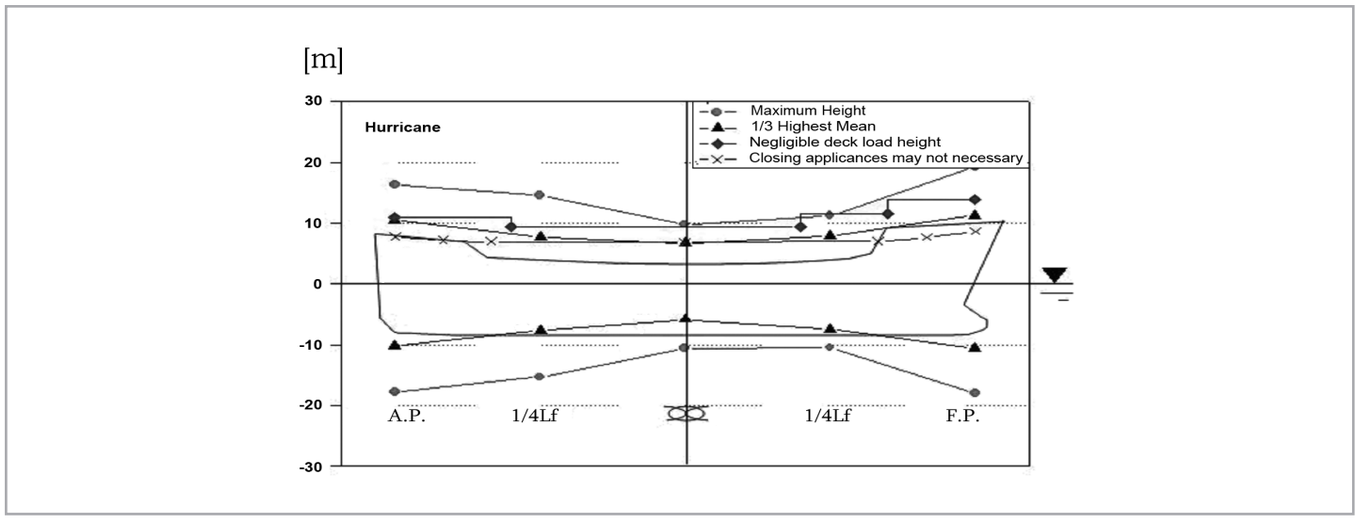

Figure 19: Relative wave height of container ship-I in hurricane

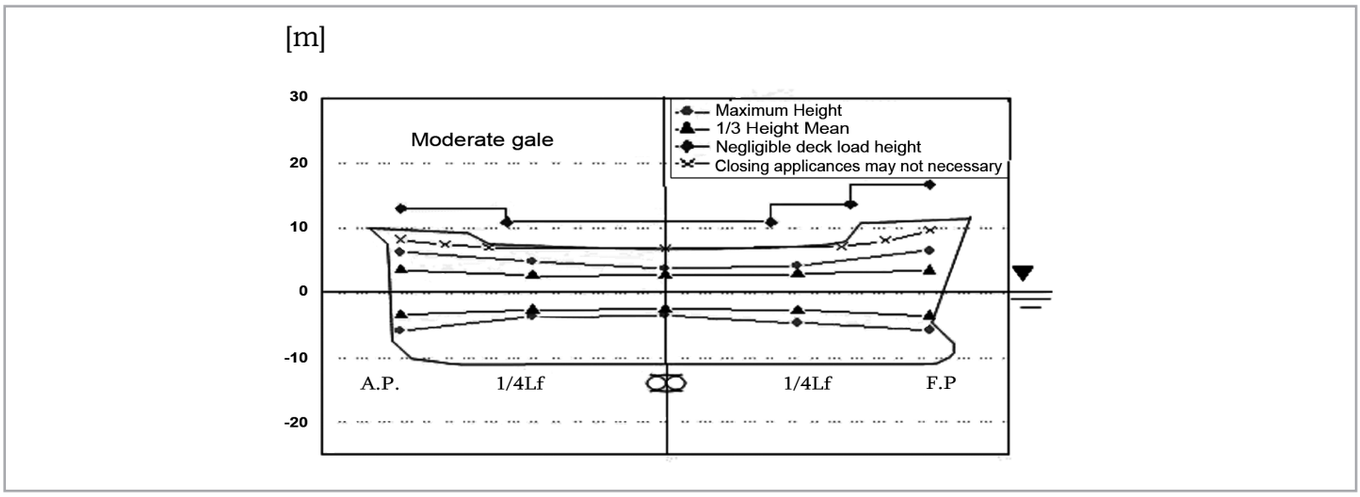

Figure 20: Relative wave height of panamax container ship in moderate gale with F_n =0.2

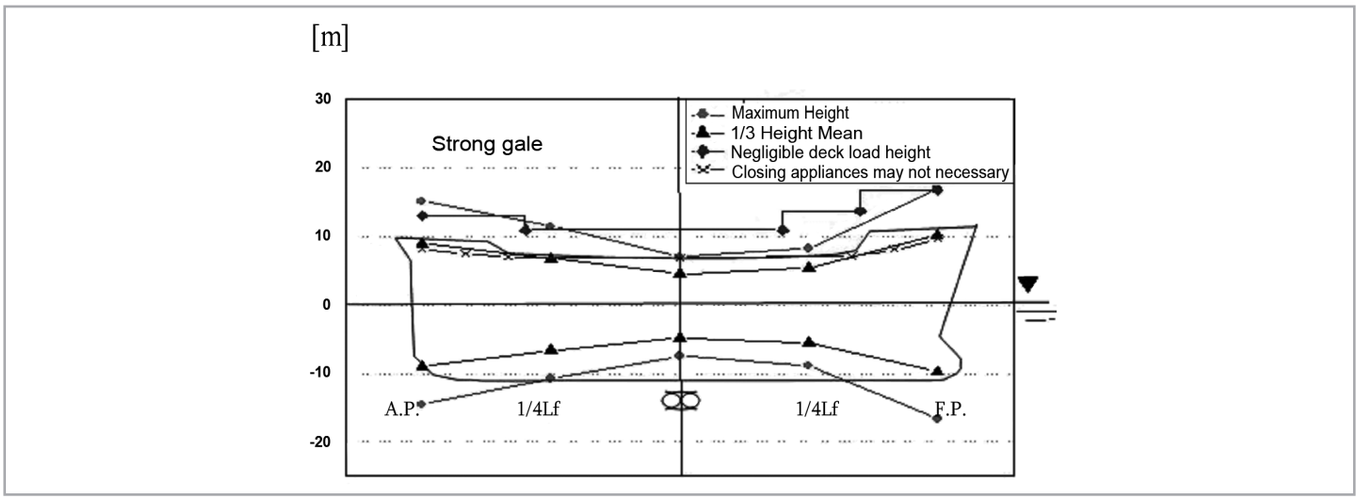

Figure 21: Relative wave height of panamax container ship in strong gale with F_n =0.2

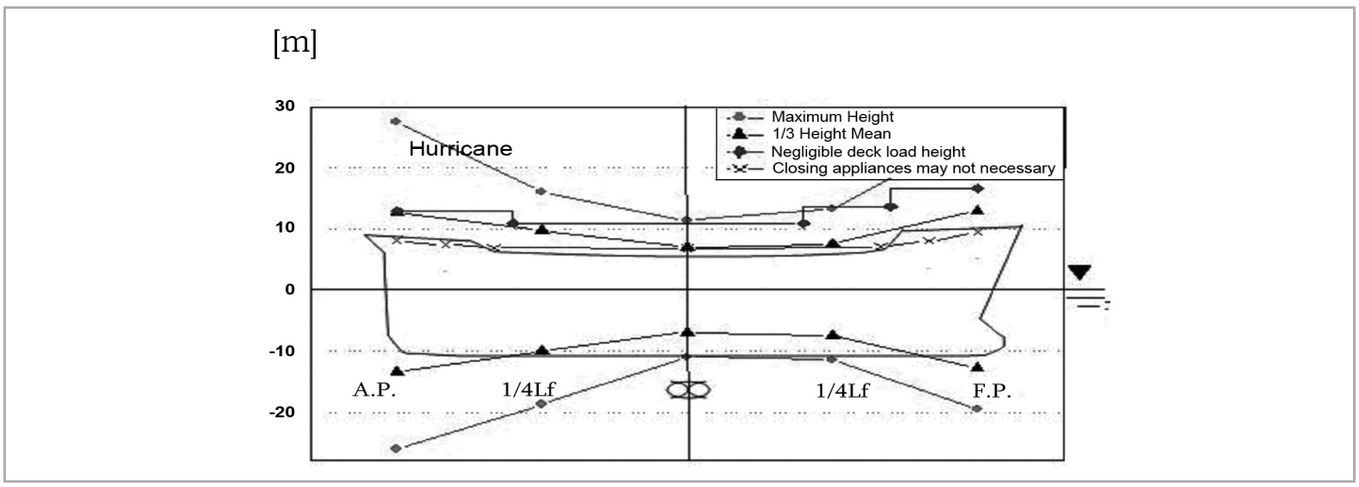

Figure 22: Relative wave height of panamax container ship in hurricane with F_n =0.2

To show the numerical result of relative wave height for the case of reducing speed and different wave heading angle, Figures 23-30 have been introduced. Figures 23-25 show the maximum and 1/3 height mean value for the case of reduced speed of 15 knots (F_n=0.15) and Figures 26-28 shows the same for the case of 12 knot (F_n=0.12) speed. From these Figures, the numerical simulation show some reduced value of both maximum and 1/3 height mean value for that reduced speed. When the wave heading angle changing from 180 *deg*. to 165 *deg*., again some reduced relative height has been noticed in this case as shown in the Figures 29-30.

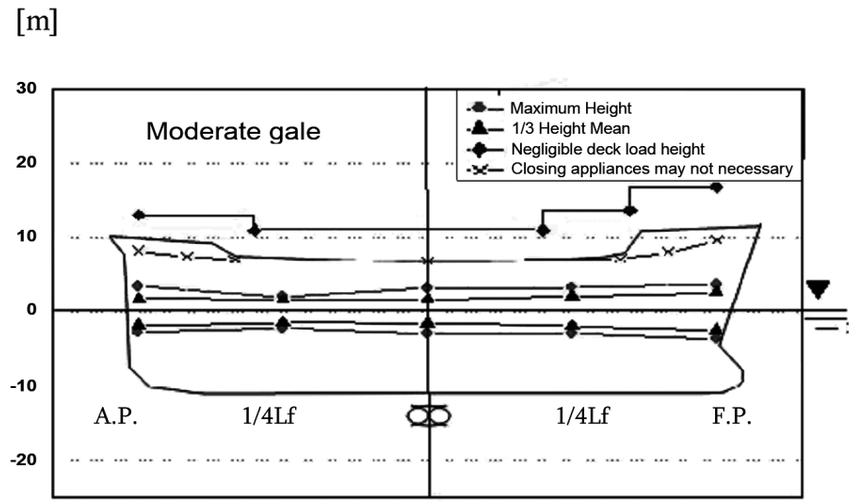

Figure 23: Relative wave height of container ship in moderate gale with F_n=0.15

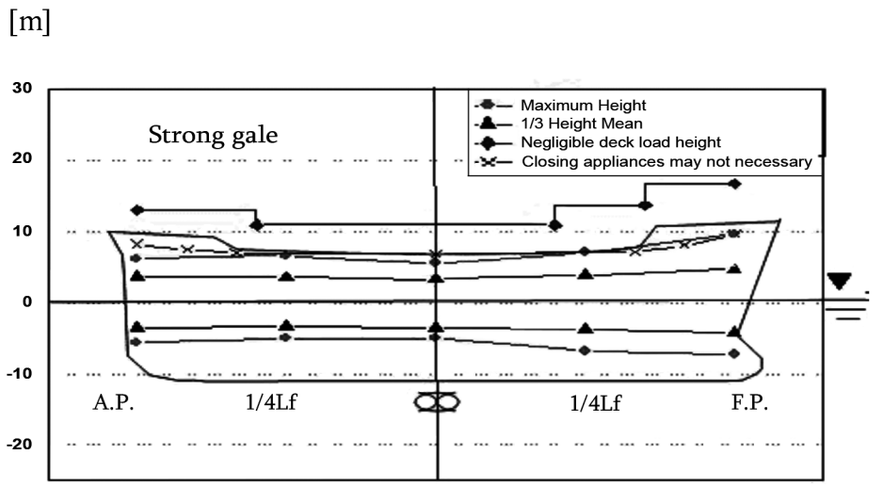

Figure 24: Relative wave height of panamax container ship in strong gale with F_n=0.15

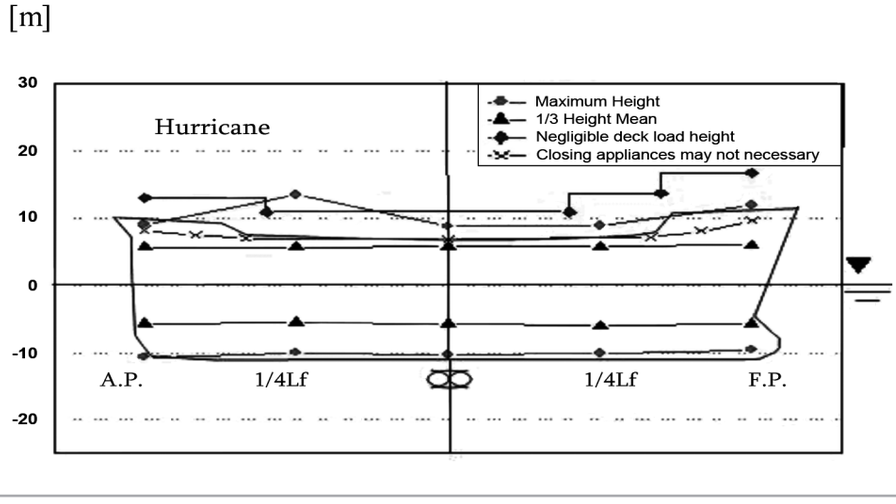

Figure 25: Relative wave height of panamax container ship in hurricane with F_n=0.15

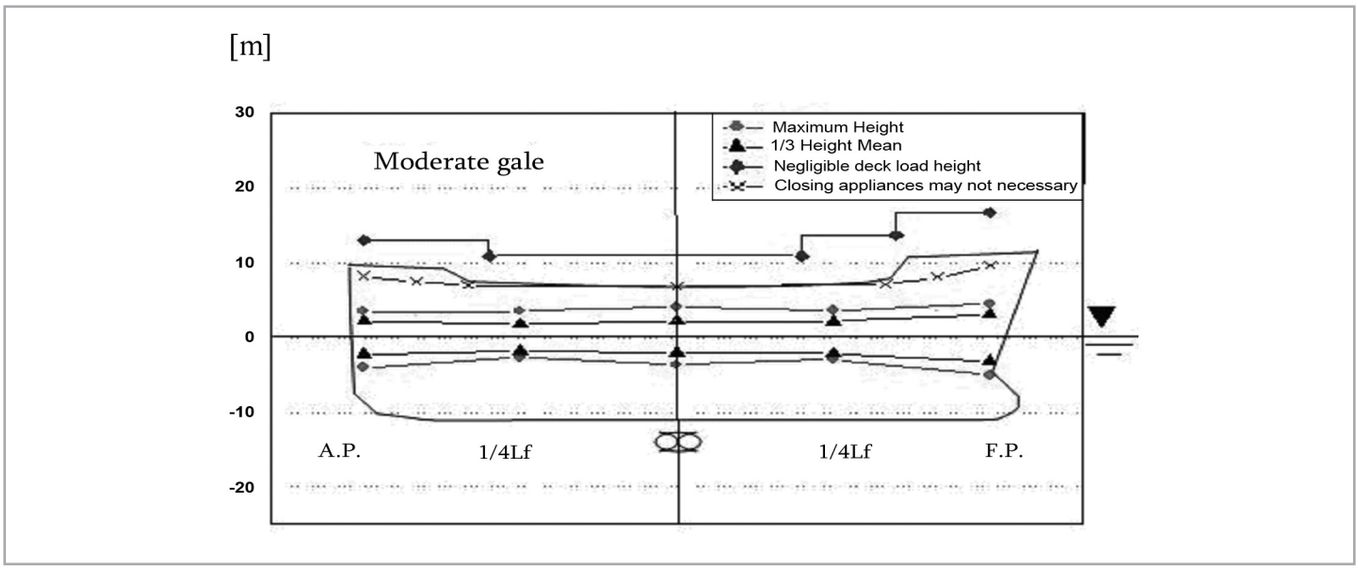

Figure 26: Relative wave height of panamax container ship in moderate gale with F_n=0.12

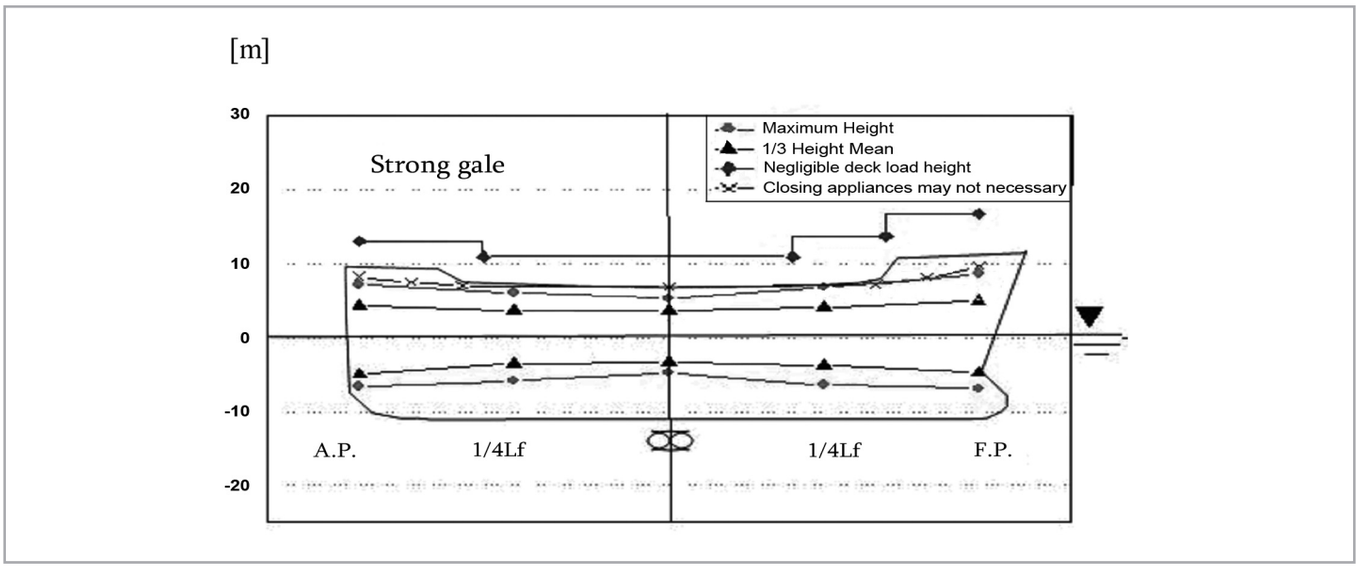

Figure 27: Relative wave height of panamax container ship in strong gale with F_n=0.12

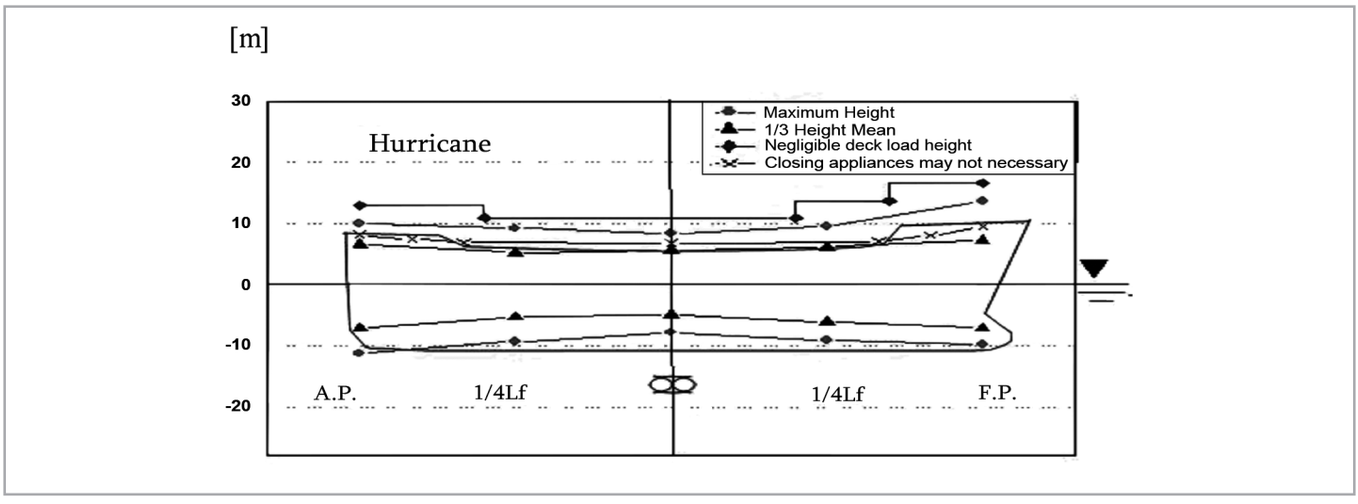

Figure 28: Relative wave height of panamax container ship in hurricane with F_n=0.12

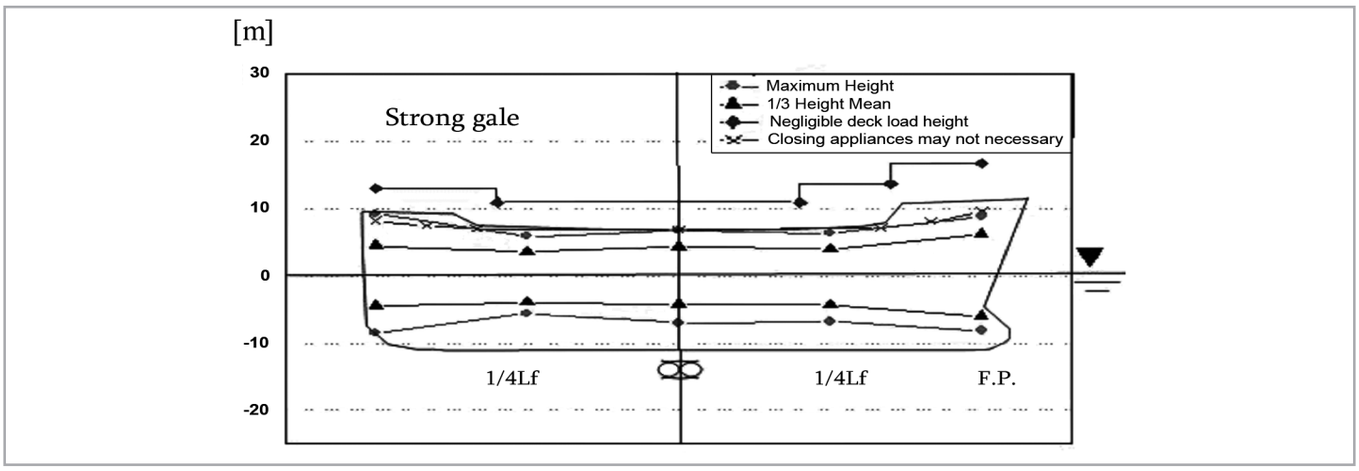

Figure 29: Relative wave height of panamax container ship at heading angle of 165⁰

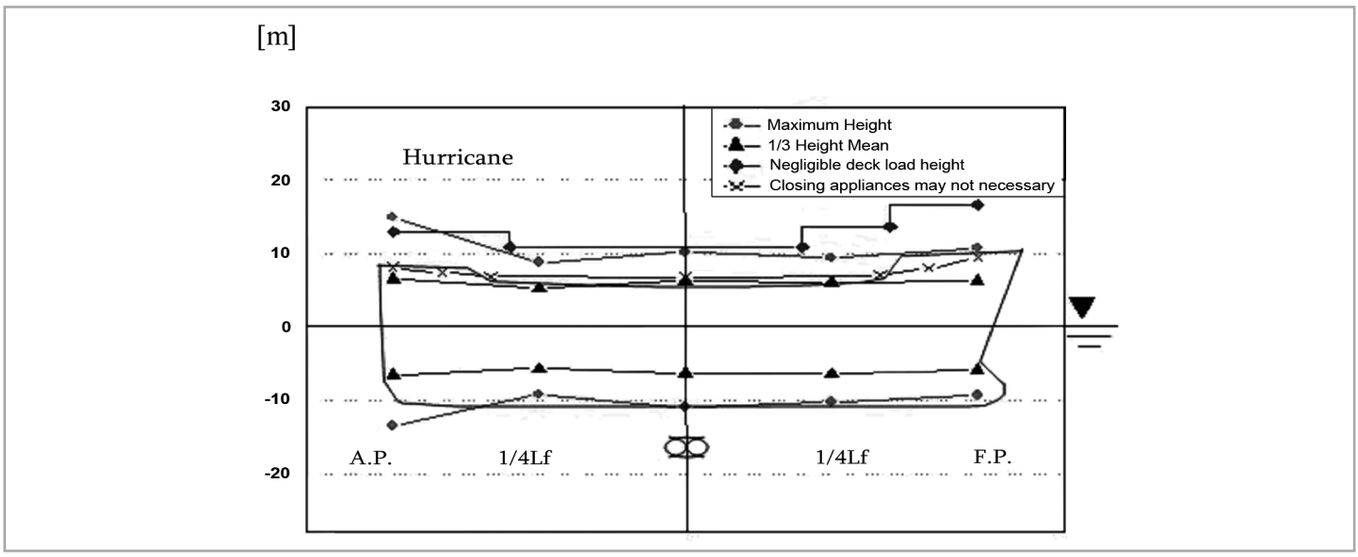

Figure 30: Relative wave height of panamax container ship at heading angle of 165⁰

6.0 CONCLUSIONS

Applying 3-D Source-sink method, numerical study of sea-keeping performances has been performed in this paper. Comparing the present numerical results of Green function for the translating pulsating source located at position (0,0, -1) with the numerical results taken from Malick and Michel [9], it is seen that the present numerical results has given quite satisfactory results both for real and imaginary part of the Green's function and its derivatives. For the case of Series60 ships with C_B=0.70, present numerical calculation has given very good predictions of motion responses for both head and oblique waves compared with the experimental data as well as with other published numerical results taken from Bailey *et al*.[10]. The results provides validity and reliability to the computation of seakeeping problems by present numerical coding. It may be worth to mention here that panels of 800 for discretisation of wetted surface with 380 panels inside the hull for adding a horizontal flat surface slightly immersed have been used to calculate motion responses of this Series60 ship. Comparison of the other hydrodynamic properties of this ship have been shown in Reference [16].

From the numerical result of time domain simulations of relative wave height of ships in short crested irregular sea, it is seen except some exception in hurricane condition, the numerical result of the 1/3 highest mean value is almost below the height at where closing appliances are not necessary as well as corresponding height to the minimum requirement of deck load. This implies that the requirement by the classification society may be reasonable height for weathertight. But the maximum value in most cases is over its height except moderate sea.

From the time domain simulation in short crested irregular wave with a speed of 20 knots (F_n=0.20) particularly for strong gale and hurricane, numerical calculation shows some relative wave height that could be dangerous for overall safety of the ship as bottom slamming is evident in this case. But for the case of reduced speed and different heading angle, we have noticed that overall seakeeping performances have been improved for these conditions as 1/3 height mean value of relative wave height has been reduced considerably .

The concept of relative wave height can be used to assess the added resistance of ship in waves, for example, added resistance prediction by Gerritsma's method. ■

NOMENCLATURE

a_{ij}	Frequency-dependent added mass
b_{ij}	Damping coefficient matrices
B	Breadth of ship (m)
B_n	Non-linear damping coefficient (only for roll)
β	Heading angle
C_B	Block coefficient of ship
C_{ij}	Hydrostatic restoring coefficient
d	Draught of ship (m)
F_n	Froude number
$\overline{F}_i$	Wave exciting forces and moments
R_{ij}	Retardation function matrix
g	Gravitational acceleration (ms^{-2})
G	Green's function
k	Wave number
L	Length of ship (m)
M_{ij}	Inertia matrix
m_{ij}	Frequency independent added mass matrix
n	Components of normal vector
P	Arbitral point in fluid
ρ	Density of water (ton s^2m^{-4})
Q	Point on body surface
r	Distance from hull boundary surface
ε_{mn}	Random phase of elementary wave
r_g	Distance from C.G of ship
S_H	Hull surface
T^i_{mn}	Complex Transfer function of exciting force
X_j	Complex motion amplitude in *j-th* mode
x_g	Centre of gravity of ship in x -axis
(x_p, y_p, z_p)	Coordinate at the arbitral point of ship
ς_A	Amplitude of incident wave (m)
ϕ_I	Diffraction potential
σ_j	Strength of source distributed over hull
ϕ_j	Radiation potential
ϕ_T	Total potential
ϕ_0	Steady potential
ϕ_w	Incident wave potential
ϕ	Unsteady potential
$\dot{\omega}$	Constant frequency chosen arbitrarily
ω	Frequency of wave
ω_e	Frequency of encounter (rad./s)
z_r	Relative wave height (m)

REFERENCES

[1] Lloyd's Register. New and forthcoming IACS/IMO legislation for the safety of bulk carriers. (2003)

[2] Nakos D.E. and Sclavounos P.D., "Ship motions by a 3-D Rankine Panel method" Proc. 18th symposium on Naval Hydrodynamic, pp.21-40. Ann Arbor, MI, USA, 1990.

[3] Maury C., Delhommeau G., Ba M,, and Guilbaud M., "Comparison between numerical computations and experiments for seakeeping on ship models with forward speed" Journal of ship research, volume 47,No.4, pp.347-364.USA, 2003.

[4] Kim B., "Some consideration on forward-speed seakeeping calculations in frequency domain" International Journal of Offshore and Polar Engineering.Volume15,No.3, pp189-197. USA. 2005.

[5] Inglis RB, and Price WG., "Calculation of Velocity Potential of a Translating, Pulsating source" Trans. RINA, Volume 123, pp 163 175,UK, 1980.

[6] Hess JL, and Smith AMO., "Calculation of Nonlifting Potential Flow About Arbitrary ThreeDimensional Bodies" Journal of Ship Research, Volume 8, No.2, pp 22-44.USA 1964.

[7] Wehausen JY, and Laitone EV, "Surface Waves" Hundbuck der Physic, Vol 9, Springer, pp 446-778, 1960.

[8] Inoue Y, and Makino Y., "The influence of Forward Speed Upon Three Dimensional Hydrodynamic Forces" JSNAJ, pp 207-215. Japan 1989.

[9] Malick Ba and Michel Guilbaud, "A fast method of evaluation for the Translating and Pulsating Green's Function" Ship Technology Research . vol.42, pp.68-80, Germany 1995.

[10] Bailey P.A., Hudson D.A., Price W.G., and Temarel P., "Comparisons between theory and experiment in a seakeeping validation" Royal Institute of Naval Architect..pp.45-78..UK 2001.

[11] Makos D.E., and Sclavounos P/D., "Ship motions by a 3-D Rankine Panel method" Proc. 18th Symposium on Naval Hydrodynamic, pp.21-40. Ann Arbor, MI, USA 1990.

[12] Inoue Y., Itatsu S. and Hiyashi N. "Ship form characteristics and motion responses in seway of various cargo ships" Kansai SNAJ, vol. 208,pp 11-25,Japan 1988.

[13] Newmark N.M., "A method of computation for structure Dynamics. Proceedings of the American Society of Civil Engineers" pp.67-94,USA 1959.

[14] Watanabe Y., Inoue S. and Murahashi T., "The modification of Rolling Resistance for Full Ship" Journal of Seibu Zosen Kai. No.27, pp.69-82, Japan 1963.

[15] Nippon Kaiji Kyoaki, Rules and Guidance, Japan (2007).

[16] Zakaria N.M.G., "A design aspect of the seakeeping performances of ships by 3-D Green Function with forward speed" Doctor of Engineering Thesis, YNU, Japan 2006.

PROFILE



DR N. M. GOLAM ZAKARIA

Dr N. M. Golam Zakaria is working as an assistant professor in the Department of Naval Architecture & Marine Engineering, Bangladesh university of Engineering and Technology (BUET), Dhaka-1000, Bangladesh. He obtained his Doctor of Engineering from Yokohama National University, Japan in year 2006.

NUMERICAL STUDY OF AN ANISOTROPICALLY SUPPORTED ROTOR WITH PARAMETRIC EXCITATION

(Date received: 7.12.2007)

Chih Feng Lee[1], Yee Wei Tan[2] and Janusz M. Krodkiewski[3]
[1]Department of Mechanical and Manufacturing Engineering, University of Melbourne
Parkville, Victoria 3010, Australia.
Email: [1]c.lee33@pgrad.unimelb.edu.au

ABSTRACT

Anisotropic structures, e.g. oil journal bearings are often employed as supporting structure for rotating machineries. Moreover, cross-section of rotating element is often non-symmetrical due to various practical reasons. This paper investigates the dynamics of a parametrically excited rotor-support system. The mathematical model of a rotor supported by an anisotropic structure in the middle and supported rigidly at the far-ends is devised. Stability analysis in the rotating speed domain is demonstrated using two numerical approaches based on Runge–Kutta method and Floquet Theory. The performance of these two methods in terms of computational cost and accuracy is compared. In addition, the influence of cross-coefficient stiffness and damping of the anisotropic support on the unstable region is discussed.

Keywords: *Anisotropic Support, Mechanical Vibrations, Rotor, Stability*

1.0 INTRODUCTION

Rotors are the rotating parts of machines. They are widely found in machineries of various sizes, *e.g.* steam turbines, centrifugal compressors, electric motors, pumps and fans. In most applications, the cross sections of rotors are not perfectly symmetrical along its two principal axes. This is due to various practical reasons, for instance, the rotor of an electric motor has slots for coil assembly and shafts are often equipped with keyways. Unsymmetrical cross section of rotor induces difference in stiffness along the two orthogonal directions.

Supporting structures of rotating machineries are often found to be anisotropic. This can be induced by using materials of non-homogenous composition such as wood, polymer laminates and fibre reinforced plastics. Moreover, irregular and unsymmetrical cross section of supporting structure leads to anisotropy. Besides, anisotropy is resulted from interaction with fluid, *e.g.* in the case of oil journal bearings which is commonly employed in turbo-machineries. The oil field in the journal bearings behaves in a nonlinear and anisotropic fashion.

Support structure can be categorised into isotropic and anisotropic support. Generally, for a two-degree-of-freedom support, the stiffness matrix along the principle axes can be represented by

$$\mathrm{K} = \begin{pmatrix} K_x & K_{xy} \\ K_{yx} & K_y \end{pmatrix} \tag{1}$$

For an isotropic support, the diagonal stiffness terms are identical, *i.e.* $K_x = K_y$ and the cross-coefficient stiffness terms are zero, *i.e.* $K_{xy} = K_{yx} = 0$. On the other hand, for an anisotropic support, the cross-coefficient stiffness terms are not identical, *i.e.* $K_x \neq K_y$. A special case for anisotropic support is orthotropic support, where $K_x \neq K_y$ and $K_{xy} = K_{yx} = 0$. The influence of diagonal stiffness terms K_x and K_y on resonance frequency is well-defined and widely studied [10]. However, the influence of cross-coefficient stiffness on resonance frequency has particular peculiarity, and will be focused in this paper.

Various studies on the influence of support anisotropy on the motion of asymmetric shaft have been done previously. Ota and Mizutani [7] investigated the influence of support stiffness on a system supported by two identical anisotropic bearings at the far-ends of rotor. A lumped mass model with a journal in the middle of the rotor is considered. However, the influence of support damping was not investigated in this paper. Rajilingham et al. [9] extended the investigation by exploring the influence of support damping characteristics. Lee *et al.* [5] approached the problem with Floquet theory and coordinate transformation method. In addition, Ganesan [2] looked into a problem with slightly different configuration. Instead of having two anisotropic support structures, the rotor is supported by an anisotropic structure in the middle and rigidly supported at the far-ends. He also studied the system stability in slowly varying rotation speed.

Parszeski *et al.* [8] investigated the problem with continuous shaft model. They showed that the problem of parametric instability of a rotor-support system could be solved when receptances of rotor-support structure are known. The receptances were obtained using rigid finite element method. Iwatsubo *et al.* [3] approached the problem with continuous shaft using Galerkin's method while Kang *et al.* [4] used transfer matrix method.

In this paper, a lumped mass model with a journal in the middle of the rotor is adopted. The rotor is supported anisotropically in the middle and supported rigidly at the far-ends. Stability analysis of free vibration is obtained by two numerical approaches based

on Runge–Kutta method and Floquet Theory. The former method numerically integrates the equation of motion, while the latter method takes account of the periodicity nature of parametric excitation. Based on Floquet Theory, the solution of periodically perturbed system can be sought using Hill's infinite determinant. By reducing the order of Hill's infinite determinant into smaller matrix, approximating solution for the critical speed region can be found. However, the size of concatenation is not well-defined and its resultant accuracy is questionable. Therefore, in order to verify the solution of Hill's infinite determinant, it is compared with the solution obtained using Runge-Kutta method.

The focus of this paper is on: (a) comparing the computational cost and accuracy of reduced order Hill's determinant and Runge-Kutta method; (b) investigating the influence of cross-coefficient stiffness terms and (c) support damping on unstable speed regions. The remainder of this paper is organised as follows. Section 2 presents the mathematical model of a rotor system with anisotropic support and parametric excitation. Classification of unstable dynamics will be discussed here. Section 3 illustrates two approaches for identification of stable and unstable operating speed regions, namely Runge-Kutta method and Hill's determinant. Section 4 compares the computational cost and accuracy of these two approaches. Section 5 discusses the influence of cross-coefficient stiffness and damping on unstable regions. Section 6 offers some concluding remarks.

2.0 PROBLEM DEFINITION

In this section, the model of rotor-bearing system is introduced, followed by categorisation of unstable dynamic motion.

2.1 Mathematical model

A model of multi-bearing rotor system is devised in order to analyse the influence of support anisotropy (see Figure 1). The rotor is a massless shaft with unsymmetrical cross-section. It is rigidly supported at both ends by two rolling element bearings with isotropic supports. Between the two supports, a journal of mass m is attached and it is supported by an anisotropic structure. Moreover, the residual unbalance of the journal is denoted by μ. The rotor rotates with constant angular speed Ω.

In the model, coordinate system xyz is stationary, while coordinate system $x_R y_R z_R$ is rotating with the shaft. Without loss of generality, the stationary axes xy coincide with the principal axes of the anisotropic support. Reaction force of shaft acting on journal, R is dependent upon the stiffness of shaft. The components of shaft stiffness along the rotating coordinates x_R and y_R are k_x and k_y respectively. If refereed to the rotating coordinates, the components of reaction force are

$$R_{xR} = k_x x_R,$$

$$R_{yR} = k_y Y_R \tag{2}$$

Likewise, the reaction force of the support on journal is dependent on its stiffness and damping. If refereed to the stationary coordinates, the components of the supporting force are

$$S_x = K_x x + K_{xy} y + C_x x\,,$$

$$S_y = K_{xy} x + K_y y + C_y y\,, \tag{3}$$

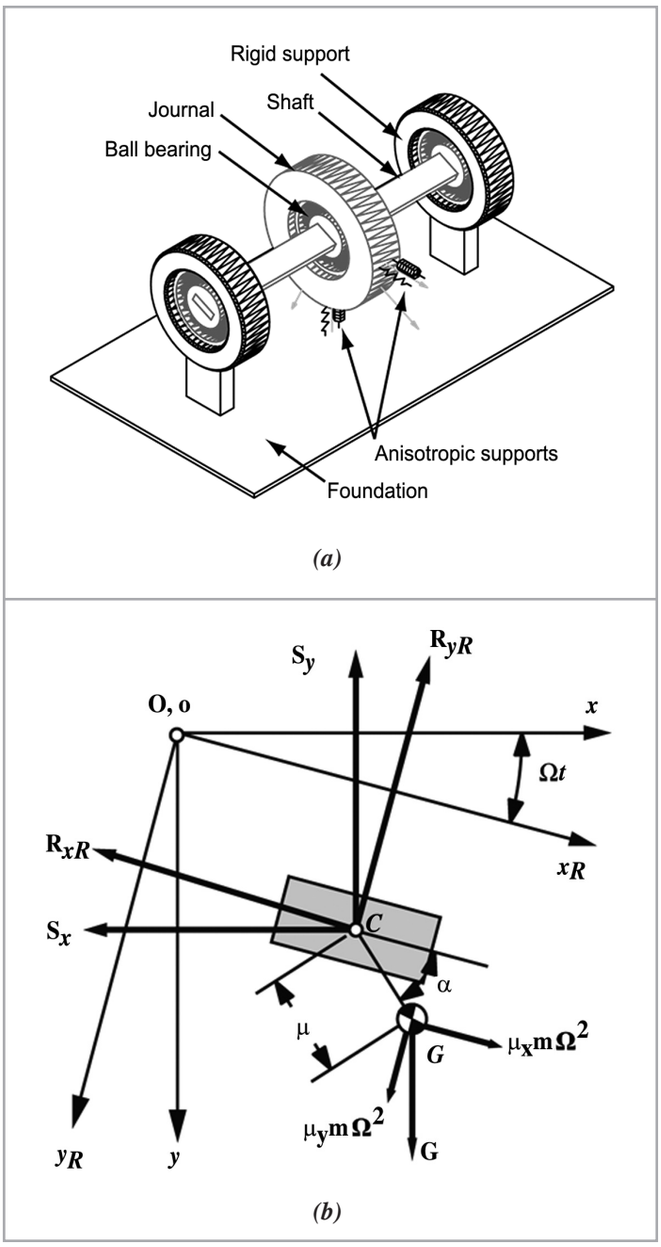

Figure 1: (a) Isometric view of the rotor-bearing-foundation system. (b) Cross-sectional view of forces acting on the rotor

where K and C are stiffness and damping coefficients of the anisotropic support.

Due to external factors such as friction, there exists external damping acting to the journal. The external damping coefficient is represented by c. In addition, due to residual unbalance in the journal, unbalance force exits, and its x and y components are denoted by q_x and q_y respectively. By applying Newton's law to the journal, the equations of motion in x and y directions are

$$m\ddot{x} + (C_x + c)\dot{x} + k_x x_R \cos(\Omega t) - k_y y_R \sin(\Omega t) + K_x x + K_{xy} y = q_x\,,$$

$$m\ddot{y} + (C_y + c)\dot{y} + k_x x_R \sin(\Omega t) + k_y y_R \cos(\Omega t) - K_{xy} x + K_y y =$$

$$G + q_y\,, \tag{4}$$

where G is gravitational force.

By referring to Figure 1, the relationships between rotating coordinate system $x_R y_R$ and stationary coordinate system xy are found to be

$$x_R = x\cos(\Omega t) + y\sin(\Omega t),$$
$$y_R = -x\sin(\Omega t) + y\cos(\Omega t), \tag{5}$$

Hence, introduction of (5) into (4) yields

$$m\ddot{x} + (C_x + c)\dot{x} + \frac{1}{2}(k_x + k_y)x + \frac{1}{2}(k_x - k_y)y\sin(2\Omega t) + \frac{1}{2}(k_x - k_y)x\cos(2\Omega t) + K_x x + K_{xy} y = q_x,$$
$$m\ddot{y} + (C_y + c)\dot{y} + \frac{1}{2}(k_x + k_y)y - \frac{1}{2}(k_x - k_y)y\cos(2\Omega t) + \frac{1}{2}(k_x - k_y)x\sin(2\Omega t) + K_y y - K_{xy} x = G + q_y, \tag{6}$$

To further analyse the problem, the following notations are introduced, namely mean and difference of diagonal stiffness terms, *i.e.* k_0 and Δk respectively.

$$k_0 = \frac{1}{2}(k_x + k_y), \quad \Delta k = \frac{1}{2}(k_x - k_y) \tag{7}$$

Then, introduction of (7) into (6) gives

$$m\ddot{x} + (C_x + c)\dot{x} + k_0 x + \Delta k y\sin(2\Omega t) + \Delta k x\cos(2\Omega t) + K_x x + K_{xy} y = q_x,$$
$$m\ddot{y} + (C_x + c)\dot{y} + k_0 y - \Delta k y\cos(2\Omega t) + \Delta k x\sin(2\Omega t) + K_y y - K_{xy} x = G + q_y. \tag{8}$$

The components of residual unbalanced force in x and y directions are

$$q_x = \mu_x m\Omega^2\cos(\Omega t) - \mu_y m\Omega^2\sin(\Omega t),$$
$$q_y = \mu_x m\Omega^2\sin(\Omega t) + \mu_y m\Omega^2\cos(\Omega t), \tag{9}$$

where

$$\mu_x = \mu\cos(\alpha),\ \mu_y = \mu\sin(\alpha) \tag{10}$$

Equation (8) can be arranged into the following matrix representation

$$\begin{pmatrix} m & 0 \\ 0 & m \end{pmatrix}\begin{pmatrix} \ddot{x} \\ \ddot{y} \end{pmatrix} + \begin{pmatrix} Cx + c & 0 \\ 0 & Cx + c \end{pmatrix}\begin{pmatrix} \dot{x} \\ \dot{y} \end{pmatrix} + \begin{pmatrix} K_x & K_{xy} \\ -K_{xy} & K_y \end{pmatrix}\begin{pmatrix} x \\ y \end{pmatrix} + \left\{\begin{pmatrix} k_0 & 0 \\ 0 & k_0 \end{pmatrix} + \begin{pmatrix} 0 & \Delta k \\ \Delta k & 0 \end{pmatrix}\sin(2\Omega t) + \begin{pmatrix} \Delta k & 0 \\ 0 & -\Delta k \end{pmatrix}\cos(2\Omega t)\right\}\begin{pmatrix} x \\ y \end{pmatrix} = \begin{pmatrix} 0 \\ G \end{pmatrix} + \begin{pmatrix} q_x \\ q_y \end{pmatrix}. \tag{11}$$

By introducing matrix notation

$$\boldsymbol{z} = \begin{pmatrix} x \\ y \end{pmatrix}, \tag{12}$$

and defining the corresponding matrices, Equation (11) is written in a compact form

$$\boldsymbol{M}\ddot{\boldsymbol{z}} + \boldsymbol{C}\dot{\boldsymbol{z}} + \boldsymbol{K}\boldsymbol{z} + (\boldsymbol{k}_0 + \Delta\boldsymbol{k}_s\sin(2\Omega\boldsymbol{t}) + \Delta\boldsymbol{k}_c\cos(2\Omega\boldsymbol{t}))\boldsymbol{z} = \boldsymbol{Q} + \boldsymbol{q}. \tag{13}$$

Then, using Euler formulae

$$\sin(2\Omega t) = \frac{e^{i2\Omega t} - e^{-i2\Omega t}}{2i}$$
$$\cos(2\Omega t) = \frac{e^{i2\Omega t} + e^{-i2\Omega t}}{2i} \tag{14}$$

the equation of motion is arranged into the following expression

$$\boldsymbol{M}\ddot{\boldsymbol{z}} + \boldsymbol{C}\dot{\boldsymbol{z}} + \boldsymbol{K}\boldsymbol{z} + \left(\boldsymbol{k}_0 + \frac{1}{2}(\Delta\boldsymbol{k}_c + \boldsymbol{i}\Delta\boldsymbol{k}_s)\boldsymbol{e}^{i2\Omega t} + \frac{1}{2}(\Delta\boldsymbol{k}_c - \boldsymbol{i}\Delta\boldsymbol{k}_s)\boldsymbol{e}^{-i2\Omega t}\right)\boldsymbol{z} = \boldsymbol{Q} + \boldsymbol{q}. \tag{15}$$

To analyse the influence of anisotropic support and non-symmetrical shaft on dynamic motion, the investigation is concentrated on dynamic motion free from any impressed force – the free vibration case. The equation of motion for free vibration is the homogeneous equation of (15), *i.e.*

$$\boldsymbol{M}\ddot{\boldsymbol{z}} + \boldsymbol{C}\dot{\boldsymbol{z}} + \boldsymbol{K}\boldsymbol{z} + \left(\boldsymbol{k}_0 + \frac{1}{2}(\Delta\boldsymbol{k}_c + \boldsymbol{i}\Delta\boldsymbol{k}_s)\boldsymbol{e}^{i2\Omega t} + \frac{1}{2}(\Delta\boldsymbol{k}_c - \boldsymbol{i}\Delta\boldsymbol{k}_s)\boldsymbol{e}^{-i2\Omega t}\right)\boldsymbol{z} = 0. \tag{16}$$

2.2 Classification of unstable regions

If there is no parametric excitation, *i.e.* $\Delta k = 0$, the system possesses two natural frequencies:

$$\omega_1 = \sqrt{\frac{k_0 + k_x}{m}}, \quad \omega_2 = \sqrt{\frac{k_0 + k_y}{m}} \tag{17}$$

With the combined effects of anisotropic supporting structure and parametric vibration, the unstable regions are often found in vicinity of the natural frequencies. The unstable regions associated with only one natural frequency are termed simple instability regions. They can be determined by:

$$\Omega_{nl} = \frac{\omega_n}{l}, \quad l = 1, 2, \ldots\ldots \tag{18}$$

Apart from the simple instability regions, some unstable regions are associated with both of the natural frequencies. They are termed combined instability regions. They can be found in vicinity of:

$$\Omega^{(\pm)}_{nml} = \frac{\omega_n \pm \omega_n}{2l}, \quad l = 1, 2, \ldots\ldots \tag{19}$$

When $l = 1$, the unstable region is called primary instability region; when $l = 2$, it is called secondary instability region.

3.0 METHODS TO DETERMINE STABILITY REGIONS

One of the operation safety concerns of rotating machineries is to avoid operating close to critical speeds. Therefore in the design stage, it is important to identify the critical speed regions. Operating under critical speed yields unstable dynamic motion, where the amplitude of vibration grows exponentially. For complex cases, such as the case expressed in (16), it is very difficult to obtain an exact analytical solution of the critical speed regions. Hence, numerical solution is sought. This section illustrates two numerical methods for determination of stable and unstable operating speed regions. They are based on Runge-Kutta method and Floquet theory.

3.1 Numerical methods for ordinary differential equations

The ordinary differential equation with time derivative, such as equation (16) can be written in the following general form

$$y(t) = \frac{dy(t)}{dt} = f(t, y). \tag{20}$$

Numerical schemes, such as Euler's method, Crank-Nicolson method and Runge-Kutta method are often employed to obtain numerical solutions for ordinary differential equations. Compared among other methods, the forth-order Runge-Kutta method has a few preferred numerical features, *e.g.* it is relatively simpler to code than Crank-Nicolson method, its numerical solution is more stable than Euler method, and it generally has fast evaluation speed. Therefore, the forth-order Runge-Kutta method is chosen in this study.

3.1.1 Runge-Kutta Method

Runge-Kutta methods has the following generalised form [1]

$$y_{i+1} = y_i + \phi(t_i, y_i, h)\, h. \tag{21}$$

where h and $\phi(t_i, y_i, h)$ are called step size and increment function respectively. The increment function can be used as a representative of the slope over interval $(t_i, t_i + h)$ and it differentiates from different orders of Runge-Kutta methods. The general form of the increment function is

$$\phi(t_i, y_i, h) = a_1 k_1 + a_2 k_2 + \ldots + a_n k_n , \tag{22}$$

where the a's are constants and the k's are

$$\begin{aligned}
k_1 &= f(t_i, y_i) \\
k_2 &= f(t_i + p_1 h, y_i + q_{11} k_1 h) \\
k_3 &= f(t_i + p_2 h, y_i + q_{21} k_1 h + q_{22} k_2 h) \\
&\vdots \\
k_n &= f(t_i + p_{n-1} h, y_i + q_{n-1,1} k_1 h + q_{n-1,2} k_2 h + \ldots + q_{n-1,n-1} k_{n-1} h)
\end{aligned} \tag{23}$$

p's and q's are constants.

Various order of Runge-Kutta methods are devised by employing different n's, specified in the increment function. The constants a's, p's and q's are evaluated by employing Taylor series expansion [1]. The most popular Runge-Kutta methods is the forth-order Runge-Kutta scheme, where its classical form has the following increment function [1]

$$\phi_{RK4}(t_i, y_i, h) = \frac{1}{6} k_1 + \frac{1}{3} k_2 + \frac{1}{3} k_3 + \frac{1}{6} k_4 , \tag{24}$$

where

$$\begin{aligned}
k_1 &= f(t_i, y_i) \\
k_2 &= f(t_i + \tfrac{1}{2} h, y_i + \tfrac{1}{2} k_1 h) \\
k_3 &= f(t_i + \tfrac{1}{2} h, y_i + \tfrac{1}{2} k_2 h) \\
k_4 &= f(t_i + h, y_i + k_3 h)
\end{aligned} \tag{25}$$

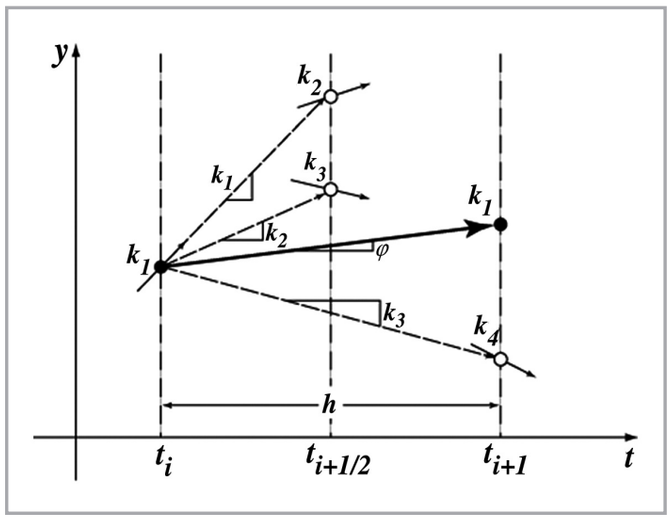

Figure 2: Graphical representation of forth-order Runge-Kutta slope estimation [1]

The step size h determines the accuracy of the solution and the speed of evaluation. Accuracy of the solution increases with the decrease of step size, however, in the expense of slower evaluation speed. Moreover, large step size can induce numerical instability. Therefore, determination of the correct step size is vital.

It is worthwhile to mention that the step size of certain variant of Runge-Kutta methods is varied during evaluation, such as the Runge-Kutta Fehlberg method. There are two notable benefits for using adaptive step size: (a) to avoid numerical instability and (b) to increase the evaluation speed by using the largest possible step size while maintaining the required accuracy tolerance. In particular for Runge-Kutta Fehlberg method, solutions obtained with forth- and firth-order are compared. Difference between the solutions is the estimated numerical truncation error [1]. Consequently, truncation error is used to determine the next step size. The strategy is to decrease the step size if the error is too large and vice-versa.

The following subsection describes the steps required to solve a set of ordinary differential equations, *e.g.* (16) using Runge-Kutta method.

3.1.2 Evaluation of a Second Order Differential Equation

Differential equations that involve one dependent variable are called ordinary differential equations. They are classified by the order of their highest derivative. For example, the highest order of derivative for the equation of motion (16) is two.

Therefore, (16) is a second order ordinary differential equation. In order to solve a set high-order differential equations using forth-order Runge-Kutta method, they are arranged into a set of first-order differential equations, which can be written concisely as

$$\dot{\boldsymbol{y}} = \boldsymbol{A}\boldsymbol{y} + \boldsymbol{B} \tag{26}$$

Equation (16) can be arranged into the form of (26), *i.e.*

$$\begin{pmatrix} \dot{z} \\ \ddot{z} \end{pmatrix} = \begin{bmatrix} 0 & 1 \\ -\boldsymbol{M}^{-1}(\boldsymbol{K}+\boldsymbol{k}_0) & -\boldsymbol{M}^{-1}\{1/2(\Delta\boldsymbol{k}_c + \boldsymbol{i}\Delta\boldsymbol{k}_s)\exp(\boldsymbol{i}2\Omega t) \\ & +1/2(\Delta\boldsymbol{k}_c - \boldsymbol{i}\Delta\boldsymbol{k}_s)\exp(-\boldsymbol{i}2\Omega t)\} \end{bmatrix} \begin{pmatrix} z \\ \dot{z} \end{pmatrix} \tag{27}$$

Henceforth, (27) can be solved using the equations as described in (21), (24) and (25).

Numerous mathematics packages such as Mathematica and MATLAB includes ordinary differential equation solvers. In particular, the results presented in this paper are obtained using MATLAB "ode45" function, which is based upon fifth- and sixth-order Runge-Kutta method with adaptive step size.

3.2 Floquet Theory

The governing differential equation of free vibration equation (16) contains coefficients that are periodic. These periodic coefficients pose excitation to the system, in which the type of excitation is termed parametric excitation. In contrast to the case of external excitation, where resonance only happens when the excitation is close to one of the natural frequencies of the system, resonance in parametric excitations may happen when the frequency of excitation is close to one half of one of the natural frequencies [6].

For systems governed by ordinary differential equations with periodic coefficients, Floquet theory is commonly used as the basis for analysis. According to Floquet theory, these systems has particular solutions of the form [6]

$$z = \exp(\gamma t)\,\varphi(t) \tag{28}$$

where γ is called characteristic exponent or Floquet exponent. It is a complex number, in which its real part is called Lyapunov exponent. $\varphi(t)$ is a periodic function, *i.e.* $\varphi(t) = \varphi(t + T)$, where T is the period of the excitation. From (16), it is noticed that $T = 2\pi/2\Omega = \pi/\Omega$. Expressing $\varphi(t)$ in Fourier series yields

$$\varphi(t) = \sum_{n=-\infty}^{\infty} \exp(i2n\Omega t)\,\varphi_n \tag{29}$$

Therefore, substituting (29) into the particular solution (28) to procure

$$z = \sum_{n=-\infty}^{\infty} \exp(\gamma t + i2n\Omega t)\,\varphi_n \tag{30}$$

It is noted that the solution (28) is unstable if, and stable for in Lyapunov sense. The following subsection illustrates a method for determining the stability boundary.

3.2.1 Hill'S Infinite Determinant

By differentiating (30), we get

$$\dot{z} = \sum_{n=-\infty}^{\infty} \exp(\gamma t + i2n\Omega t)(\gamma + i2n\Omega)\,\varphi_n, \qquad \ddot{z} = \sum_{n=-\infty}^{\infty} \exp(\gamma t + i2n\Omega t)(\gamma + i2n\Omega)^2\,\varphi_n \tag{31}$$

Substituting (30) and (31) into (16) yields

$$\sum_{n=-\infty}^{\infty} \left\{ \left[\boldsymbol{M}(\gamma + i2n\Omega)^2 + \boldsymbol{C}(\gamma + i2n\Omega) + \boldsymbol{K} + \boldsymbol{k}_0 \right] \varphi_n \exp(\gamma t + i2n\Omega t) \right\}$$
$$+ \frac{1}{2}(\Delta\boldsymbol{k}_c + i\Delta\boldsymbol{k}_s) \sum_{n=-\infty}^{\infty} \left\{ (\varphi_n \exp(\gamma t + i(2n+1)\Omega t) \right\}$$
$$+ \frac{1}{2}(\Delta\boldsymbol{k}_c - i\Delta\boldsymbol{k}_s) \sum_{n=-\infty}^{\infty} \left\{ (\varphi_n \exp(\gamma t + i(2n-1)\Omega t) \right\} \tag{32}$$

Equating the coefficients for each of the exponential terms $\exp(\gamma t + i2n\Omega t)$ in (32) to zero, we get the following infinite set of equations, corresponding to φ_m (where $m = -\infty, \ldots, \infty$)

$$\left[\boldsymbol{M}(\gamma + i2n\Omega)^2 + \boldsymbol{C}(\gamma + i2n\Omega) + \boldsymbol{K} + \boldsymbol{k}_0 \right] \varphi_m + \frac{1}{2}(\Delta\boldsymbol{k}_c + i\Delta\boldsymbol{k}_s)\varphi_{m+1}$$
$$+ \frac{1}{2}(\Delta\boldsymbol{k}_c + i\Delta\boldsymbol{k}_s)\varphi_{m+1} = 0 \tag{33}$$

Presenting (33) in matrix notation gives

$$\begin{pmatrix} \ddots & \vdots & \vdots \\ \cdots & \boldsymbol{M}(\gamma - i2\Omega)^2 + \boldsymbol{C}(\gamma - i2\Omega) + \boldsymbol{K} + \boldsymbol{k}_0 & \frac{1}{2}(\Delta\boldsymbol{k}_c + i\Delta\boldsymbol{k}_s) \\ \cdots & \frac{1}{2}(\Delta\boldsymbol{k}_c + i\Delta\boldsymbol{k}_s) & \boldsymbol{M}\gamma^2 + \boldsymbol{C}\gamma + \boldsymbol{K} + \boldsymbol{k}_0 \\ \cdots & 0 & \frac{1}{2}(\Delta\boldsymbol{k}_c + i\Delta\boldsymbol{k}_s) \\ \iddots & \vdots & \vdots \end{pmatrix}$$
$$\begin{pmatrix} \vdots & \iddots \\ 0 & \cdots \\ \frac{1}{2}(\Delta\boldsymbol{k}_c - i\Delta\boldsymbol{k}_s) & \cdots \\ \boldsymbol{M}(\gamma + i2\Omega)^2 + \boldsymbol{C}(\gamma + i2\Omega) + \boldsymbol{K} + \boldsymbol{k}_0 & \cdots \\ \vdots & \ddots \end{pmatrix} \begin{pmatrix} \vdots \\ \varphi_{-1} \\ \varphi_0 \\ \varphi_{+1} \\ \vdots \end{pmatrix} = \begin{pmatrix} \vdots \\ 0 \\ 0 \\ 0 \\ \vdots \end{pmatrix} \tag{34}$$

For a nontrivial solution, the determinant of the coefficient matrix in (34) is equal to zero. Hence, as a function of Floquet exponent and rotation speed, Hill's infinite determinant is

$$\boldsymbol{D}(\gamma, \Omega) = \begin{pmatrix} \ddots & \vdots \\ \cdots & \boldsymbol{M}(\gamma - i2\Omega)^2 + \boldsymbol{C}(\gamma - i2\Omega) + \boldsymbol{K} + \boldsymbol{k}_0 \\ \cdots & \frac{1}{2}(\Delta\boldsymbol{k}_c + i\Delta\boldsymbol{k}_s) \\ \cdots & 0 \\ \iddots & \vdots \end{pmatrix} \tag{35}$$

$$\begin{pmatrix} \vdots & \vdots & \ddots \\ \frac{1}{2}(\Delta \boldsymbol{k}_c + i\Delta \boldsymbol{k}_s) & 0 & \cdots \\ \boldsymbol{M}\gamma^2 + \boldsymbol{C}\gamma + \boldsymbol{K} + \boldsymbol{k}_0 & \frac{1}{2}(\Delta \boldsymbol{k}_c - i\Delta \boldsymbol{k}_s) & \cdots \\ \frac{1}{2}(\Delta \boldsymbol{k}_c + i\Delta \boldsymbol{k}_s) & \boldsymbol{M}(\gamma + i2\Omega)^2 + \boldsymbol{C}(\gamma + i2\Omega) + \boldsymbol{K} + \boldsymbol{k}_0 & \cdots \\ \vdots & \vdots & \ddots \end{pmatrix} = 0$$

As mentioned in the previous subsection, solution (28) is unstable if $\mathrm{Re}(\gamma) > 0$. The transition curves separating stable and unstable motion correspond to $\mathrm{Re}(\gamma) = 0$ [6]. Therefore, (35) is solved as a function of rotation speed and characteristics exponent with only imaginary parts, where $\mathrm{Im}(\gamma) = \mu$. In addition, periodic motion with period 2Ω corresponds to solution at $\gamma = 0$, while 4Ω corresponds to $\gamma = \pm i$. The roots can be plotted as Figure 3, and the stability boundary is located at

$$\mathrm{Re}(D(\mu,\Omega)) = 0 \quad \text{and} \quad \mathrm{Im}\,(D(\mu,\Omega)) = 0 \tag{36}$$

3.2.2 Reduced-Order Hill'S Determinant

When $\Delta k_c + i\Delta k_s$ is small, approximate solution can be obtained by considering the central row and column of (35) [6]. A nth order Hill's reduced order determinant matrix $D(\mu, \Omega)$ has $2n + 1$ rows. For example, a first order Hill's determinant has three rows

$$D_1(\mu, \Omega) = \begin{bmatrix} \boldsymbol{M}(i\mu - i2\Omega)^2 + \boldsymbol{C}(i\mu - i2\Omega) + \boldsymbol{K} + \boldsymbol{k}_0 & \frac{1}{2}(\Delta \boldsymbol{k}_c - i\Delta \boldsymbol{k}_s) & 0 \\ \frac{1}{2}(\Delta \boldsymbol{k}_c + i\Delta \boldsymbol{k}_s) & \boldsymbol{M}(i\mu)^2 + \boldsymbol{C}(i\mu) + \boldsymbol{K} + \boldsymbol{k}_0 & \frac{1}{2}(\Delta \boldsymbol{k}_c - i\Delta \boldsymbol{k}_s) \\ 0 & \frac{1}{2}(\Delta \boldsymbol{k}_c + i\Delta \boldsymbol{k}_s) & \boldsymbol{M}(i\mu + i2\Omega)^2 + \boldsymbol{C}(i\mu + i2\Omega) + \boldsymbol{K} + \boldsymbol{k}_0 \end{bmatrix} \tag{37}$$

To obtain a better approximation, higher-order determinant has to be considered. It is generally unclear what order of determinant has to be considered in order to obtain a valid solution. Therefore, the solution of different orders will be compared and discussed in the following section.

4.0 COMPUTATIONAL ISSUES

In the previous section, it is shown that the stable region can be obtained using Runge-Kutta method and reduced order of Hill's infinite determinant. This section assesses the accuracy and evaluation time of both methods quantitatively.

To study the computing requirement for different orders of Hill's determinant, the computational grid size is fixed as 0.05 [rad/s], and computing time is recorded. It is found that lower computing requirement is required by reducing the order of Hill's determinant (see Table 1). Moreover, percentage increase in computing time diminishes with higher order. To identify the accuracy of solution of the reduced order determinant, it is compared with the solution obtained using Runge-Kutta method, and is tabulated in Table 2. Unstable regions in the rotating speed domain from 0–40 [rad/s] are identified and classified into primary and secondary simple or combined instability regions. Numerical values of the instability boundaries obtained from reduced order of Hill's determinant and Runge-Kutta method are compared, and their percentage differences are calculated. It is observed that:

(i) By increasing the order of Hill's determinant, new unstable regions can be found. In this example, the boundaries of secondary instability region are not revealed by the first-order Hill's determinant.

(ii) By increasing the order of Hill's determinant, better accuracy could be obtained. However, the improvement of accuracy is very minor (approximately 1%) for order more than two.

(iii) Longer computation time is required for higher order Hill's determinant.

(vi) Locating stability boundary is more efficient using Hill's determinant. Estimated evaluation time using Runge-Kutta method is 6400 [s], and 78 [s] for second order Hill's determinant (0.05 [rad/s] accuracy using a Pentium 4 3.0 GHz machine).

Table 1: Evaluation time for reduced order Hill's determinant

Order	Evaluation Time [s]	Time Increase [%]
0	29	–
1	78	169
2	125	60
3	173	38

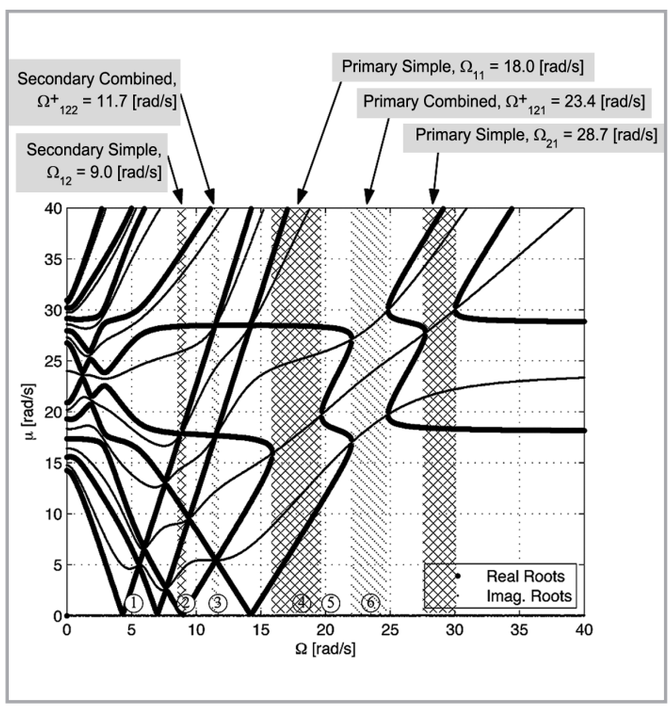

Figure 3: Whirl speed chart calculated using 2nd order Hill's determinant for system supported by orthotropic structure with small damping. The unstable region is hatched

Table 2: Comparison of stability boundaries obtained using different orders of Hill's determinant and Runge-Kutta method

	Secondary Simple		Secondary Combined		Primary Simple		Primary Combined		Primary Simple	
	lower	upper	lower	upper	lower	upper	lower	upper	lower	upper
Runge-Kutta	8.84	8.99	11.49	11.55	15.91	19.67	22.04	24.83	27.74	30.02
Order 1	-	-	-	-	15.84	19.62	22.01	24.82	27.72	30.02
Order 2	8.74	8.90	11.48	11.56	15.90	19.68	22.04	24.83	27.73	30.02
Order 3	8.84	8.99	11.48	11.56	15.90	19.68	22.04	24.83	27.73	30.02
(% diff.) Order 1	-	-	-	-	0.44%	0.25%	0.14%	0.04%	0.07%	0.00%
(% diff.) Order 2	1.13%	1.00%	0.09%	0.09%	0.06%	0.05%	0.00%	0.00%	0.04%	0.00%
(% diff.) Order 3	0.00%	0.00%	0.09%	0.09%	0.06%	0.05%	0.00%	0.00%	0.04%	0.00%

5.0 INFLUENCE OF ANISOTROPIC SUPPORTING STRUCTURE

This section discusses the influence of cross-coefficient stiffness of anisotropic support on the stability region in rotating speed domain. In the following analysis, anisotropic support is categorised into two cases, *i.e*. orthotropic structure and non-orthotropic structure.

5.1 Case $K_{xy} = K_{yx} = 0$ (Orthotropic Structure)

Orthotropic support is a special case of anisotropic support, when the cross-coefficient stiffness terms K_{xy} and K_{yx} are zero. Orthotropic supporting structures include supporting structure with unsymmetrical dimension in the two principal axes and supporting structure constructed with laminating materials, such as wood, polymer laminates and fibre reinforced plastics.

In this subsection, numerical simulation of two cases will be discussed. First, a system with orthotropic support and small damping will be discussed, followed by the same system with large damping.

The simulation parameters for parametric excited system supported with orthotropic structure with small damping are tabulated in Table 3 and the rotating speed associated with simple and combined instability regions are tabulated in Table 4. According to numerical experiments, the unstable regions in the rotating speed domain are found in vicinity of simple and positive combined critical speeds Ω_{nl} and Ω^{+}_{nml} . However, unstable region associated with the negative combined critical speed Ω^{-}_{nml} does not exist. Moreover, it is noticed that the largest unstable region is associated with the primary unstable region. Unstable regions of higher order are usually smaller and are likely to diminish due to the existence of damping.

Spectrum analysis of time history shows that there is only one frequency associated with simple unstable region. On the other hand, there are at least two frequencies associated with the combined unstable regions. The associated frequencies are found to be the natural frequencies of the non-parametrically excited case, as defined in (17). In addition, in the stable regions, the spectrum contains various frequencies, where some of them include the simple and combined critical speeds, as defined in (18) and (19) (see Figures 3 and 4).

Table 3: Simulated system parameters for orthotropic support structure with small damping

Parameters	Values	Parameters	Values
m	50 kg	K_{xy}	0 N/m
k_o	11250 N/m	c	20 N.s/m
Δk	6750 N/m	C_x	0 N.s/m
K_x	5000 N/m	C_y	0 N.s/m
K_y	30000 N/m		

Table 4: Angular speed associated with simple and combined instability regions

Simple	Values [rad/s]	Combined	Values [rad/s]
Ω_{11}	18.0	$\Omega^{(+)}_{121}$	23.35
Ω_{21}	28.7	$\Omega^{(-)}_{121}$	5.35
Ω_{12}	9.0	$\Omega^{(+)}_{122}$	11.68
Ω_{22}	14.4	$\Omega^{(-)}_{122}$	2.68
Ω_{13}	6.0	$\Omega^{(+)}_{123}$	7.78
Ω_{23}	9.6	$\Omega^{(-)}_{123}$	1.78

Unstable region diminishes as damping increases. This is shown in the simulation with parameters tabulated in Table 5. Figure 5 shows that when damping is large, unstable regions in the low frequency range (0–40 [rad/s] in this case) vanish, in exception to the primary simple unstable region associated with Ω_{11}. This is because Ω_{11} is associated with the natural frequency in x, and the damping in x is relatively smaller compared to the damping in y.

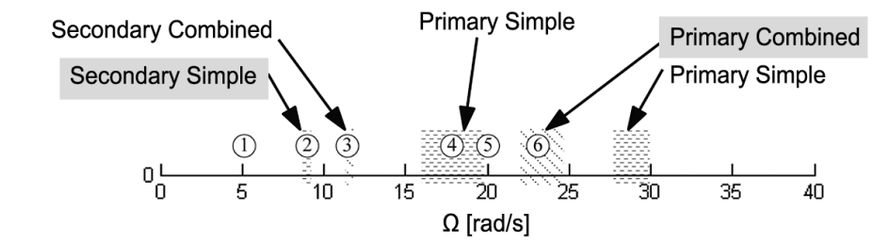

(a)

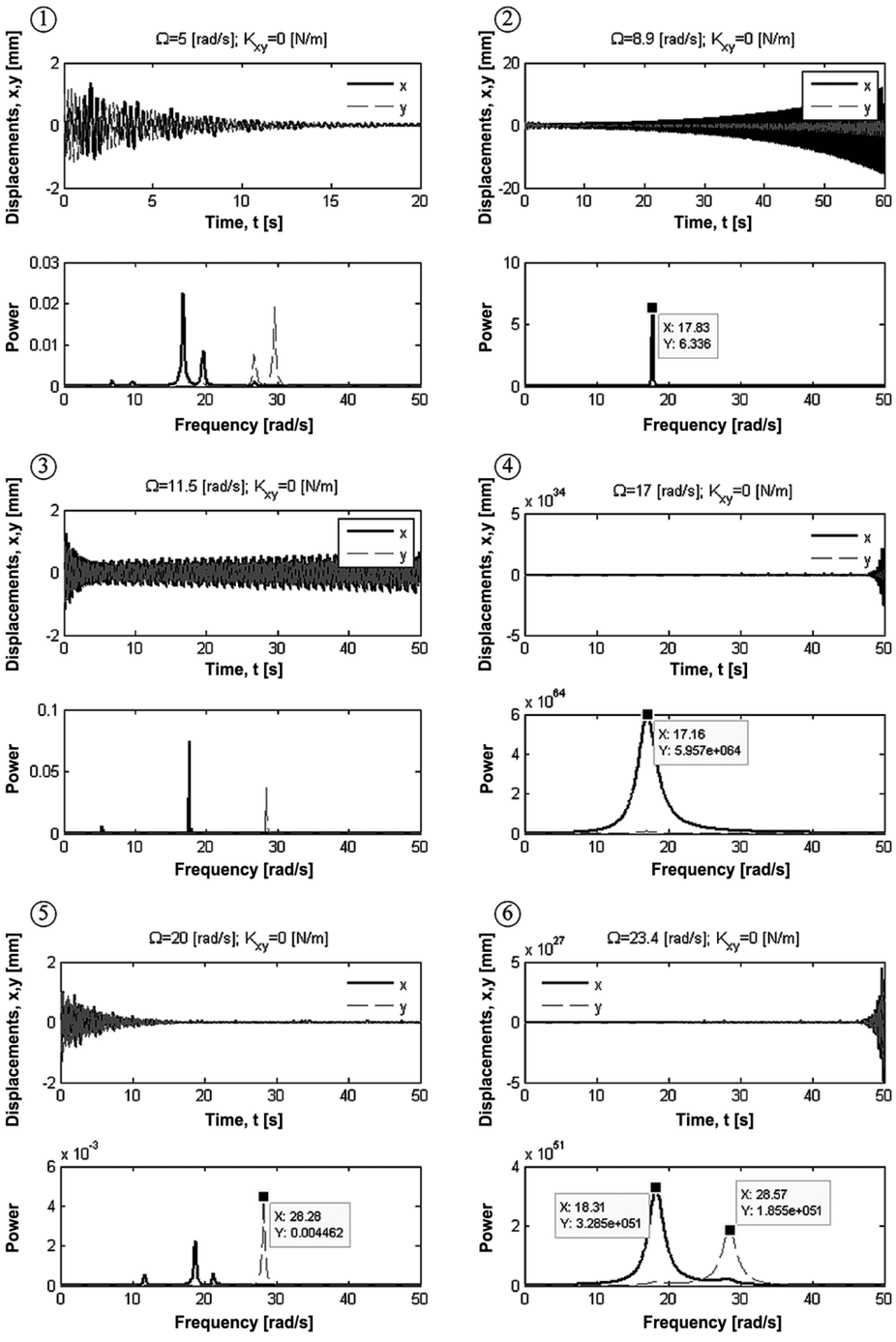

(b)

Figure 4: (a) Unstable regions in rotating speed domain. (b) Time history diagrams and frequency spectrums for various rotating speeds

5.2 Case $K_{xy} = -K_{yx} \neq 0$

The cross-coefficient stiffness terms for non-orthotropic structure are nonzero. This class of anisotropic structure includes oil journal bearings, which are widely used to support rotor in turbomachineries. For anisotropic structure in general, at the principal axes of anisotropy, the cross-coefficient stiffness terms, K_{xy} and K_{yx} have same magnitude with opposite sign.

In this subsection, numerical experiment of a system with large cross-coefficient stiffness and small structural damping (at support) is considered. The system parameters are tabulated in Table 6.

Table 5: Simulated system parameters for orthotropic support structure by large damping

Parameters	Values	Parameters	Values
m	50 kg	K_{xy}	0 N/m
k_o	11250 N/m	c	20 N.s/m
Δk	6750 N/m	C_x	100 N.s/m
K_x	5000 N/m	C_y	500 N.s/m
K_y	30000 N/m		

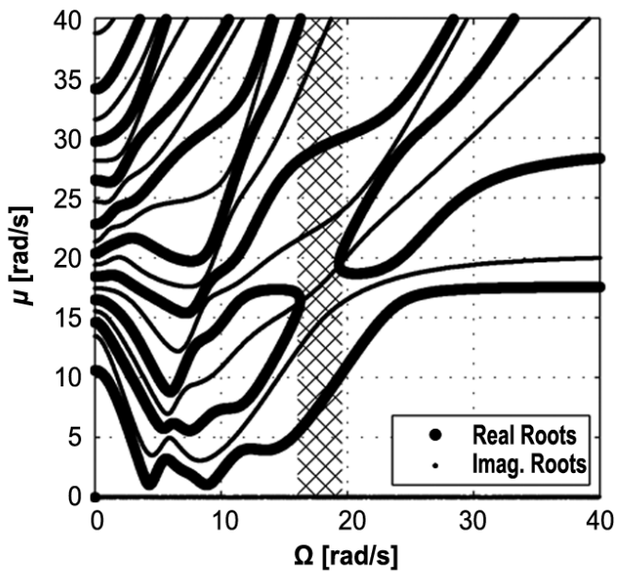

(a)

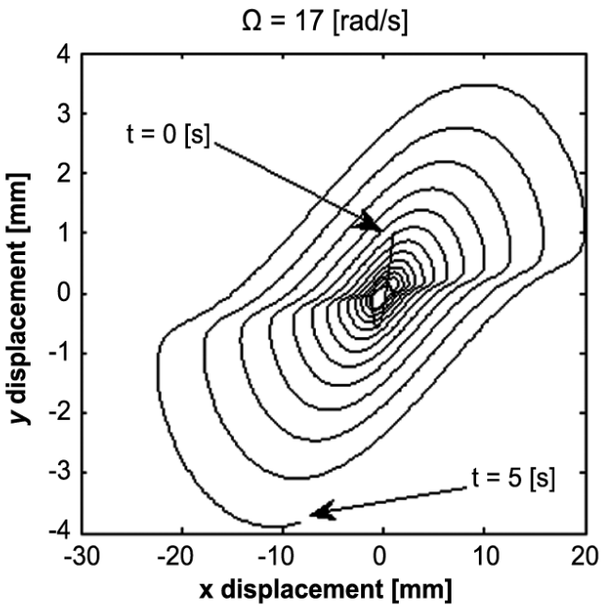

(b)

Figure 5: (a) Whirl speed chart for system supported by orthotropic structure with large damping. The unstable region is hatched. (b) x-y displacement from 0 to 5 seconds for unstable motion

Table 6: Simulated system parameters for anisotropic support structure with small damping

Parameters	Values	Parameters	Values
m	50 kg	K_{xy}	2000 N/m
k_o	11250 N/m	c	20 N.s/m
Δk	6750 N/m	C_x	0 N.s/m
K_x	5000 N/m	C_y	0 N.s/m
K_y	30000 N/m		

Compared with the orthotropic case, strong cross-coefficient stiffness yields new unstable regions (see Figure 6). From simulation, a new secondary simple instability region is found in vicinity of Ω_{21}. Apart, new primary combined instability region is also found in vicinity of $\Omega^{(-)}_{121}$ (see rotating speed range from 5 to 7 [rad/s] in Figure 6). Note that this unstable region associated with negative sign is not found in the orthotropic case. Although $\Omega^{(-)}_{121}$ is very close to the other tertiary speeds (such as Ω_{13} and $\Omega^{(+)}_{123}$), it can be justified that this unstable region is associated with the primary speed. This is because the secondary and tertiary unstable regions are comparatively narrower, and are likely to diminish due to the existence of damping. Conversely, this new found unstable region is large, and is classified as primary combined instability region.

In addition, by observing the location of the stability boundaries, it is found that the boundaries for primary simple instability regions always fall on the line $\mu = \Omega$. Moreover, for secondary simple instability regions, the boundary falls on the line $\mu = 2\Omega$. In fact, for nth order simple instability regions, the stability boundary falls on $\mu = n\Omega$ (see Figure 6).

Figure 7 shows the relationship between unstable region with the magnitude of cross-coefficient stiffness K_{xy} and external damping c. As K_{xy} increases: (a) Overall unstable region increases; (b) Combined instability regions increases; (c) If there are two adjoining unstable regions, they combine as K_{xy} increases. Moreover, unstable regions decrease as external damping increases.

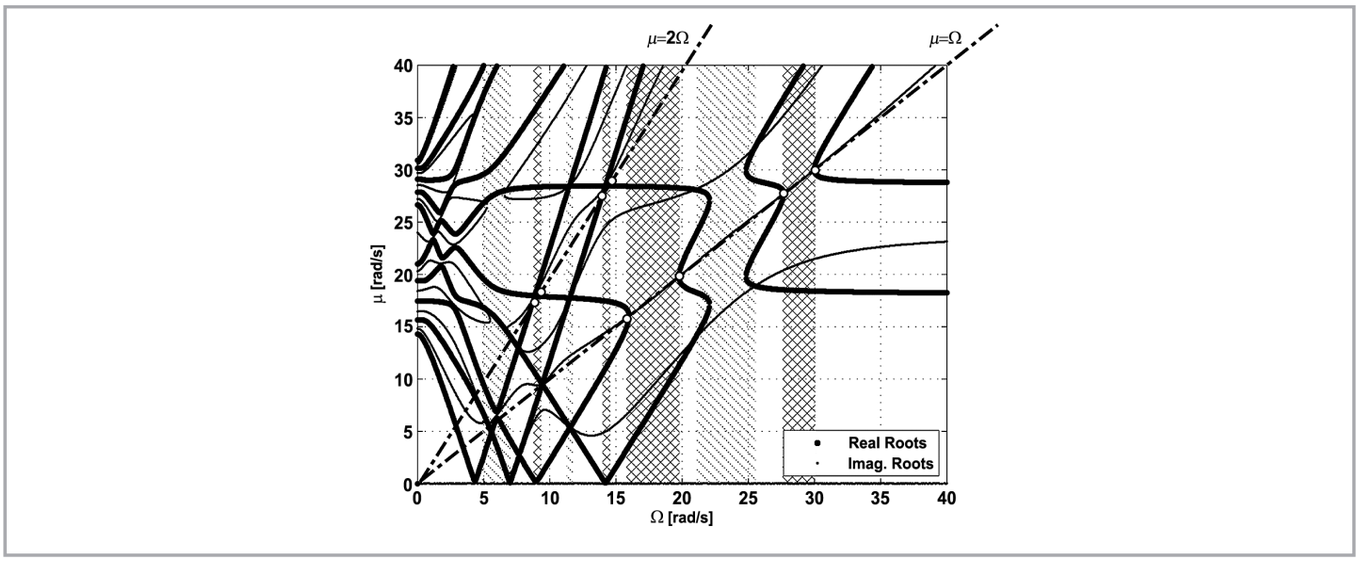

Figure 6: Whirl speed chart for system supported by anisotropic structure with large cross-coefficient stiffness and small damping. The unstable region is hatched

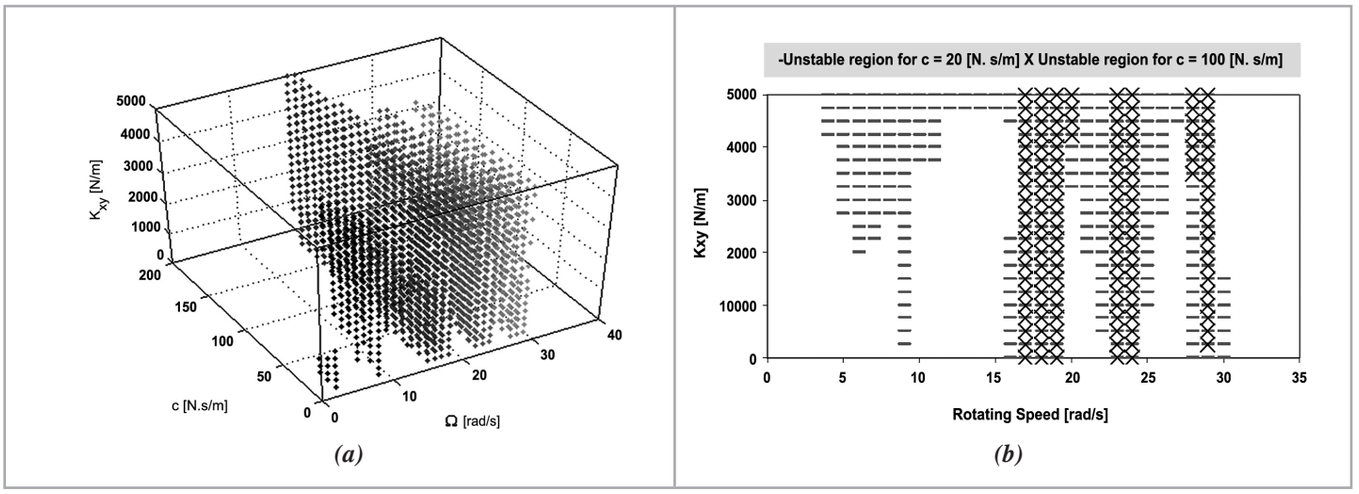

Figure 7: (a) Unstable region (dotted) as a function of external damping, cross-coefficient stiffness and rotating speed. (b) Influence of damping to unstable region.

6.0 CONCLUSIONS

Rotor dynamics subjected to parametric excitation are evaluated by means of Runge-Kutta method and Floquet theory. By comparing the results obtained using these two methods, it is found that the discrepancy is very low (approximately 1%).

Moreover, computation time and resources needed for evaluation of Hill's determinant is significantly more efficient than Runge-Kutta method. By inspection of whirl speed chart, the researcher can immediately have an idea of where the unstable speed region is. On the other hand, in order to produce instability region from Runge-Kutta method, one has to assess multiple time histories, which each of them is evaluated with different rotation speed, and this is very time consuming. However, the time history produced can be utilised to procure vibration frequencies using Fast Fourier Transform (FFT).

Although higher-order Hill's determinant produces better approximation and revealing higher order unstable regions, this comes with the expense of higher computational load. The recommended strategy is to start with first and second-order Hill's determinant. By determining the percentage improvement of the solutions, one can then assess the need to further evaluate solution of higher-order.

In addition, higher cross-coefficient stiffness of anisotropic support increases the overall unstable region. On the other hand, higher damping in supporting structure reduces unstable region. ■

REFERENCES

[1] Chapra S., and Canale R. (2003). Numerical Methods for Engineers, 4th Edition, Mcgraw-Hill, ISBN 0072431938.

[2] Ganesan, R. (2000). "Effects of bearing and shaft asymmetries on the instability of rotors operating at near-critical speeds." Mechanism and Machine Theory. 35: pp. 737-752.

[3] Iwatsubo, T., Tomita, A., and Kawai, R. (1973). "Vibrations of asymmetric rotors supported by asymmetric bearings." Archive of Applied Mechanics (Ingenieur Archiv). Springer, Berlin. 42(6): pp. 416-432.

[4] Kang, Y., Lee, and Y.-G., Chen, S.-C. (1997). "Instability analysis of unsymmetrical rotor-bearing systems using the transfer matrix method." Journal Sound and Vibration. 199(3): pp. 381-400.

[5] Lee, C.-W., Han, D.-J., Suh, J.-H., and Hong, S.-W. (2007). "Modal analysis of periodically time-varying linear rotor systems." Journal of Sound and Vibration. 303(3-5): pp. 553-574.

[6] Nayfeh A., and Mook D. (1979). Nonlinear Oscillations, John Wiley and Sons, ISBN 0471035556.

[7] Ota, H., and Mizutani, K. (1978). "Influence of unequal pedestal stiffness on the instability regions of a rotating asymmetric shaft." Transaction of the ASME, Journal of Applied Mechanics. 45: pp. 400-407.

[8] Parszeski, Z.A., Krodkiewski, J.M., and Rucinski, J. (1986). "Parametric instabilities of rotor-support systems with asymmetric stiffness and damping matrices." Journal of Sound and Vibration. 109(1): pp. 111-125.

[9] Rajalingham, C., Bhat, R.B., and Xistris, G.D. (1992). "Influence of support flexibility and damping characteristics on the stability of rotors with stiffness anisotropy about shaft principle axes." International Journal of Mechanical Sciences. 34(9): pp. 717-726.

[10] Tondl, A. (1965), Some Problems of Rotor Dynamics, Chapman and Hall, London.

PROFILES



LEE CHIH FENG
Lee Chih Feng is a postgraduate student at the University of Melbourne, Australia. He obtained B.Eng. (Hons) in Mechanical and Manufacturing Engineering from the same university in 2005. His research interests cover dynamics and automatic control.



TAN YEE WEI
Tan Yee Wei is an engineer involved in the field of water purification. He graduated from the University of Melbourne in 2005 with a B.Eng. (Hons) in mechanical engineering. His interests include modelling and simulation.



DR KRODKIEWSKI
After his graduation from the Technical University of Lodz in Poland, Dr Krodkiewski joined its Institute of Applied Mechanics in 1964. From the same University, in 1971, he obtained his doctorate in Mechanical Engineering. Since 1981 he has worked for the University of Melbourne and currently, as a senior fellow, is responsible for teaching Mechanics of Rigid Bodies, Dynamics of Machines and Dynamics of Rotors.

DERIVATION OF SWITCHING ANGLES OF THE CASCADED MULTILEVEL VOLTAGE SOURCE INVERTER SUBJECTED TO A NEW PULSE WIDTH MODULATION SCHEME

(Date received: 5.10.2007)

Zainal Salam[1] and Junaidi Aziz[2]
[1]Falcuty of Electrical Engineering, Universiti Teknologi Malaysia,
81310 UTM, Skudai, Johor Darul Takzim
[2]The University of Nottingham,
United Kingdom,
Email: [1]zainals@fke.utm.my

ABSTRACT

A new modulation scheme for a five-level cascaded multilevel inverter is proposed. Unlike other schemes, the proposed method is based on the symmetric regular sampling unipolar PWM with a single carrier and multiple modulating signals. The paper will detail the method to obtain the switching angles of this PWM scheme. This algorithm is implemented using a low-cost fixed-point microcontroller on an experimental five-level cascaded inverter test rig. The results from the test rig are compared with MATLAB simulation for verification.

Keywords: *Harmonics, MATLAB, Multilevel Inverter, PWM*

1.0 INTRODUCTION

Recently there is a surge in interest in the research related to multilevel inverters. The main impetus for this is the fact that electrical equipment and machineries have begun to demand for power converters in the range of several Megawatts to be connected to a medium voltage network (2.3-6.9*kV*) [1]. Typical applications are electric train locomotives, heavy-duty ac drives, conveyer belts, and unified power-flow controllers. However, power (semiconductor) switches with the suitable switching frequency at ratings above 5*kV* are rare. Furthermore the ones that are available are prohibitively expensive to develop large power conversion systems for the above-mentioned applications. It is therefore uneconomical to achieve the required inverter output voltage using the existing power switches.

One approach to solve this problem is to utilise the multilevel voltage source inverter (MVSI) structure. Multilevel inverter is an array of power semiconductor switches and capacitor voltage sources, which is switched in a manner that an output voltage of stepped waveform is generated. For the normal two-level voltage source inverter, the maximum voltage output level is determined by the voltage blocking capability of each power switch. In contrast, for MVSI, the stress on each switch can be reduced in proportional to the number of output voltage levels. Thus with MVSI, higher input DC link voltage can be utilised using lower rated power switches. For example in high speed train locomotives which has DC link voltage of typically 2.5-3.5*kV*, standard IGBT switches rated at 1.8-2.4*kV* could be used in the five-level MVSI arrangement. In comparison, the 4.5*kV* and above IGCT used in single level inverter would be a much more expensive proposition.

Besides this important point, there are other advantages of the MVSI. It is possible to remove the expensive and bulky step-up transformer for applications that does not require galvanic isolation such as adjustable speed drives. Furthermore MVSI is known to improve harmonics performance, resulting in reduced switching losses. This is particularly crucial for high power application as increased power losses can complicate thermal management system design. With several levels in output waveform constructed using MVSI, the *dV/dt* on each power switch is reduced and so thus the EMI problem.

The development of MVSI began in the early 1980's when Nabae *et. al*. [2] proposed the neutral-point clamped (NPC) pulse width modulation (PWM) inverter. Since then several multilevel topologies have evolved; most common are the NPC or Diode-Clamped Multilevel Inverter [2-4], Flying-Capacitor Multilevel Inverter [5] and Modular Structured Multilevel Inverter [6]. In addition there are emerging multilevel topologies such as the asymmetric hybrid cells [7] and soft-switching multilevel inverters [8]. To aid the reader in understanding some of the basic concepts of MVSI, a brief description of the three main MVSI topologies and the common modulation Pulse Width Modulation (PWM) techniques is given in the following paragraphs.

1.1 Diode-Clamped Multilevel Inverter (DCMI)

The DCMI uses capacitors in series to divide up the dc bus voltage into a set of voltage levels. An example of a single-phase four-level DCMI and its output voltage waveform is shown in Figure 1. To produce N-levels of the phase voltage, the DCMI requires *N*-1 capacitors on the dc bus. Thus for a four-level inverter, the dc bus consists of three capacitors C_1, C_2 and C_3.

For a dc bus voltage of *Vdc*, the voltage across each capacitor is *Vdc*/3. Consequently the voltage stress for each power device is limited to *Vdc*/3, through the clamping diodes.

Although each power switch only required to block a voltage level of *Vdc*/3, each clamping diodes need to have different voltage ratings for reverse voltage blocking. Assuming that each blocking diode voltage rating is the same as the power switches, the relationship between the diodes and the output voltage levels is expressed as (*N*-1)×(*N*-2)]. This represents a quadratic increase with respect to *N*, and for high level inverters, the system impractical to implement. Furthermore, the voltage unbalance problem across the capacitor make this topology is unattractive to handle real power flow control.

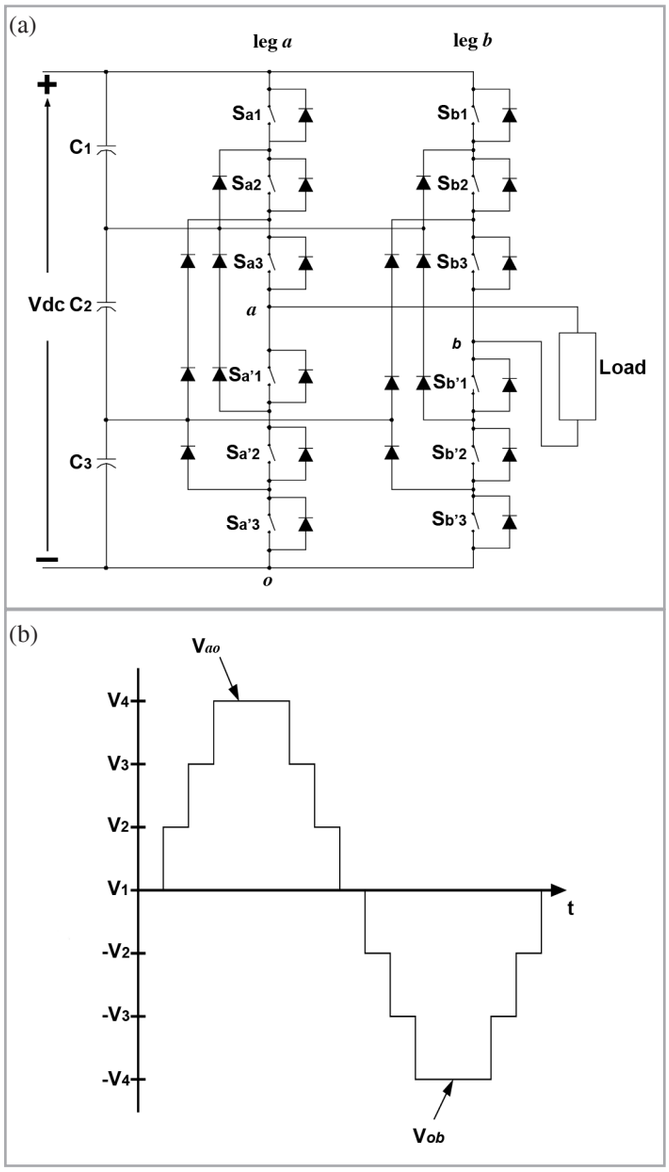

Figure 1(a): A single-phase four-level DCMI (b): Output voltage waveform

1.2 Flying-Capacitor Multilevel Inverter (FCMI)

Figure 2 illustrates the fundamental building block of a single-phase four-level FCMI. The voltage level defined is similar to that of the DCMI. To generate *N*-level staircase output voltage, *N*-1 capacitors on the dc bus are needed. It is obvious that two inner-loop balancing capacitors for phase leg *a*, C_{a1} and C_{a2} are independent from those for phase leg *b*. Both phase leg share the same dc link capacitors, C_1, C_2 and C_3.

The advantage of this topology is that it eliminates the clamping diode problems present in the DCMI. In addition, the large amount of capacitance provide extra ride through capabilities during power outage. Similar to DCMI, the harmonic content is proportional with the level of the inverter, thus it's possible to avoid the output filters. Furthermore, this topology naturally limits the *dV/dt* stress across the devices and introduces additional switching states that can be used to maintain the charge balance in the capacitors. However, FCMI has several technical difficulties that complicate its practical application for-high power converters. To maintain the charge balance in the capacitors, the dc-link capacitors need a controller, thus adding complexity to the control of the overall circuit. Furthermore, an excessive number of storage capacitors are required when the number of inverter level is high. Therefore it is more difficult to package the bulky capacitors.

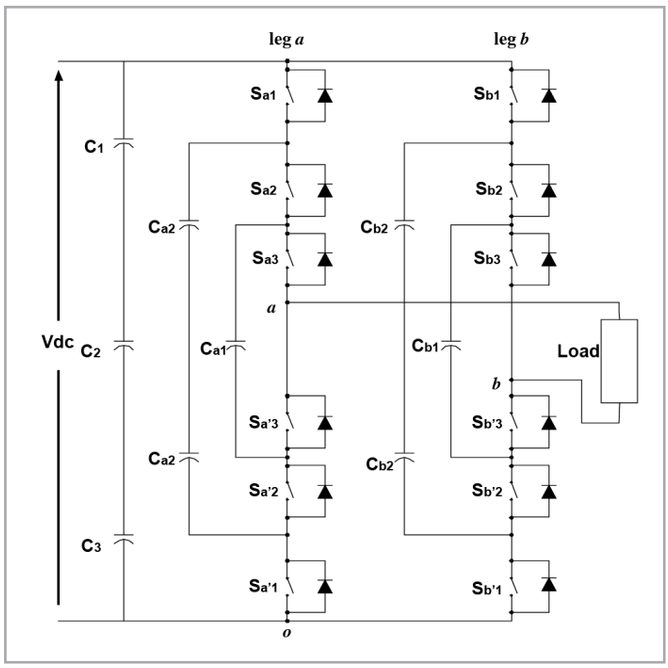

Figure 2: Circuit of a single-phase four-level FCMI

1.3 Cascaded Multilevel Inverters (CMI)

The CMI, shown in Figure 3, utilises separate dc sources to construct the multilevel phase voltage by means of H-bridges inverter modules. Due to its modular structure, it is also known as the Modular Structured Multilevel Inverters. CMI inherits several advantages over other multilevel topologies in terms of circuit modularity, protection and packaging. In addition the cascaded structure requires the least number of components among all multilevel topologies to achieve the same output voltage levels. Furthermore it does not suffer the voltage-balancing problem as experienced by the DCMI. The CMI inverter is well suited for renewable energy applications because naturally, renewable energy sources provide separate dc sources. This topology will be discussed in more details in the following sections.

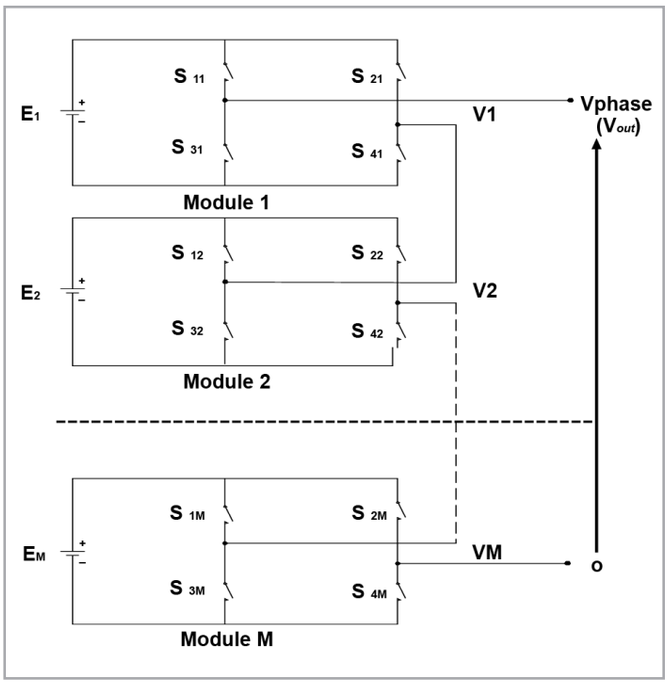

Figure 3: Structure of a CMI

1.4 MVSI Modulation Techniques

In general, the modulation control of MVSI is more complicated than the two-level VSI due to the need to cater for the transitions between the voltage levels (or steps). This was demonstrated by previous works, for example [5, 9-12]. Efforts from these researchers have established the sinusoidal natural sampling PWM (SPWM) as the most popular modulation method. Other modulation methods such as the space vector PWM modulation (SVPWM) [13] and harmonics elimination PWM (HEPWM) [14] has also been applied to multilevel topologies for specific applications.

The SPWM for MVSI is based on the intersection of a single sinusoidal reference with *N*-1 triangular carrier signals. The resulting intersection points become the switching instants of the PWM pulses. As far as the carrier signals alignment is concerned, three carrier phase shifting (or commonly known as the disposition method) schemes are suggested:

- *Alternative phase opposition disposition* (APOD) where the carrier signals above the zero line of sinusoidal modulating waveform are 180 out of phase with those below the zero line,
- *Phase disposition* (POD), where each carrier signal is phase shifted by 180 from its adjacent carriers, and
- *Phase disposition* (PD) where all the carrier signals are in phase.

Figures 4 (a) through (c) shows these disposition techniques. Each of these variations has particular harmonic benefits, which have been argued extensively in [11].

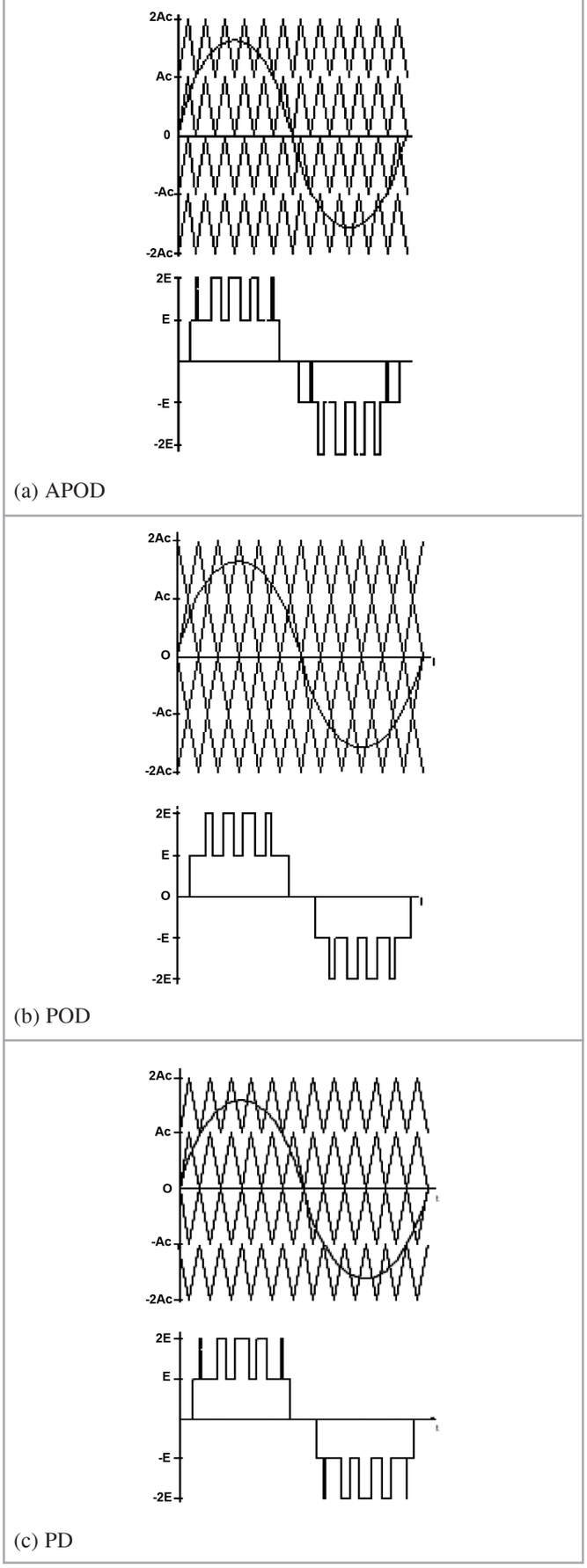

Figure 4: Phase disposition of the five-level MVSI

While the literature on the modulation techniques for MVSI can be considered extensive, there seems to be inadequate description on how such scheme can be implemented effectively on a digital system. For the multi carrier schemes described in [16], digital implementation results in an inherent "jump" in more than one level of the output voltage during level transitions. The level jumps seriously distort the output voltage waveform, thus degrading its harmonics spectra. The same authors proposed software solutions to check and then to avoid these undesired conditions. However the correction scheme is rather complicated and its practical implementation can be quite cumbersome.

This work attempts to propose an alternative switching scheme for the CMI that utilizes the symmetric regular sampling unipolar PWM. Unlike other schemes, the method is based on the intersection of a single carrier waveform with multiple modulating signals. It was discovered that by using this technique, switching transitions can be programmed effectively using a simple fixed-point microprocessor. It was also observed that the level jumping problem vanished. The paper begins by outlining the principle of the modulation and the derivation trigonometric equations that define the switching instant. The algorithm is then implemented using a fixed point 16-bit microcontroller and tested on a five-level CMI prototype. Typical results were compared with MATLAB simulation to verify the correctness of the proposed scheme

2.0 THE PROPOSED MODULATION SCHEME

2.1 Modulation Principle

The proposed scheme is implemented on a CMI. For convenience, an *N*-level, single-phase CMI is redrawn as Figure 5. The *ac* output voltage of each module is connected in series to form an output voltage, *Vout*. The number of H-bridge module (M), depends on the number of levels (N) required and can be written as:

$$M = \frac{N-1}{2} \tag{1}$$

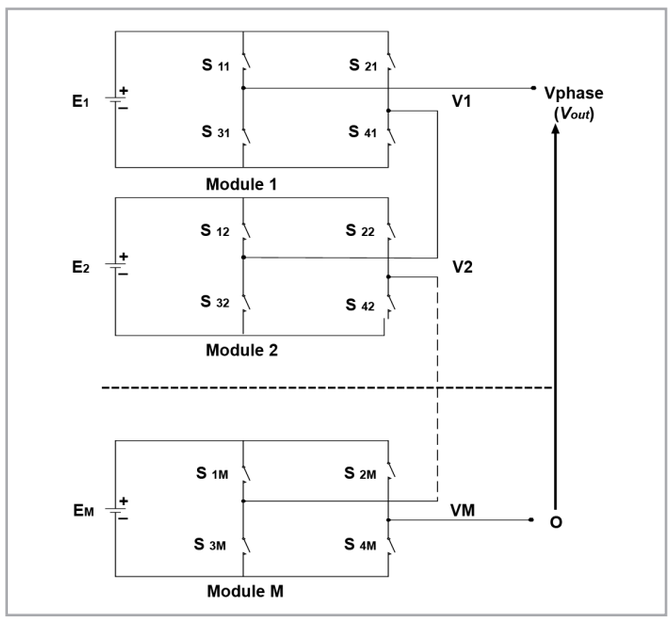

Figure 5: CMI structure

It is usually assumed that *N* is odd, as this would give an integer-valued *M*. By different combinations of the four switches, S_{1M} through S_{4M}, each module can generate three different voltage outputs, *i.e.* +E, –E, and 0. The total output voltage is then constructed by the sum of the output voltage from each module. For example, a five level inverter would have an output levels of +2E, +E, 0, –E, and –2E.

The proposed modulation scheme is based on the classical unipolar, symmetric PWM switching technique. The method compares several modified sinusoidal modulation signals *su*(*k*) with a single triangular carrier signal *c*(*k*) as shown in Figure 5. Each of these modified modulation signals have the same frequency (f_o) and amplitude (A_m). The carrier signal is a train of triangular waveform with frequency f_c and amplitude A_c. Equations (2) and (3) define the modulation index and ratio for *N*-level inverter with M number of modules:

$$m_i = \frac{A_m}{A_c} \cdot \frac{1}{\frac{(N-1)}{2}} = \frac{A_m}{MA_c} \tag{2}$$

$$m_f = f_c / f_o \tag{3}$$

The variable *k* represents a position of each modulated width pulses, initiated from $k = 1, 2, 3 \ldots m_f/2$. Intersection between the modified modulation signals and the carrier signal defines the switching instant of the PWM pulses.

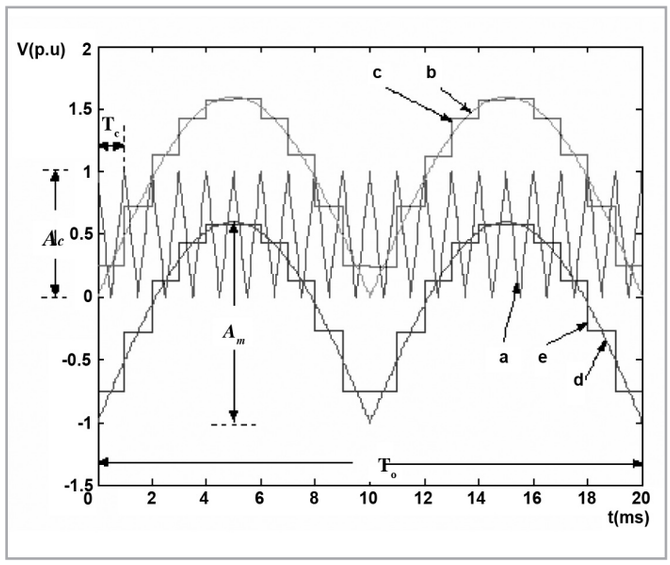

Figure 6: The modified sinusoidal modulation signals with a single carrier signal. Waveform labels: (a) Carrier signal c(k), (b) Absolute sinusoidal modulation signal $m_1(t)$, (c) Modified sinusoidal modulation signal $s_1(k)$ of $m_1(t)$, (d) Shifted absolute sinusoidal modulation signal $m_2(t)$, (e) Modified sinusoidal modulation signal $s_2(k)$ of $m_2(t)$

To illustrate the principle of the proposed scheme, a five-level inverter at $m_i = 0.4$ and $mi = 0.8$ for E = 100V is shown in Figures 6 and 7, respectively. For clarity, a low value of m_f, *i.e.* 20 is arbitrary chosen. For a five level output, two modulation signals namely $s_1(k)$ and $s_2(k)$ and single triangular carrier $c(k)$ are involved in the modulation process. Signal $s_2(k)$ is actually $s_1(k)$ that shifted down by the amplitude of triangular carrier signals A_c. In general signal $s_u + 1(k)$ is shifted down by A_c from

$s_u(k)$. The PWM pulses $V_1(k)$ is generated from the comparison between $s_1(k)$ and $c(k)$, while $V_2(k)$ is from comparison between $s_2(k)$ and $c(k)$. The comparison is designed such that if $s_1(k)$ is greater than $c(k)$, a pulse-width $V_1(k)$ is generated; if $s_2(k)$ is greater than $c(k)$, $V_2(k)$ is generated. On the other hand if there is no intersection, then $V_1(k)$ and $V_2(k)$ remain at 0. It can be seen in Figure 7 that for the case of $m_i \leq 0.5$, only $s_1(k)$ and carrier signal $c(k)$ is involved in the modulation process. There is no intersection for $s_2(k)$. Therefore, the output pulse $V_2(k)$ is zero. The output voltage V_{out}, which is the sum of $V_1(k)$ and $V_2(k)$, is then similar to the conventional three-level unipolar PWM case. For m_i>0.5, as depicted in Figure 8, both modulating signal, *i.e.* $s_1(k)$ and $s_2(k)$ intersect the carrier and therefore V_1 and V_2 pulses are generated. As a result, a multilevel output voltage V_{out} is formed.

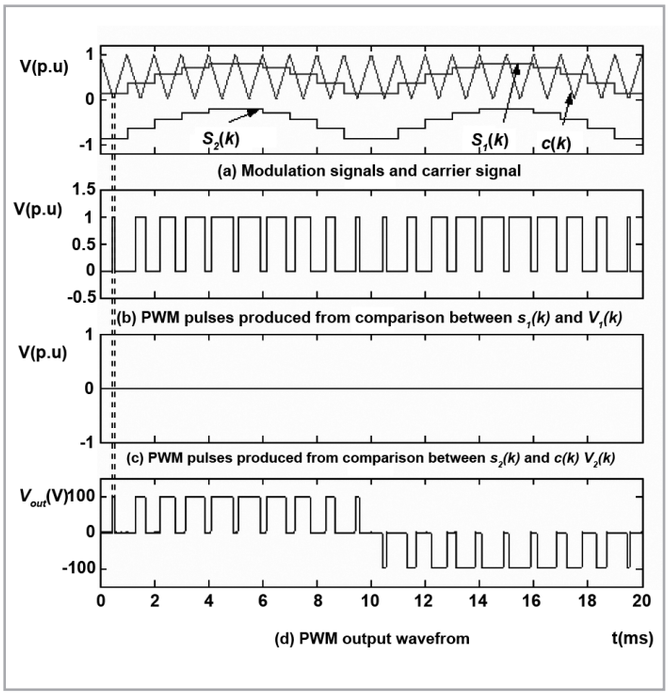

Figure 7: Proposed modulation scheme for m_i = 0.4, m_f = 20. Traces: (a) Modulation signals and carrier signal (b) PWM pulses produced from comparison between $s_1(k)$ and c(k), $V_1(k)$; (c) PWM pulses produced from comparison between $s_2(k)$ and c(k), $V_2(k)$; (d) PWM output waveform

For a *N*-level inverter there are *M* modulating waveform, which corresponds to *M* number of *H*-bridge modules. The nth level transitions occur at:

$$m_i = \frac{n}{m}\ ;\ n = 1...M\text{ -}1 \qquad (4)$$

For example for a 9 level inverter, *N*=9; therefore *M*=4. The transition occurs when the modulation index m_i reaches 0.25, 0.5 and 0.75. Note that the definition of modulation index used in this discussion is given by Equation (2).

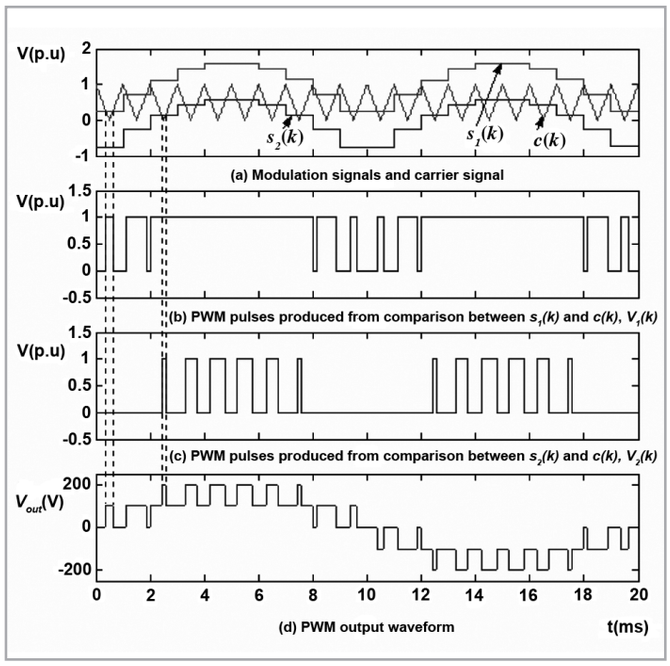

Figure 8: Proposed modulation scheme for m_i = 0.8, m_f = 20. Traces: (a) Modulation signals and carrier signal; (b) PWM pulses produced from comparison between $s_1(k)$ and c(k), $V_1(k)$; (c) PWM pulses produced from comparison between $s_2(k)$ and c(k), $V_2(k)$; (d) PWM output waveform

2.2 Derivation of the Switching Angle Equations

It can be seen that the kth rising edge is defined as the intersection of the negative slope carrier $c^-(k)$ and two set of modulating signals $s_1(k)$ and $s_2(k)$. Since the waveform is symmetrical, the intersection of the positive slope carrier $c^+(k)$ and the modulating signals is not required. It can be deduced from the rising edge equations, *i.e.* the intersection between $c^-(k)$ and $s_1(k)$ or $s_2(k)$ as shown in Figure 8.

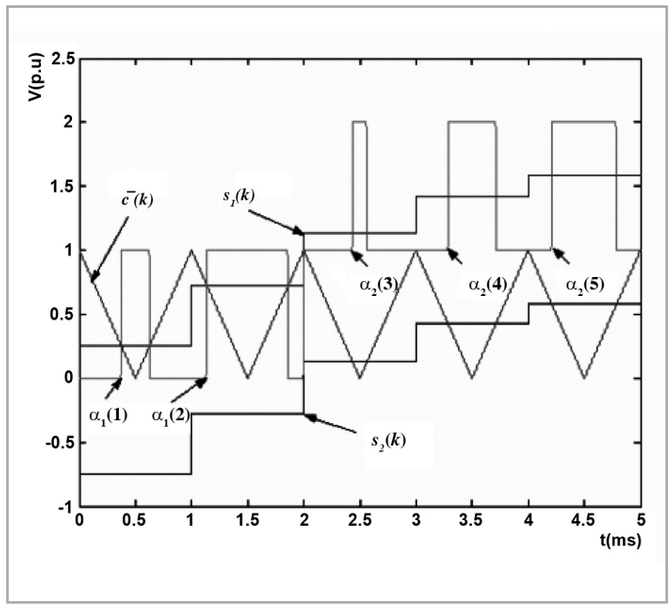

Figure 9: Intersection between single carrier and modified sinusoidal modulation signals

The straight-line equation for the carrier wave is denoted by $c^{-}(k)$ for the negative slope. It can be expressed as:

$$c^{-}(k) = \left(\frac{-A_c}{\frac{T_c}{2}}\right)\alpha_k + hA_c;\ k = 1, 2, 3....;\ h = 1, 3, 5....$$

$$f_c = \frac{1}{T_c} \tag{5}$$

Where f_c is a carrier frequency and f_o is a modulating signal frequency. The symmetric regular sampled modulation signals $s_1(k)$ and $s_2(k)$ can be expressed as:

$$s_1(k) = A_m \sin\left[\omega(i) + \frac{\pi}{m_f}\right] \text{and } s_2(k) =$$

$$A_m \sin\left[\omega(i) + \frac{\pi}{m_f}\right] - A_c \tag{6}$$

Where $i = 0, 1, 2... \frac{m_f}{2} - 1$ when $s_1(k)$ and $s_2(k)$ intersects with $c^{-}(k)$. The angular frequency, in (6) is represented by $2\pi/m_f$. Using the arithmetic regression and the kth raising edge (α_1, (k)) of PWM signal $V_1(k)$ is produced by the intersection between $s_1(k)$ and $c^{-}(k)$, *i.e.*:

$$\left(\frac{-A_c}{\frac{T_c}{2}}\right)\alpha_1(k) + hA_c = A_m \sin\left[\omega(i) + \frac{\pi}{m_f}\right];$$

$$h = 2k - 1 \text{ and } i = k - 1 \tag{7}$$

Solving, this rising edge k^{th} transition point $\alpha_1(k)$ is represented by:

$$\alpha_1(k) = \frac{T_c}{2}\left[(2k-1) - \frac{A_m}{A_c}\sin\left[\omega(k-1) + \frac{\pi}{m_f}\right]\right] \tag{8}$$

Using the same method, *i.e.* the intersection between $s_2(k)$ with $c^{-}(k)$, every rising edge of PWM signal $V_2(k)$ can be expressed as:

$$\alpha_2(k) = \frac{T_c}{2}\left[2k - \frac{A_m}{A_c}\sin\left[\omega(k-1) + \frac{\pi}{m_f}\right]\right] \tag{9}$$

Equations (8) and (9) can be generalised to produce a general switching angle for an N-level inverter:

$$\alpha_u(k) = \frac{T_c}{2}\left[(2k + u - 2) - \frac{A_m}{A_c}\sin\left[\omega(k-1) + \frac{\pi}{m_f}\right]\right] \tag{10}$$

Where $u = 1, 2...$ M and M = $\frac{N-1}{2}$. Equation (10) can be used to generate the kth PWM pulses for a cascaded inverter of any level N. Note that the variable u corresponds to the particular H-bridge module that the switching will be subjected on. It follows that α_u is the switching angle for the kth pulse of a particular bridge module. It can also be noted that this equation (10) is non-transcendental. All the variables at the right hand side of this equation are known and therefore the switching angles can be calculated directly. Its practical implementation using digital technique is therefore quite straightforward.

3.0 HARDWARE IMPLEMENTATION

3.1 Generation of PWM Waveform

A five-level 250 *Watts* experimental rig is built to prove the effectiveness of the proposed modulation technique. The inverter input voltages are fixed at 100*V* dc for each H-bridge module with pure resistive load. The PWM signal generation is performed by the SIEMENS SAB-C167CR-LM fixed-point microcontroller. Integrated on-chip peripherals such as Serial Port, bi-directional Parallel Port, Timers, PWM module and Peripheral Interfaces

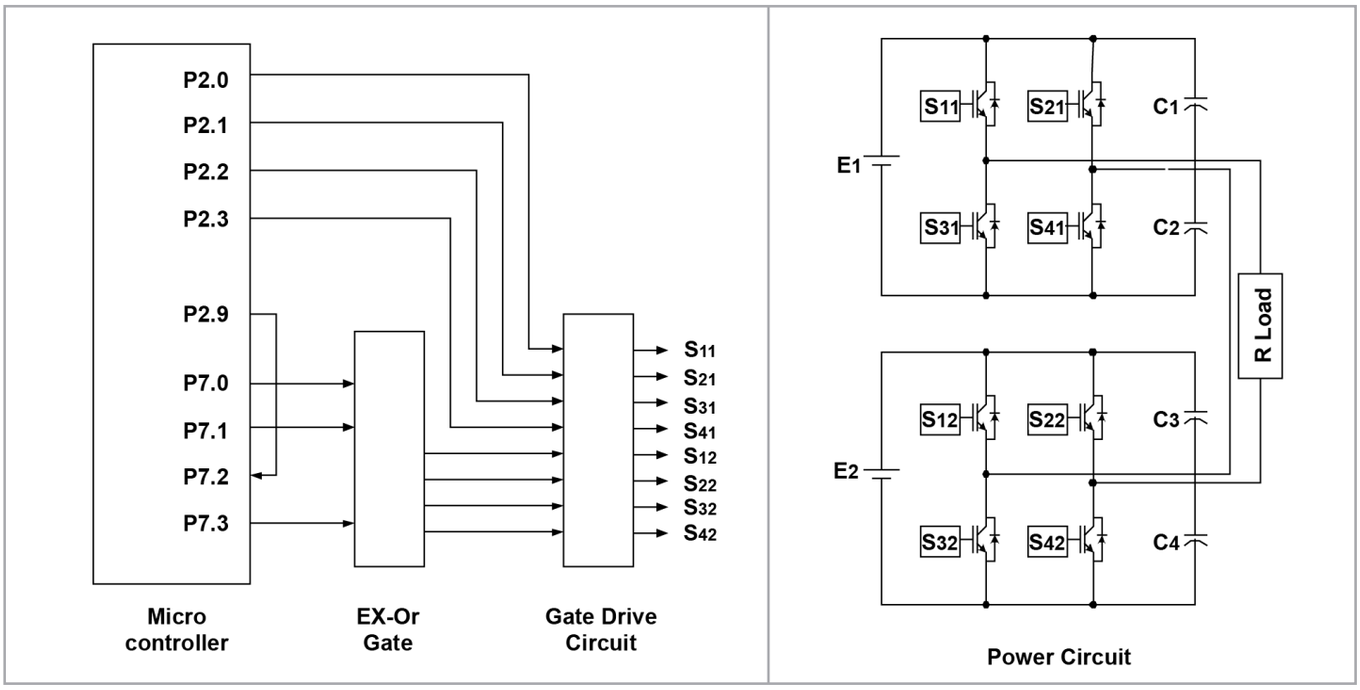

Figure 15: Functional block diagram of the inverter system

units make the interfacing task much easier and with higher reliability. To obtain a five-level output voltage as described in the simulation section, three signals need to be generated, namely the fundamental frequency square wave, the PWM signal $V_1(k)$ and the PWM signal $V_2(k)$. These signals are generated using on chip PWM module. The PWM module eliminates the requirement for complicated external timers. It allows the generation of up to four independent PWM signals. The standard PWM is selected to generate fundamental frequency square wave, meanwhile the symmetrical PWM is dedicated to generate V_a and V_b.

3.2 Overall Functional Block Diagram

The functional block diagram of the microcontroller ports, its associated logic gates, IGBT gate driver and power circuit are shown in Figure 15. The PWM signals ($V_1(k)$ and $V_2(k)$) and 50Hz square wave are generated by the PWM module and latched out via C167 microcontroller parallel ports P7.0, P7.1 and P7.3, respectively. The fast external interrupt signal for P7.2, which operates as input trigger for P7.1 is activated via port P.2.9. The enable signals for IGBT gate drive are also supplied by microcontroller via ports P2.0 through P2.3.

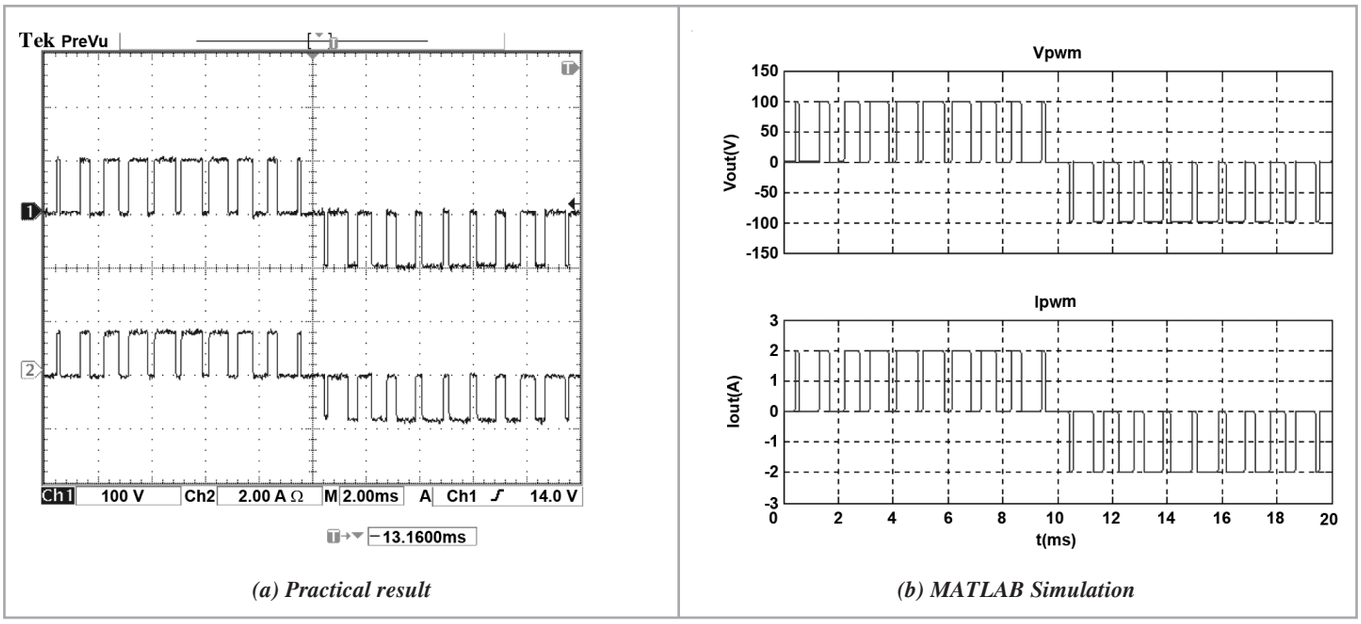

(a) Practical result *(b) MATLAB Simulation*

Figure 16: Output waveforms for m_i = 0.4; m_f = 20.
Top trace: Output voltage. Vertical scale 100V/div. Bottom trace: Output current.
Vertical scale 2A/div. Horizontal scale 2ms/div.

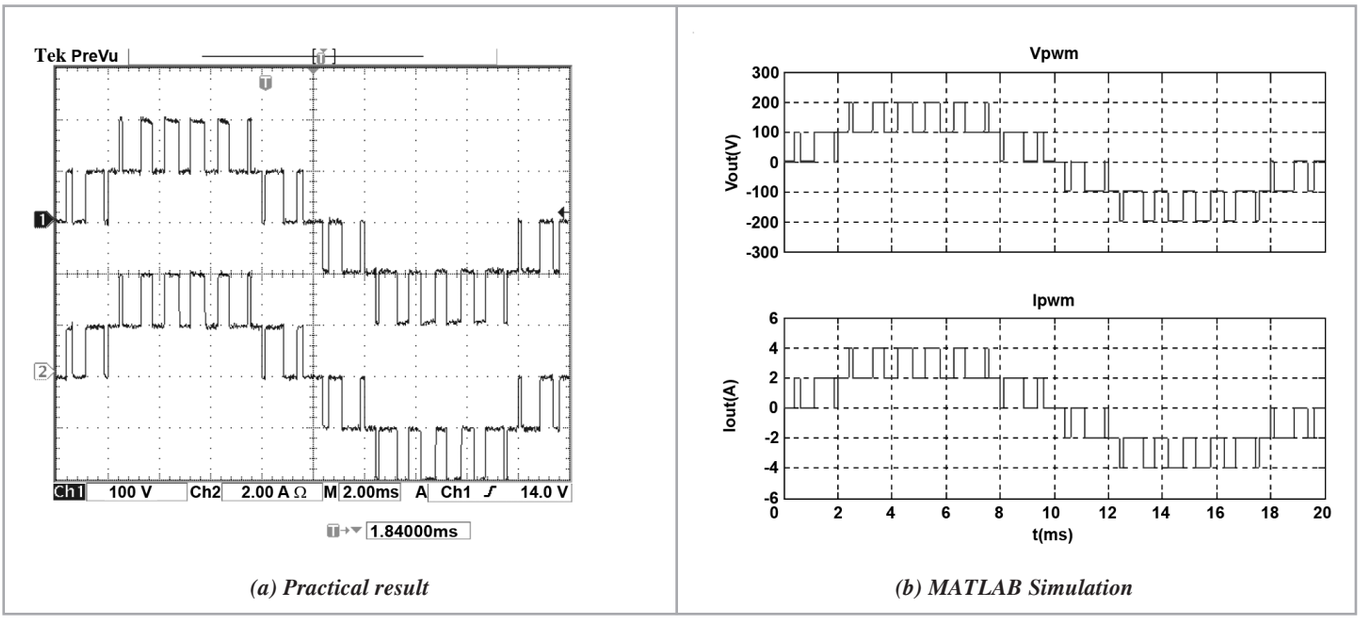

(a) Practical result *(b) MATLAB Simulation*

Figure 17: Output waveform for m_i = 0.8; m_f = 20
Top trace: Output voltage. Vertical scale 100V/div. Bottom trace: Output current.
Vertical scale: 2A/div.Horizontal scale 2ms/div.

As illustrated in Figure 15, two modules of cascaded power circuit are required for a five-level inverter. Both modules are connected in series and constructed from IGBT switches and *dc* link capacitors. Power switches used for the inverter are type IRG430CKD IGBTs, manufactured by International Rectifier.

3.3 Results

Figure 16 shows the oscillogram of the output voltage and current of the inverter for m_i = 0.4 and m_f = 20. For comparison, MATLAB simulation results are shown side-by side. As can be observed, the output voltage is similar to a three-level inverter, because m_i <0.5. For m_i = 0.8 and m_f = 20 shown in Figure 17, the five-level PWM waveform is obtained. Clearly the output voltage is consistent with the theoretical prediction.

For the case of m_f = 20 and m_i = 0.4, the output voltage harmonic spectrum are shown in Figure 18, while for the case of m_f = 20; m_i = 0.8 it is illustrated in Figure 19. As can be seen, the magnitude of the fundamental voltage for the latter case is doubled but the harmonics remain about the same. As a result, the ratio of its harmonics to a normalised fundamental is approximately half of the former.

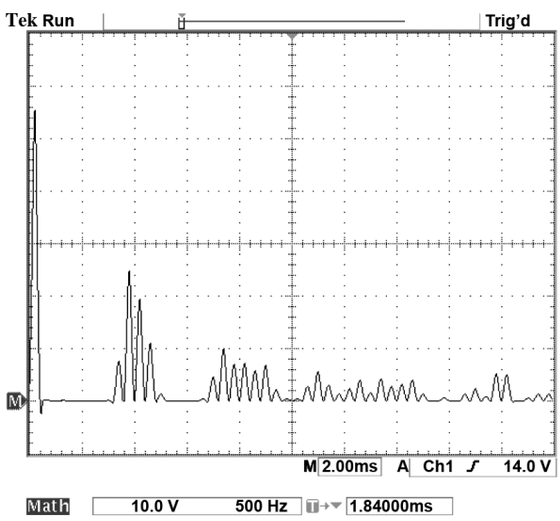

(a) Practical

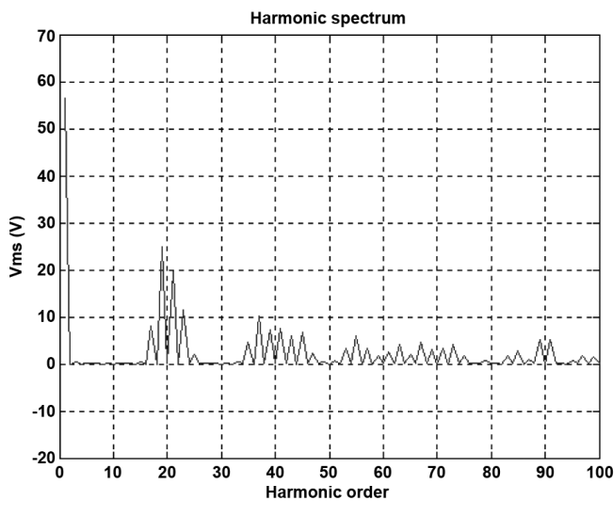

(b) MATLAB Simulation

Figure 18: Harmonics of output voltage for m_i = 0.4; m_f = 20. Vertical scale 10V/div.Horizontal scale 500Hz/div

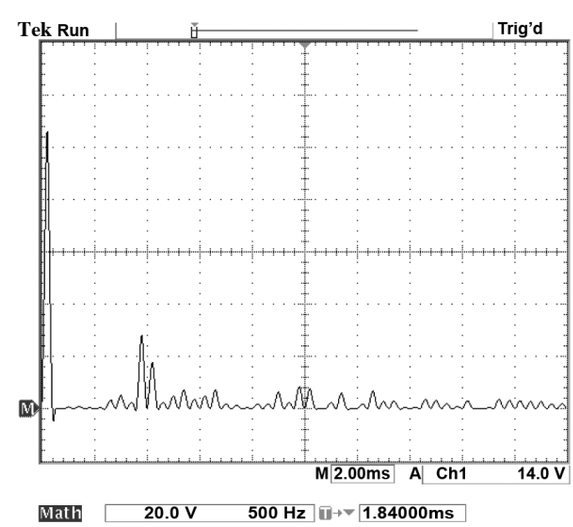

(a) Practical

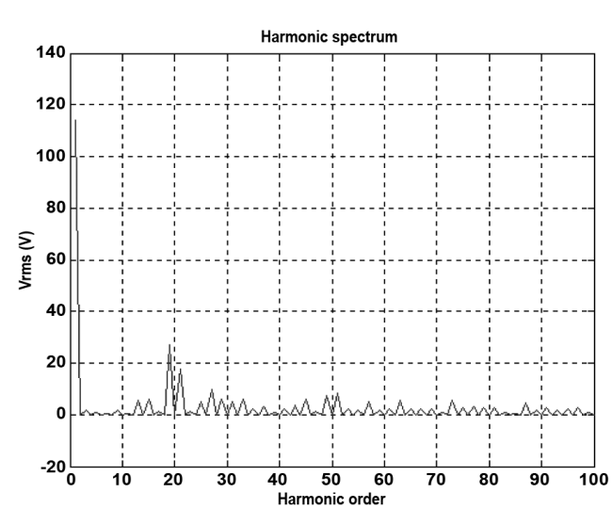

(b) MATLAB Simulation

Figure 19: Harmonics f output voltage for m_i = 0.8; m_f = 20. Horizontal scale 500Hz/div

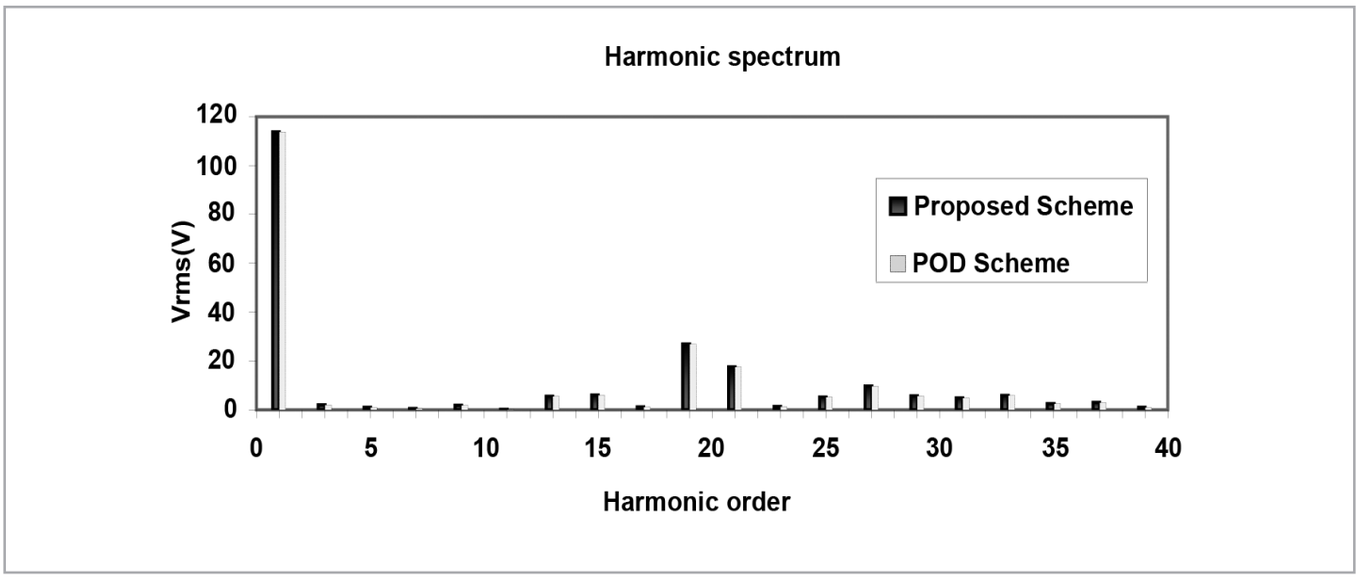

Figure 20: Comparison of harmonic spectrum between the proposed scheme and POD scheme

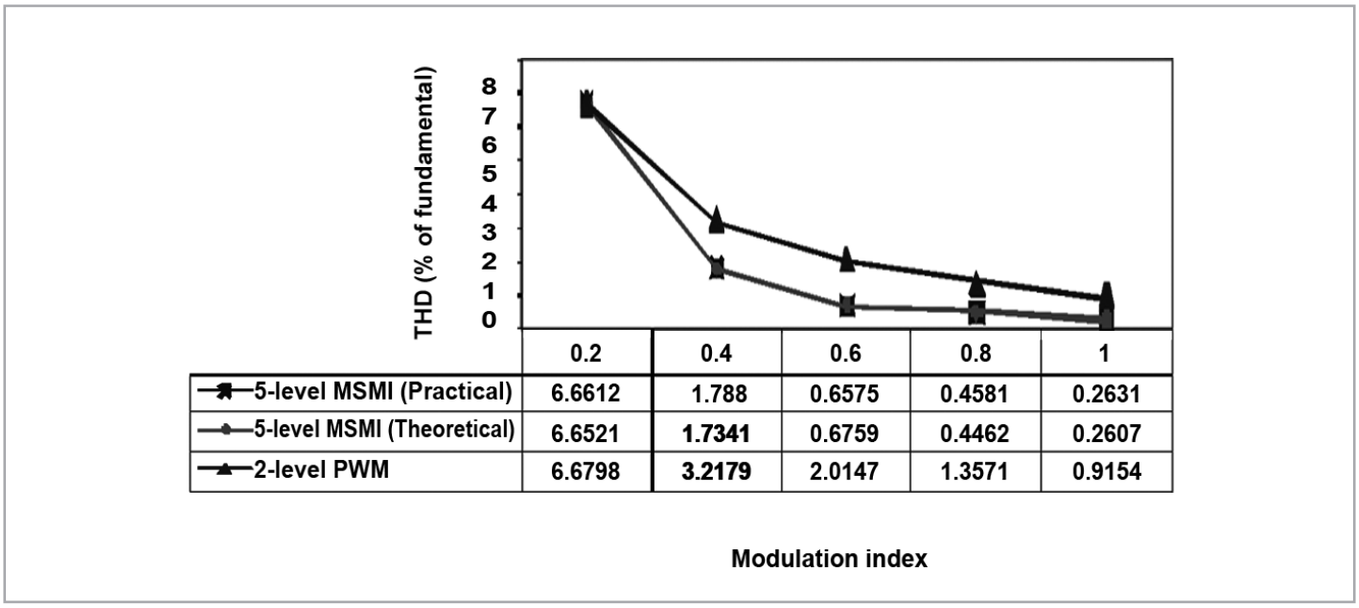

	0.2	0.4	0.6	0.8	1
5-level MSMI (Practical)	6.6612	1.788	0.6575	0.4581	0.2631
5-level MSMI (Theoretical)	6.6521	1.7341	0.6759	0.4462	0.2607
2-level PWM	6.6798	3.2179	2.0147	1.3571	0.9154

Figure 21: Variation of THD for five-level and two-level SPWM inverter configuration

Figure 20 shows the comparison the harmonic profile of the proposed modulation technique with the POD scheme (using symmetrical regular sampling PWM). It can be observed that the proposed technique produces identical spectra to the POD scheme for all major harmonics. It can be suggested that both strategies produce harmonic components of the same magnitude and frequencies despite the obvious difference between the two modulation principles.

Figure 21 shows the comparison of the voltage THD between a five-level single-phase CMI and a conventional two-level inverter configuration. The figure shows that for both cases, a poor THD are obtained when the inverter operated at low modulation index. This is to be expected because at $m_i \leq 0.5$, the cascaded inverter essentially behaves like a conventional three-level inverter. A better THD is obtained when the inverter operated at higher modulation index, particularly when mi > 0.5. For example, at modulation index equals 1.0, it was found that THD is three times superior compared to a conventional two-level inverter.

4.0 CONCLUSIONS

This paper presents a new switching scheme for the modular structured multilevel inverter. The proposed scheme is based on symmetric regular sampled unipolar PWM, with multiple modulating waveforms and a single carrier. Mathematical equations that define the PWM switching instants are derived. Due to the non-transcendental nature of the equation, digital implementation is possible. A low power inverter test rig is built and the PWM algorithm is programmed using a low-cost fixed-point microcontroller. Several tests to quantify the performance of the inverter with the proposed modulation scheme are carried out. The results were compared with MATLAB simulation and are found to be in very close agreement. ■

REFERENCE

[1] J.S. Lai, and F.Z. Feng, "Multilevel converters–A new breed of power converters", IEEE Transaction on Industrial Applications, Vol IA-32, May/June 1996, pp.509-517.

[2] A. Nabae, I. Takahashi, H. Akagi, "A neutral -point clamped PWM inverter." IEEE Transaction on Industrial Applications, vol. IA-17, Sep/Oct 1981, pp.518-523.

[3] T.A. Meynard, and H. Foch, "Multi-level Choppers for high voltage applications," European Power Electronics and Drives Journal, Vol. 2, No. 1, March. 1992, pp.41-48.

[4] C. Hochgraf, R. Lasseter, D. Divan, and T.A. Lipo, "Comparison of multilevel inverters for static var compensation," in Conf. Record of the IEEE-IAS Annual Meeting, IAS' 94, pp.921–928.

[5] P. Hammond, "A new approach to enhance power quality for medium voltage ac drives," IEEE Transaction on Industrial Applications, Vol IA-32, Vol. IA-33, Jan./Feb. 1997, pp. 202–208,

[6] E. Cengelci, S. U. Sulistijo, B. O. Woom, P. Enjeti, R. Teodorescu, and F. Blaabjerge, "A new medium voltage PWM inverter topology for adjustable speed drives," in Conf. Record of the IEEE-IAS Annual Meeting, IAS' 98, pp.1416–1423.

[7] M. D. Manjrekar, P. K. Steimer, and T. A. Lipo, "Hybrid multilevel power conversion system: a competitive solution for high-power applications," IEEE Transaction on Industrial Applications, Vol. IA-36, May/June 2000, pp.834–841.

[8] X. Yuan and I. Barbi, "Zero voltage switching for three level capacitor clamping inverter," IEEE Transaction on Power Electronics Vol. 14, July 1999, pp.771–781.

[9] L. Tolbert and T. G. Habetler, "Novel multilevel inverter carrier-based PWM method," IEEE Transaction on Industrial Applications, Vol. IA-35, Sept./Oct. 1999, pp.1098–1107.

[10] Y. Liang and C. O. Nwankpa, "A new type of STATCOM Based on cascading voltage-source inverters with phase-shifted unipolar SPWM," IEEE Transaction on Industrial Applications, Vol. IA-35, Sept/Oct. 1999, pp.1118–1123.

[11] B.P. McGrath and D.G. Holmes, "Multicarrier PWM Strategies for Multilevel Inverters." IEEE Transaction on Industrial Electronics, Volume 49, Issue 4, Aug. 2002, pp.858 – 867.

[12] B.P. McGrath and D.G. Holmes, "An Analytical Technique for the Determination of Spectral Components of Multilevel Carrier-Based PWM Methods." IEEE Transactions on Industrial Electronics, Vol. 49, Issue 4, Aug. 2002, pp.847 – 857

[13] N. Celanovic and D. Boroyevic, "A fast space vector modulation algorithm for multilevel three-phase converters," in Conf. Record of the IEEE-IAS Annual Meeting IAS'99, pp.1173–1177.

[14] L. Li, D. Czarkowski, Y. Liu, and P. Pillay, "Multilevel selective harmonic elimination PWM technique in series-connected voltage inverters," in Conf. Record of the IEEE-IAS Annual Meeting, IAS '98, pp.1454–1461.

[15] Carrara G. *et al*., "A New Multilevel PWM Method; A Theoretical Analysis", 21st Annual IEEE Power Electronics Specialist Conference, PESC '90 pp.363-371.

[16] A. Dell'Aquila *et al*. "Novel Multilevel PWM Inverter Implementation", 23rd International Conference on Industrial Electronics, Control and Instrumentation, IECON 97. Vol. 2, pp.710– 715.

PROFILES



DR ZAINAL SALAM

Zainal Salam has been a lecturer at UTM for 23 years and is currently the Professor in Power Electronics at the Faculty of Electrical Engineering, UTM. He has been working in several researches and consulting works with SIRIM and GBT on battery powered converters. Currently he is the Director of the Inverter Quality Control Center (IQCC) UTM which is responsible to test PV inverters that are to be connected to the local utility grid.

His research interests include all areas of power electronics, renewable energy, power electronics and machine control. Dr Zainal has written over 100 technical papers for various journals and conferences. He is currently working on high frequency inverters for PV applications.



JUNAIDI ABDUL AZIZ

Junaidi Abdul Aziz received the B.S and M Eng. degrees in electrical engineering from the Universiti Teknologi Malaysia in 2000 and 2002, respectively, and he received the Ph.D. degree in 2008 from the University of Nottingham. Since 2001, he has been with the Department of Energy Conversion at the Universiti Teknologi Malaysia, where he is presently a lecturer. His research interests include electric vehicle, ground power unit (GPU) and multilevel inverter.

HYBRID INPUT SHAPING AND PID CONTROL OF A FLEXIBLE ROBOT MANIPULATOR

(Date received: 5.10.2007)

M. A. Ahmad[1], Z. Mohamed[2] and Z.H. Ismail[2]
[1]Faculty of Electrical and Electronics Engineering,
Universiti Malaysia Pahang, Karung Berkunci 12,
25000, Kuantan Pahang, Malaysia.
[2]Faculty of Electrical Engineering, Universiti Teknologi Malaysia,
81310, Skudai, Johor Bahru, Malaysia.
Email: mashraf@ump.edu.my.com[1], zahar@fke.utm.my[2]

ABSTRACT

This paper presents experimental investigations into the development of hybrid input shaping and PID control for vibration suppression and input tracking of a flexible robot manipulator. Initially, a PID controller is developed for control of rigid-body motion of the system. This is then extended to incorporate a feedforward controller based on input shaping techniques for vibration control. Experimental results of the response of the manipulator with the controllers are presented in time and frequency domain. The effects of derivative order of the input shaper on the performance of the system are also investigated. The performances of the hybrid control schemes are assessed in terms of input tracking capability and level of vibration reduction in comparison to the PID control. Finally, a comparative assessment of the hybrid control schemes is presented.

Keywords: *Flexible Manipulator, Input Shaping, PID control, Vibration Control*

1.0 INTRODUCTION

Flexible robot manipulators exhibit many advantages over their rigid counterparts: they require less material, are lighter in weight, have higher manipulation speed, lower power consumption, require smaller actuators, are more manoeuvrable and transportable, are safer to operate due to reduced inertia, have less overall cost and higher payload to robot weight ratio. However, the control of flexible manipulators to maintain accurate positioning is challenging. Due to the flexible nature and distributed characteristics of the system, the dynamics are highly non-linear and complex. Problems arise due to precise positioning requirements, system flexibility leading to vibration, the difficulty in obtaining accurate model of the system and non-minimum phase characteristics of the system [1].

The control strategies for flexible manipulator systems can be classified as feedforward (open-loop) and feedback (closed-loop) control. Feedforward control techniques are mainly developed for vibration suppression and involve developing the control input through consideration of the physical and vibrational properties of the system, so that system vibrations at response modes are reduced. This method does not require any additional sensors or actuators and does not account for changes in the system once the input is developed. A number of techniques have been proposed as feedforward control schemes for control of vibration in flexible structures. These include utilisation of Fourier expansion [2], development of computed torque [3], utilisation of single and multiple-switch bang-bang control functions [4] and construction of input functions from ramped sinusoids or versine functions [5]. Moreover, command shaping techniques have also been investigated in reducing system vibration in flexible manipulators. These include filtering techniques based on low-pass, band-stop and notch filters [6,7] and input shaping [8,9]. Previous experimental studies on a single-link flexible manipulator have shown that input shaping gives higher level of vibration reduction and robustness than filtering techniques. However, the major drawback of feedforward control schemes is their limitation in coping with parameter changes and disturbances to the system [10]. Moreover, the technique requires relatively precise knowledge of the dynamics of the system.

Feedback control techniques use measurement and estimate of the system states for control of rigid body motion and vibration suppression. Feedback controllers can be designed to be robust to parameter uncertainty. In general, control of flexible manipulators can be made easier by locating every sensor exactly at the location of the actuator, as collocation of sensors and actuators guarantees stable servo control [11]. In the case of flexible manipulator systems, the end-point position is controlled by obtaining the parameters at the rotating and end-point of the manipulator and using the measurements as a basis for applying control torque at the rotating. Thus, the feedback control can be divided into collocated and non-collocated control. By applying control torque based on non-collocated sensors, the problem of non-minimum phase and of achieving stability is of concern. Several approaches utilising closed-loop control strategies have

been reported for control of flexible manipulators. These include linear state feedback control [12,13], adaptive control [14,15], robust control techniques based on H-infinity [16] and variable structure control [17] and intelligent control based on neural networks [18] and fuzzy logic control schemes [19].

This paper presents experimental investigations into the development of hybrid input shaping and PID control for vibration suppression and input tracking of a flexible robot manipulator. To demonstrate the effectiveness of the control schemes, initially a PID controller as a feedback control is developed for control of rotating angle motion of flexible manipulator system. This is then extended to incorporate a feedforward controller based on input shaping techniques for vibration suppression of the manipulator. The performances of the controllers are assessed in terms of the input tracking capability and vibration reduction as compared to the response with PID control. The effects of derivative order of the input shaper on the performance of the system are also investigated. Finally, a comparative assessment and further analysis of the control strategies is discussed.

2.0 FLEXIBLE MANIPULATOR SYSTEM

A description of the single-link flexible manipulator system considered in this work is shown in Figure 1, where $\{O\ X_o\ Y_o\}$ and $\{O\ X\ Y\}$ represent the stationary and moving coordinates frames respectively, s represents the applied torque at the hub. E, I, ρ, A, IH, r, and M_P represent the Young modulus, area moment of inertia, mass density per unit volume, cross-sectional area, hub inertia, radius and payload mass of the manipulator respectively. In this work, the motion of the manipulator is confined to the $\{O\ X_o\ Y_o\}$ plane. The rotation of $\{O\ X\ Y\}$ relative to frame $\{O\ X_o\ Y_o\}$ is described by the angle θ. The displacement of the link from the axis OX at a distance x is designated as $\upsilon(x, t)$. Since the manipulator is long and slender, transverse shear and rotary inertia effects are neglected [20]. This allows the use of the Bernoulli–Euler beam theory to model the elastic behavior of the manipulator. The manipulator is assumed to be stiff in vertical bending and torsion, allowing it to vibrate dominantly in the horizontal direction and thus, the gravity effects are neglected. Moreover, the manipulator is considered to have constant cross-section and uniform material properties throughout.

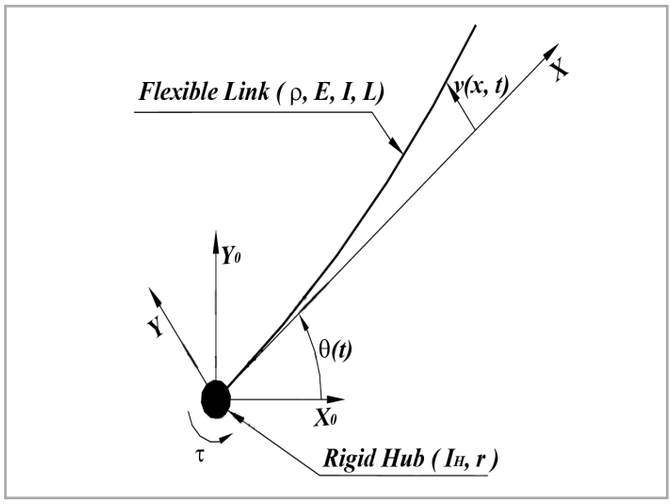

Figure 1: Mechanical model of the flexible manipulator

2.1 Lab-Scale Experimental of Flexible Manipulator

The experimental work for this research was carried out at the University of Technology Malaysia robotic laboratory. Figure 2 shows a single-link flexible manipulator system consists of a flexible aluminum beam and a KollMorgern Servo Disk DC motor JR12M4CH with a built-in optical encoder used to measure the load shaft angular position. The system parameters of flexible robot manipulator are described precisely in [21]. The encoder has the high resolution up to 3000 counts in quadrature and signal from encoder is sent directly to computer through data acquisition board PCL 818. The light-weight flexible beam is clamped to the shaft of the motor through a coupling and is confined to turn only in the horizontal plane, thus the gravity effect is neglected. The tip deflection of the link is computed by an accelerometer ADXL202JQC which is installed at the tip of the flexible link. This accelerometer is capable of tracing deflection within the amount of 0.2 angstroms or $1/10^{th}$ of an atomic diameter. The control voltage for driving the motor is sent to the servo amplifier through a similar PCL 818 board.

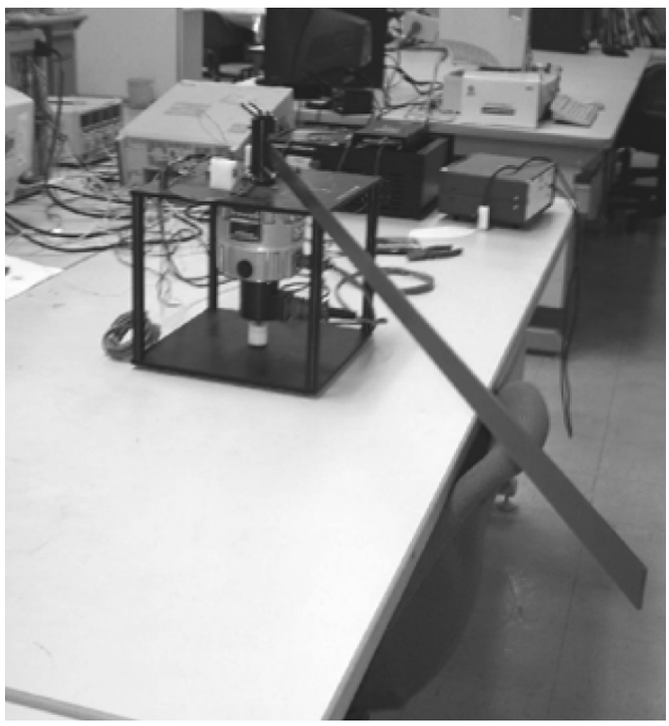

Figure 2: Actual flexible-link test bed in UTM

The setup of the control system is schematically shown in Figure 3. The control algorithms are coded in Matlab/Simulink, compiled with the Matlab/Real Time Windows Target. Real-Time Windows Target includes an analog input and analog output that provide connections between the physical I/O board (PCL 818) and the real-time model. Rotating-angle and acceleration measurements are fed back and use to derive the actuator command. From these two signals, a closed loop system with PID controller can be built to control the rotation of the flexible link.

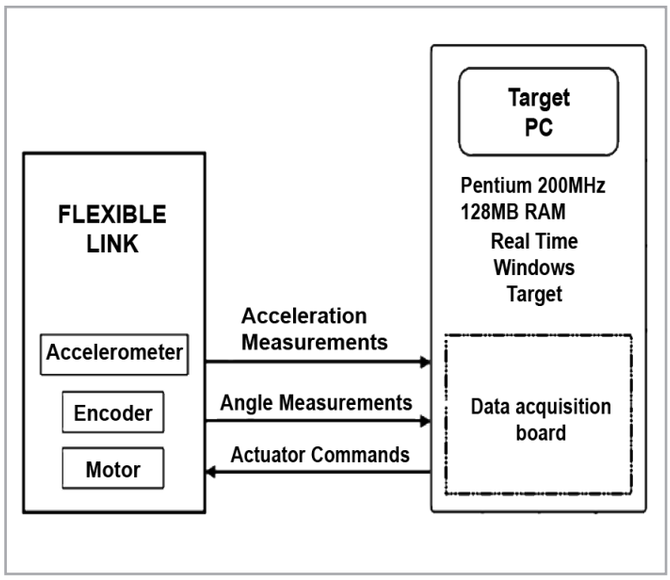

Figure 3: Flow diagram of the system

3.0 CONTROL SCHEMES

In this section, the proposed control schemes for rigid body-motion and vibration control of a flexible manipulator are designed. Initially, a PID control is developed. Then input shaping techniques are incorporated in the closed-loop system for control of vibration of the system.

3.1 PID controller

To demonstrate the performance of the hybrid control schemes, a PID control strategy is adopted for control of rigid-body motion of the manipulator. A block diagram of the PID controller is shown in Figure 4, where K_p, K_d and K_i are the proportional, derivative and integral gains respectively, θ represents rotating angle, r is the reference rotating angle. Essentially, the task of this controller is to position the flexible robot arm to the specified angle of demand. The rotating angle signal is fed back and used to control the rotating angle of the manipulator. The control signal $U(s)$ in Figure 4 can thus be obtained as

$$U(s) = \left(K_p + K_d s + \frac{K_i}{s}\right)[R(s) - \theta(s)] \tag{1}$$

where s is the Laplace variable. Hence the closed-loop transfer function is obtained as

$$\frac{\theta(s)}{R(s)} = \frac{\left(K_p + K_d s + \frac{K_i}{s}\right) G(s)}{1 + \left(K_p + K_d s + \frac{K_i}{s}\right) G(s)} \tag{2}$$

where $G(s)$ is the open-loop plant from the input torque to the rotating angle. In this study, the Ziegler-Nichols approach is utilized to tune the controller parameter of K_p, K_d and K_i.

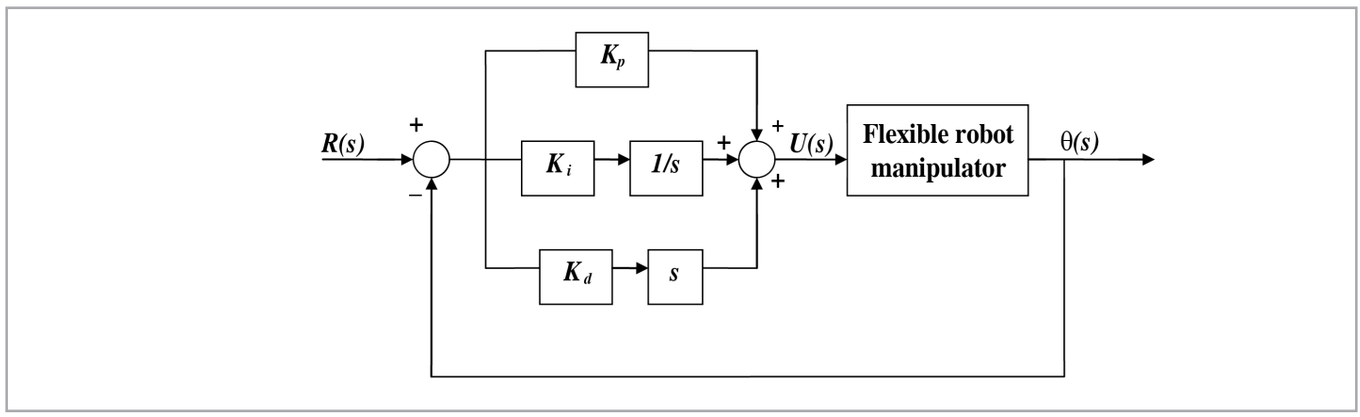

Figure 4: The PID control structure

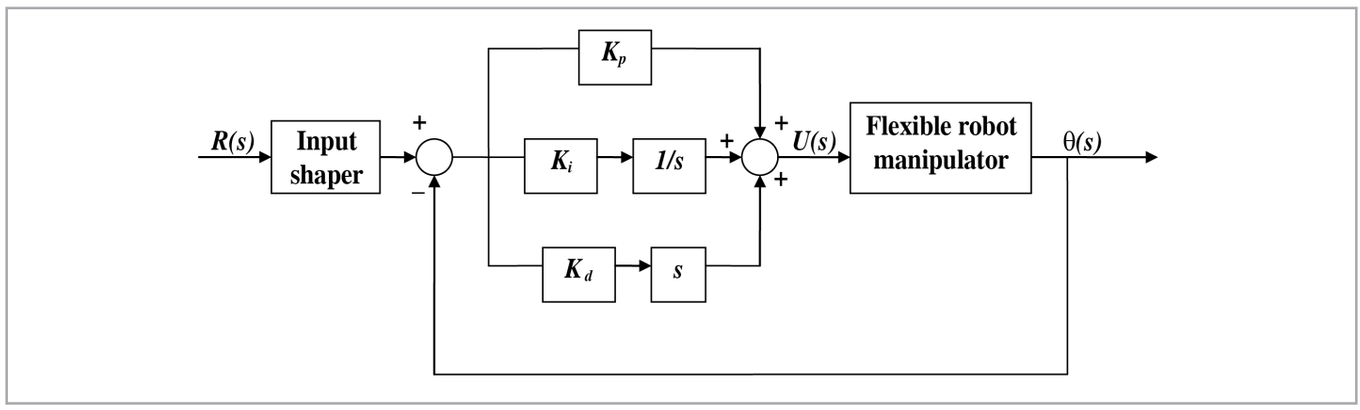

Figure 5: The PID and input shaper control structure

3.2 Hybrid PID and Input Shaping control

A hybrid control structure for control of rigid body motion and vibration suppression of the flexible manipulator based on a PID and input shaping control is proposed in this section. The input shaping techniques were designed on the basis of vibration frequencies and damping ratios of the flexible manipulator system. In this experiment, the first two natural frequencies are considered as these dominantly characterize the dynamic behavior of the single-link flexible manipulator system. The input shapers thus designed were used for pre-processing the reference input. The shaped inputs were then applied to the system in the closed-loop configuration with PID controller to reduce the vibrations of the manipulator. In this study, the input shaping control schemes is designed using a two-impulse sequence (ZV) and four-impulse sequence (ZVDD). A block diagram of the hybrid control schemes is shown in Figure 5.

The input shaping method involves convolving a desired command with a sequence of impulses known as input shaper. The design objectives are to determine the amplitude and time location of the impulses based on the natural frequencies and damping ratios of the system. The corresponding design relations for achieving a zero residual single mode vibration of a system and to ensure that the shaped command input produces the same rigid body motion as the unshaped command yields a two-impulse sequence with parameters as

$$t_1 = 0,\ t_2 = \frac{\pi}{\omega_d},$$

$$A_1 = \frac{1}{1+H},\ A_2 = \frac{H}{1+H}\ . \qquad (3)$$

where ω_n and ζ represent the natural frequency and damping ratio respectively, $H = e^{\frac{-\zeta\pi}{\sqrt{1-\zeta^2}}}$, $\omega_d = \omega_n\sqrt{1-\zeta^2}$, t_j and A_j are the time location and amplitude of impulse j respectively. The robustness of the input shaper to errors in natural frequencies of the system can be increased by solving the derivatives of the system vibration equation. This yields a four-impulse sequence with parameters as

$$t_1 = 0,\ t_2 = \frac{\pi}{\omega_d},\ t_3 = \frac{2\pi}{\omega_d},\ t_4 = \frac{3\pi}{\omega_d}$$

$$A_1 = \frac{1}{1+3H+3H^2+H^3},\ A_2 = \frac{3H}{1+3H+3H^2+H^3},$$

$$A_3 = \frac{3H^2}{1+3H+3H^2+H^3},\ A_4 = \frac{H^3}{1+3H+3H^2+H^3} \qquad (4)$$

where H is as in equation (3).

To handle higher vibration modes, an impulse sequence for each vibration mode can be designed independently. Then the impulse sequences can be convoluted together to form a sequence of impulses that attenuate vibration at higher modes. In this manner, the vibration reduction can be accomplished by convolving a desired input reference with the input shaper. This yields a shaped input that drives the system to a desired location with reduced vibration.

4.0 EXPERIMENTAL RESULTS

This section presents experimental results of the applications of hybrid control schemes on the flexible robot manipulator. The corresponding results are presented in time and frequency domain. The manipulator is required to follow a unit step trajectory of 45 degree as shown in Figure 6. System responses, namely the rotating angle, end-point acceleration and power spectral density, are observed. To investigate the vibration of the system in the frequency domain, power spectral density (PSD) of the response at the end-point is obtained. The performances of the hybrid controllers are assessed in terms of input tracking and vibration suppression in comparison to the PID control.

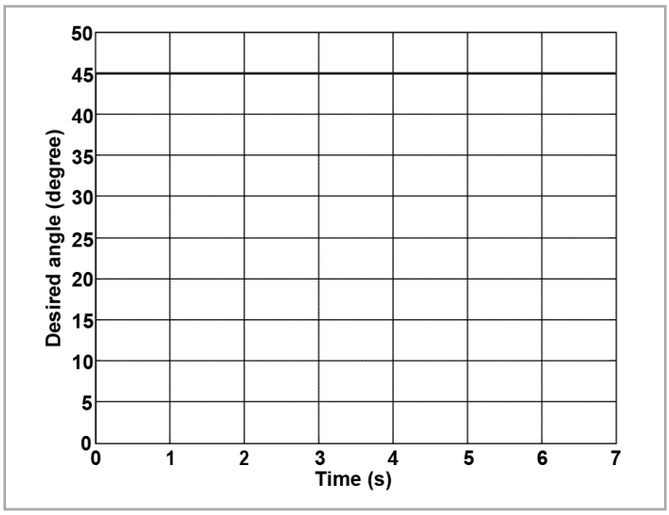

Figure 6: The reference rotation angle

4.1 PID controller

In this experiment, the unshaped reference input of the motor is a 45 degree step command. The feedback parameters of the PID controller are chosen experimentally to realize a good-compromise rotating-angle response in terms of overshoot and settling time. The sampling frequency is set to 1 ms. Utilizing the Ziegler Nichols method with several adjustments, the final gains are chosen as

$K_p = 0.0145$, $K_i = 0.0015$ and $K_d = 0.0155$.

Figure 7 shows the response of the system and power spectral density with the PID controller. The experimental results show that, with the PID controller, the magnitudes of the first two vibration modes are 2.02 *mV* and 4.17 *mV*, respectively from the power spectral density measurement. It is also noted that the vibration modes at the end point is dominated by the first two vibrational modes, which are obtained as 7.813 *Hz* and 22.95 *Hz*, respectively. These results were considered as the system response without vibration control and will subsequently be used to design and evaluate the performance of the hybrid control

strategies. The steady-state rotation angle of 45 degree for the flexible manipulator system was achieved within the settling times and overshoot of 3.013 *s* and 0.00% respectively, while for the end point acceleration response; the maximum acceleration range is ±0.50 *V*.

4.2 Hybrid control

In the case of hybrid PID and input shaping control schemes, an input shaper was designed based on the dynamic behaviour of the closed loop system obtained using only the PID control. In designing the hybrid PID with two impulses (PID-ZV) and four impulses (PID-ZVDD) sequence, the magnitudes and time locations of the impulses were obtained by solving equations (3) and (4). For digital implementation of the input shaping, locations of the impulses were selected at the nearest sampling time. Figures 8 and 9 show the rotating angle, end point acceleration and power spectral density response with PID-ZV and PID-ZVDD respectively for the first two modes of vibration. It is noted that the hybrid controller is capable of reducing the system vibration while maintaining the input tracking capability of the manipulator. The vibration magnitudes of the hybrid control have significantly been reduced as compared to the response with PID control. With PID-ZV control, the magnitudes of the first two vibration modes were obtained at 0.51 *mV* and 0.71 *mV* respectively, while with PID-ZVDD control, the magnitudes were obtained at 0.49 *mV* for both vibration modes. It is noted that, higher levels of vibration reduction were obtained using PID-ZVDD as compared to the PID-ZV control schemes. This is also evidenced in end-point acceleration response, where the maximum acceleration ranges of PID-ZVDD is lower than PID-ZV control schemes. Table 1 summarises the levels of vibration magnitude reduction of the system responses at the first two modes in comparison to the PID control. In overall, the hybrid control schemes results a slower rotation angle response as compared to the PID control. The steady-state rotation angle of 45 degree for PID-ZV and PID-ZVDD control were achieved within the settling times of 3.255 *s* and 3.339 *s*. It shows that, with PID-ZVDD, the system response is slightly slower as compared to PID-ZV control. Hence, it is shown that the speed of the system response reduces with the increase in number of impulse sequence. The corresponding setting time and overshoot of the rotation angle response using PID-ZV and PID-ZVDD control schemes is depicted in Table 1.

Table 1: Experimental results using PID, PID-ZV and PID-ZVDD controller

Controller	Time domain			Frequency domain	
	Rotating angle		Acceleration	First mode	Second mode
	Settling time (*s*)	Overshoot (%)	Maximum range (*V*)	Vibration magnitude (*mV*)	Vibration magnitude (*mV*)
PID-ZV	3.255	0.00	±0.37	0.51	0.77
PID-ZVDD	3.339	0.00	±0.29	0.49	0.49
PID	3.013	0.00	±0.50	2.02	4.17

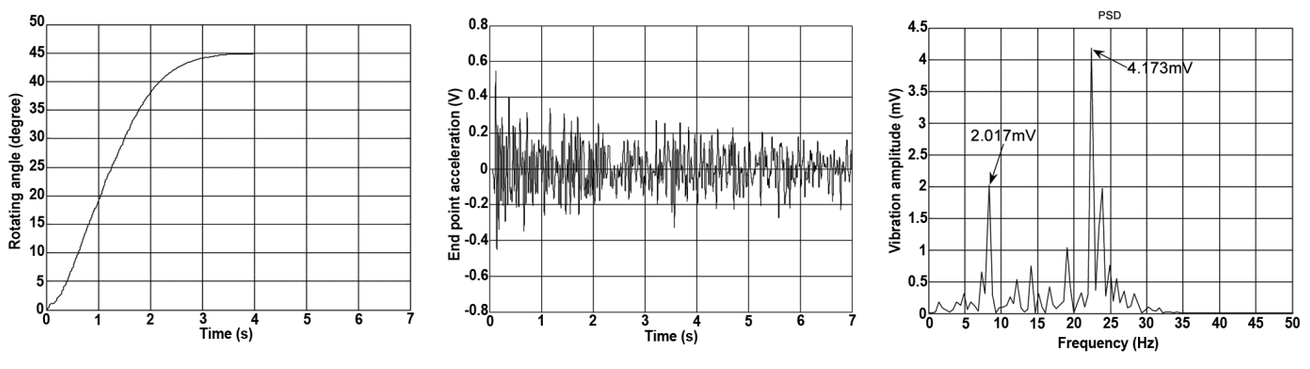

(a) Rotating angle (b) End point acceleration (c) Power spectral density

Figure 7: Response of the manipulator with PID Controller

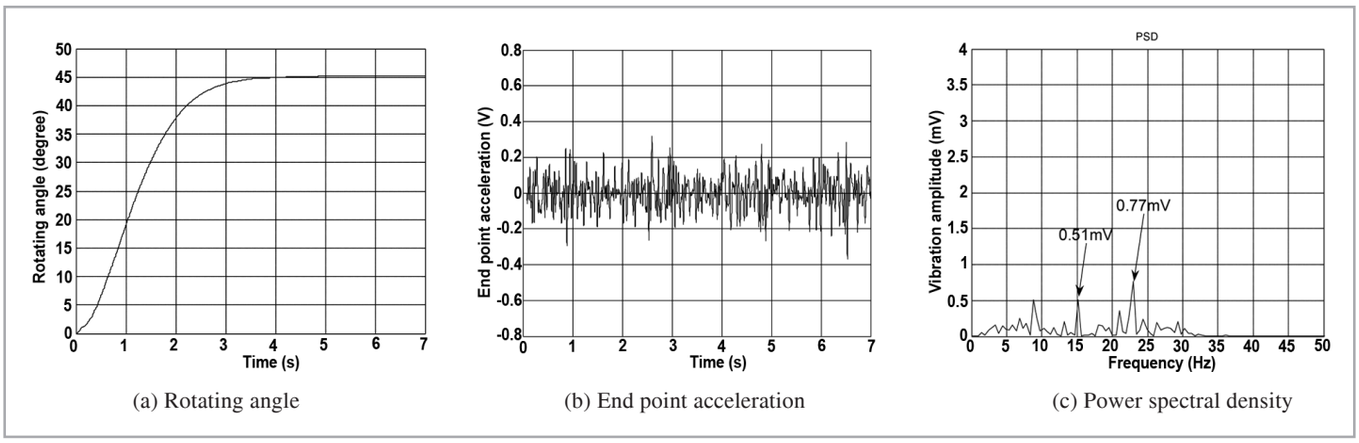

(a) Rotating angle (b) End point acceleration (c) Power spectral density

Figure 8: Response of the manipulator with PID-ZV controller

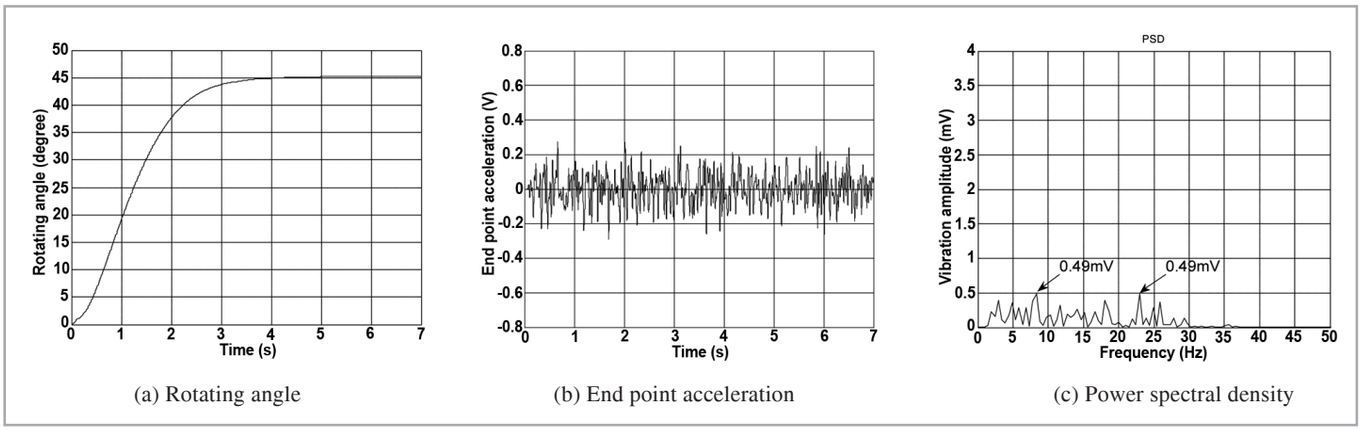

(a) Rotating angle (b) End point acceleration (c) Power spectral density

Figure 9: Response of the manipulator with PID-ZVDD controller

6.0 CONCLUSION

Experimental investigations into the development of hybrid input shaping and PID control for vibration suppression and input tracking of a flexible robot manipulator have been presented. The hybrid control schemes have been developed based on PID with ZV shaper (PID-ZV) and PID with ZVDD shaper (PID-ZVDD). The proposed control schemes have been implemented and tested within the experimental environment of a single-link flexible robot manipulator. The performances of the control schemes have been evaluated in terms of input tracking capability and vibration suppression at the resonance modes of the manipulator. Acceptable performance in input tracking control and vibration suppression has been achieved with both control strategies. A comparison of the results has demonstrated that the PID-ZVDD control provides higher level of vibration reduction as compared to the PID-ZV control. In term of speed of the responses, PID-ZVDD control results in a slower tracking response as compared to PID-ZV control. It is noted that the proposed hybrid controllers are capable of reducing the system vibration while maintaining the input tracking performance of the manipulator. ■

REFERENCE

[1] Azad, A.K.M. Analysis and design of control mechanism for flexible manipulator systems. PhD. Thesis, 1994 (Department of Automatic Control and Systems Engineering, The University of Sheffield, UK).

[2] Aspinwall, D.M. Acceleration profiles for minimising residual response. *Transactions of ASME: Journal of Dynamic Systems, Measurement and Control*, 1980, 102(1), 3-6.

[3] Bayo, E. Computed torque for the position control of open-loop flexible robots. In Proceedings of IEEE International Conference on *Robotics and Automation*, Philadelphia, 1988, 316-321.

[4] Onsay, T. and Akay, A. Vibration reduction of a flexible arm by time optimal open-loop control. *Journal of Sound and Vibration*, 1991, 147(2), 283-300.

[5] Meckl, P.H. and Seering, W.P. Experimental evaluation of shaped inputs to reduce vibration of a cartesian robot. *Transactions of ASME: Journal of Dynamic Systems, Measurement and Control*, 1990, 112(6), 159-165.

[6] Singhose, W.E., Singer, N.C. and Seering, W.P. Comparison of command shaping methods for reducing residual vibration. In Proceedings of European Control Conference, Rome, 1995, 1126-1131.

[7] Tokhi, M.O. and Poerwanto, H. Control of vibration of flexible manipulators using filtered command inputs. In Proceedings of International Congress on *Sound and Vibration*, St. Petersburg, 1996, 1019-1026.

[8] Singer, N.C. and Seering, W.P. Preshaping command inputs to reduce system vibration. *Transactions of ASME: Journal of Dynamic Systems, Measurement and Control*, 1990, 112(1), 76-82.

[9] Mohamed, Z. and Tokhi, M.O. Vibration control of a single-link flexible manipulator using command shaping techniques. *Proceedings IMechE-I: Journal of Systems and Control Engineering*, 2002, 216, 191-210.

[10] Khorrami, F., Jain, S. and Tzes, A. Experiments on rigid body-based controllers with input preshaping for a two-link flexible manipulator. *IEEE Transactions on Robotics and Automation*, 1994, 10(1), 55-65.

[11] Gevarter, W.B. Basic relations for control of flexible vehicles. *AIAA Journal*, 1970, 8(4), 666-672.

[12] Cannon, R.H. and Schmitz, E. Initial experiment on the end-point control of a flexible one-link robot. *International Journal of Robotics Research*, 1984, 3(3), 62-75.

[13] Hasting, G.G. and Book, W.J. A linear dynamic model for flexible robot manipulators. *IEEE Control Systems Magazine*, 1987, 7, 61-64.

[14] Feliu, V., Rattan, K.S. and Brown, H.B. Adaptive control of a single-link flexible manipulator. *IEEE Control Systems Magazine*, 1990, 10(2), 29 –33.

[15] Yang, T.-C., Yang, J.C.S. and Kudva, P. Load-adaptive control of a single-link flexible manipulator systems. *IEEE Transactions on Systems, Man and Cybernetics*, 1992, 22(1), 85-91.

[16] Moser, A.N. Designing controllers for flexible structures with H-infinity/μ-synthesis. *IEEE Control Systems Magazine*, 1993, 13 (2), 79-89.

[17] Moallem, M., Khorasani, K. and Patel, R.V. Inversion-based sliding control of a flexible-link manipulator. *International Journal of Control*, 1998, 71(3), 477-490.

[18] Gutierrez, L.B., Lewis, P.L. and Lowe, J.A. Implementation of a neural network tracking controller for a single flexible link: comparison with PD and PID controllers. *IEEE Transactions on Industrial Electronics*, 1998, 45(3), 307-318.

[19] Moudgal, V.G., Passino, K.M. and Yurkovich, S. Rule-based control for a flexible-link robot. *IEEE Transactions on Control Systems Technology*, 1994, 2(4), 392-405.

[20] Tokhi, M.O., Mohamed, Z. and Shaheed, M.H. Dynamic Modelling of Flexible Manipulator System Incorporating Payload: Theory and Experiments. *Journal of Low Frequency Noise, Vibration and Active Control*, 2000, 19(4), 209-229.

[21] Quanser Student Handout, Rotary Flexible Link Module. http://www.quanser.com

PROFILES



MOHD ASHRAF AHMAD

Mohd Ashraf Ahmad is born at Colorado, United State of America in 1983. He received his first degree in B.Eng. Electrical Mechatronics in 2006 from University of Technology Malaysia (UTM) in Johor, Malaysia. In 2008, he received a Master degree in M.Eng. Mechatronics and Automatic Control from University of Technology Malaysia (UTM). He has an experience as a research assistant at Robotic Laboratory in University of Technology Malaysia (UTM) in 2005. As a research assistant, he has developed an experimental investigation for vibration control of flexible robot manipulator. Currently, he is a lecturer in Faculty of Electrical and Electronics Engineering, Universiti Malaysia Pahang (UMP). He has currently published more than 23 paper work in various International Conference and has already published three Journals in the field of vibration control. The latest publications are: Vibration and input tracking control of a flexible manipulator using hybrid fuzzy logic controller (Kagawa, Japan: IEEE International Conference of Mechatronics and Automation, 2008) Hybrid input shaping and feedback control schemes of a flexible robot manipulator (Seoul, Korea: The 17th World Congress International Federation of Automatic Control, 2008). His current research interests are vibration control, input shaping, gantry crane and flexible robot manipulator.

EXPERIMENTAL INVESTIGATION OF AN AIR ENHANCEMENT DEVICE ON THE PERFORMANCE OF A SPARK IGNITION ENGINE

(Date received: 30.3.2009)

Mior Azman M. Said[1], Mutarazmin A. Mubin[2], Shaharin A. Sulaiman[3] and Rahmat I. Shazi[4]

[1, 3, 4] Department of Mechanical Engineering,
Universiti Teknologi Petronas, 31750 UTP, Tronoh, Perak
[2] Petronas Penapisan (Melaka) Sdn Bhd,
76300 Sungai Udang, Melaka
Email: [1]miorazman@petronas.com.my, [2]mutarazmin_mubin@petronas.com.my,
[3]shaharin@petronas.com.my, [4]rahmats@petronas.com.my

ABSTRACT

Air enhancement devices for air intake manifold systems of automotive engines have been widely available in the market with the claim that they can improve fuel-air mixing and thus bring more power to the engine performance and better fuel efficiency. However, there is lack of evidence to complement the claim. The objective of this study is to investigate the ability of an air enhancement device in improving the performance of a Spark Ignition (SI) engine. The investigation is performed by an experiment on a four-stroke single-cylinder engine test bed, in which the air enhancement device is installed at the downstream of the air intake manifold. The result is compared to the performance of the engine without the air enhancement device. It is shown that the brake power, brake mean effective pressure (BMEP) and torque increase significantly with the engine speed when operated at 30% to 50% of the open throttle positions. However, no distinct difference in the results is observed when the engine is running at higher throttle openings.

Keywords: *Engine, Internal Combustion, Spark Ignition, Volumetric Efficiency*

1.0 INTRODUCTION

Historically, the price for crude oil used to be USD 150 per barrel [1]. Due to the increase of fuel price, vehicle owners may consider seeking for devices that can lower their vehicles' fuel consumption without compromising the performance of the engine. One of the approaches to reduce fuel consumption is by using an air enhancement system that is mounted at the air intake manifold of the engine. Forced induction systems such as turbochargers and superchargers have been used to overcome some of the performance issues [2]. However, turbocharging does not completely eliminate the problem of "turbo lag" as it cannot produce sufficient charging pressure at low engine speed when there is little energy in the exhaust [3]. As for supercharging, it has problem with parasitic loss, which takes additional power from the engine especially at full load [4].

The amount of air that enters the intake manifold of a *Spark Ignition* (S.I.) engine depends on the pressure differential between the air above and below the throttle valve [2]. The air above the throttle valve is the atmospheric pressure, which is around 101 *kPa*. The air below the partially closed throttle valve is at less than atmospheric pressure, which is called negative pressure as created by the piston during the intake strokes. When the piston leaves top dead center (TDC) and move down the cylinders the space above the pistons gets larger. The stroke will lower the pressure in the intake manifold and creates the partial vacuum called intake manifold vacuum.

Normal engines use atmospheric pressure as a force to induce air into the intake manifold. These engines are called naturally aspirated or normally aspirated engines. At the same speed, an engine can produce more power if more air-fuel mixture is forced into the cylinders [5]. Forcing additional air-fuel mixture into the cylinders is referred as forced induction, which increases the volumetric efficiency of the engine; and this can be achieved by allowing higher pressures during the power strokes

There are many air enhancement devices available in the market recently, which are intended to increase the volumetric efficiency of the engine. One of the devices is reported to use crossed pin at a location before the throttle body of the engine to produce a swirl effect inside the manifold and consequently induce more air-fuel mixture in the cylinders [6, 7]. With a similar concept, another device, which uses a conical-shaped element, alters the pressure and velocity of the gas flow in order to improve fuel efficiency [8]. Some of these devices are reported to improve fuel efficiency for about 3-5% [9, 10]. In contrary, in

a more recent work by Mohd-Abidin [11] on a similar device, it was reported that such device had a detrimental effect on engine's performance.

There is also a device that employs an air induction element with a honeycomb treatment structure to provide a uniform directional air flow pattern for reduction of turbulence and improvement of air velocity delivery to the carburetor [12]. Another device system, which is integrated with the engine air management system, consists of an electronically controlled inlet air compressor [13]. The system is claimed to use the concept of turbo charger system with the capability of improved performance without sacrificing the fuel economy.

However, for most of the devices introduced, there is lack of evidence to support the claims by the manufacturers of their advantages. Therefore a study has to be conducted to determine the most suitable method to design a modified air enhancement system.

In the present work, the mechanism and design of an airflow enhancement device or the airflow enhancer that forcefully induces the flow of air into the combustion chamber of a Spark-Ignition (S.I.) engine is studied. The manufacturer claims that the device enables cars to have better power and fuel consumption by a three-stage mechanism that results in a mixture of fuel and air molecules with separated positive and negative ions. The effects of using the airflow enhancer in terms of engine performance at various throttle positions are studied using a petrol engine test bed.

2.0 DESCRIPTION OF THE AIRFLOW ENHANCER

The name of the air enhancement system product will not be revealed in this paper to prevent influencing consumers' judgment on a particular brand. The authors will refer the particular commercial product in generic term as the 'airflow enhancer.' For the same reason, detailed description of the device will not be disclosed. Tubular in shape, the airflow enhancer resembled a nozzle, of which the internal diameter of the inlet was about four times greater than the outlet. The airflow enhancer was installed at the intake manifold after the throttle, as illustrated in Figure 1. The mechanism operation of the airflow enhancer can be divided into three stages. In the first stage, the surrounding air will be drawn into the device inlet to pass through a built-in strainer. In the second stage, the air will pass through an array of air splitter before being directed into a nozzle for compression. In the final stage, the air accumulated in the cavity would be pressurised due to the reduction in the cross-sectional area of the airway. A Neodymium magnet was installed at a downstream point of the compressed air flow within the device. It has been claimed that the diatomic oxygen molecules that passed through the magnetic field would be polarised and would also increase the negative ions in the air to result in increases in burn time, temperature, and cylinder pressure, and consequently would increase the engine torque and power output [14].

3.0 EXPERIMENTAL SET-UP AND PROCEDURE

The experiments were conducted using an engine test bed. Shown in Figure 2 is the schematic of the engine test bed. A photograph of the test bed is shown in Figure 3. A 1.8 *litre* Ford 16-valve S.I. engine that was coupled to a dynamometer was used to determine the horsepower and torque of the engine. Table 1 shows the specifications of the engine. The dynamometer, Cusson Model SE 150, was of eddy current type with a maximum capacity of 150 *kW* and speed up to 8000 *RPM*. The fuel tank continuously fed the engine during the experiment and all the

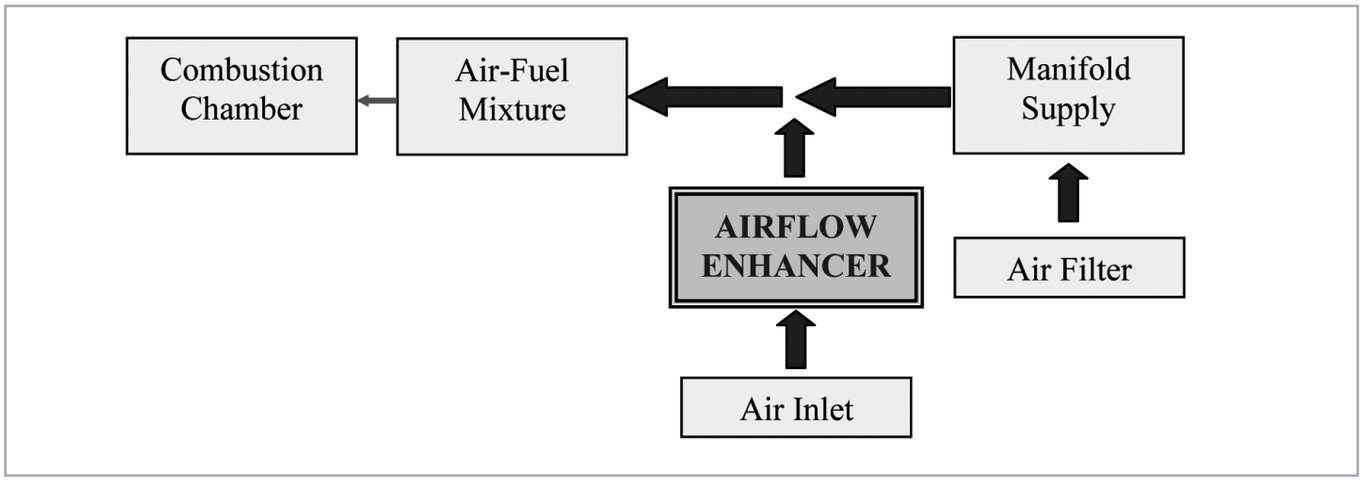

Figure 1: Mounting location of the airflow enhancer

tests were conducted using Petrol RON 92 fuel, which was available and purchased from the local retailer. The air intake would pass through the air filter prior to entering the intake manifold at the body of the engine. The exhaust gas from the combustion chambers would be diverted into the exhaust pipe, as shown in Figure 2. A data acquisition system was connected to all the measurement transducers within the engine test bed to obtain the torque, brake mean effective pressure (BMEP) and brake power (accurate to ± 0.5 *kW*). The measurements were displayed and recorded by a desktop computer. The airflow enhancer was installed at the intake manifold in the arrangement as shown in Figure 1.

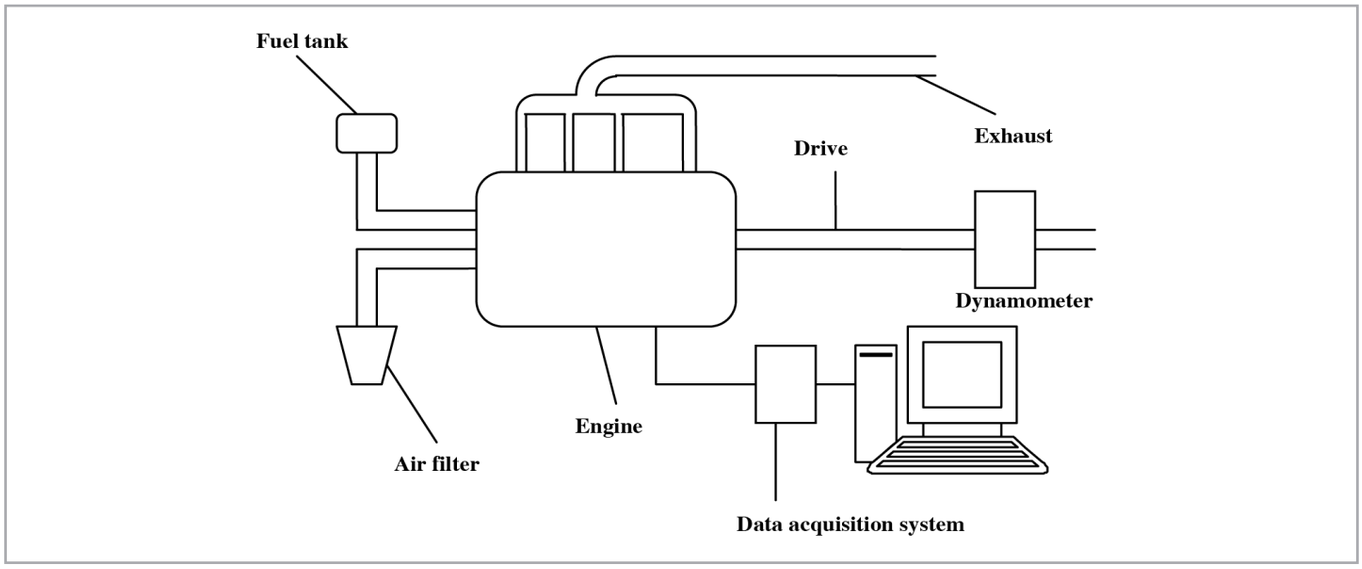

Figure 2: Experimental set-up

The engine's performance testing was conducted with and without the airflow enhancer. The engine was initially allowed to warm up. After a steady temperature within the engine's radiator was achieved, the engine was stopped to install the airflow enhancer. The engine was then restarted and the air vent-screw was adjusted to obtain the previous engine speed. A load on the engine was established to allow a starting speed of 1000 *rpm*. The experiment conditions were varied by changing the throttle opening positions and the engine speeds from 30 to 100 % and 500 to 3500 *rpm*, respectively, as indicated in Table 2. For each condition, the brake power, torque, BMEP, speed, fuel consumptions, air flow rate, and temperatures were recorded when the readings were stable. As shown in Table 2, there were experiments that could not be carried out for 30 and 40% throttle positions and at certain engine speeds. This was because the engine torque was very low that it could not run at such speeds. In other cases, instability in the measurement readings was displayed and thus it was decided that experiments were not performed under such conditions.

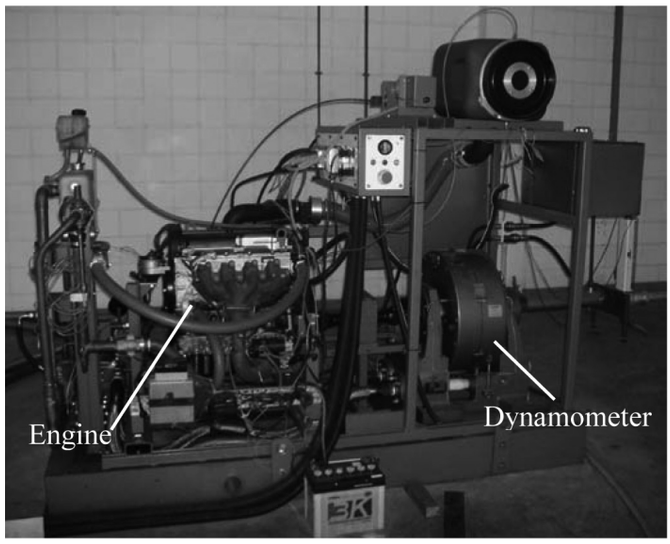

Figure 3: Photograph of the engine test bed

Table 1: Engine technical data

Specification	Data
Make	Ford
Type	SI 1.8 DOHC 16V
Emission standard	83 US
Identification code	RDA
Firing order	1-3-4-2
Bore (mm)	80.6
Stroke (mm)	88.0
Cubic capacity (cc)	1796
Compression ratio	10:1
Max. engine speed (rev/min)	5950
Power output (DIN-kW) at 5500 rev/min	77
Torque (Nm) at 4000 rev/min	153

Table 2: Experiment conditions

	Engine Speed (RPM)						
Throttle (%)	500	1000	1500	2000	2500	3000	3500
30		x	x	x			
40		x	x	x	x		
50	x	x	x	x	x	x	x
60	x	x	x	x	x	x	x
100	x	x	x	x	x	x	x

4.0 RESULTS AND DISCUSSIONS

Shown in Figure 4(a) is the variation of the measured torque with engine speed at throttle opening positions between 30% and 100%. The continuous lines represent the results for experiments with the airflow enhancer installed, and the dashed lines represent those without. In general, Figure 4(a) shows that the measured torque decreases with the engine speed, except for that of 100% opening, which exhibits gradual increase in torque with the engine speed. In Figure 4(b) the change in torque as a result of the use of the airflow enhancer is shown. Obviously, the torque increases up to 25% for experiments with low engine throttle (30% to 50%). As for 50% of the throttle opened, the increase in torque is shown only at engine speeds of higher than 2000 *RPM*. The slight drop in the graph for 30% of the open throttle at an engine speed of 2000 *RPM* is probably related to the fact that the torque at such condition was approaching a zero value. At other conditions, the differences in the results are small (<5%).

The variation of the BMEP with engine speed is shown in Figure 5(a), for the same experiment conditions as described for Figure 4 and with the same representations of symbols and lines. It is shown in Figure 5(a) that the BMEP decreases with the engine speed. However, this is an exception when operated at 100% opening position, in which the engine experienced a gradual increase in BMEP with the engine speed. Although at an engine speed of between 3000 and 3500 *RPM*, the BMEP starts to drop slightly, it is uncertain of whether it would further drop at a much higher engine speed.

In Figure 5(b) the change in BMEP as a result of the use of the airflow enhancer is shown. The trend of the graph is similar to that of Figure 4(b), in which the BMEP increases up to 25% for experiments with low engine throttle. As for 50% opening, the increase in BMEP is shown only at engine speeds of higher than 2000 *RPM*. At other conditions, the differences in the results are very small; *i.e.* less than 5%.

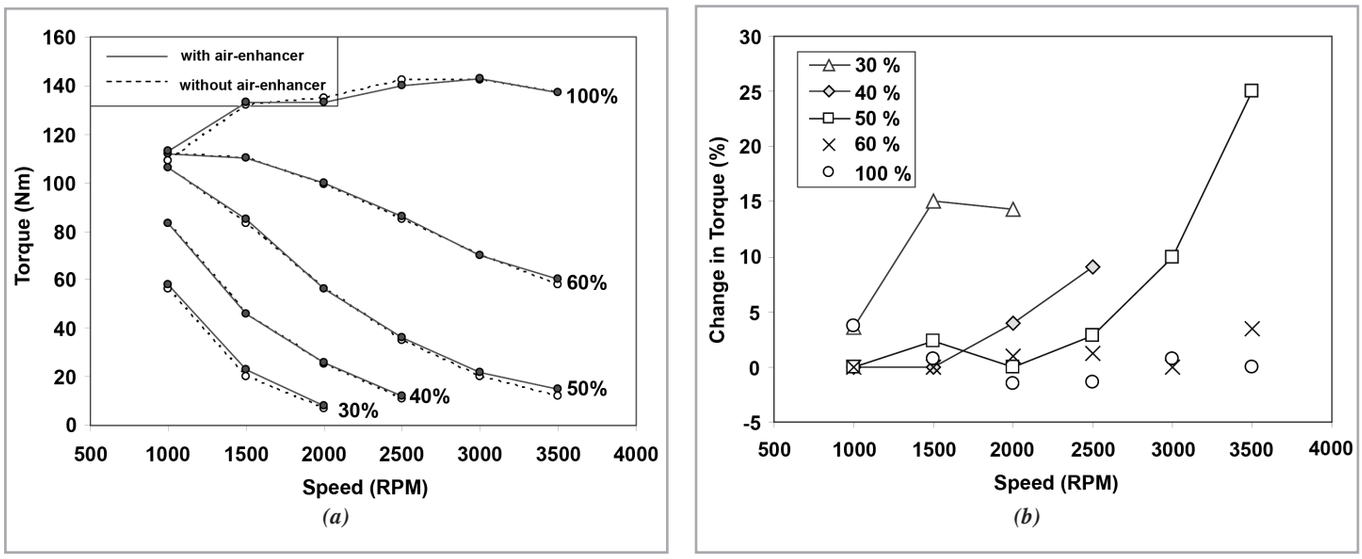

Figure 4: Variation of the measured torque with engine speed at different throttle opening positions with and without the airflow enhancer, (b) changes in the torque

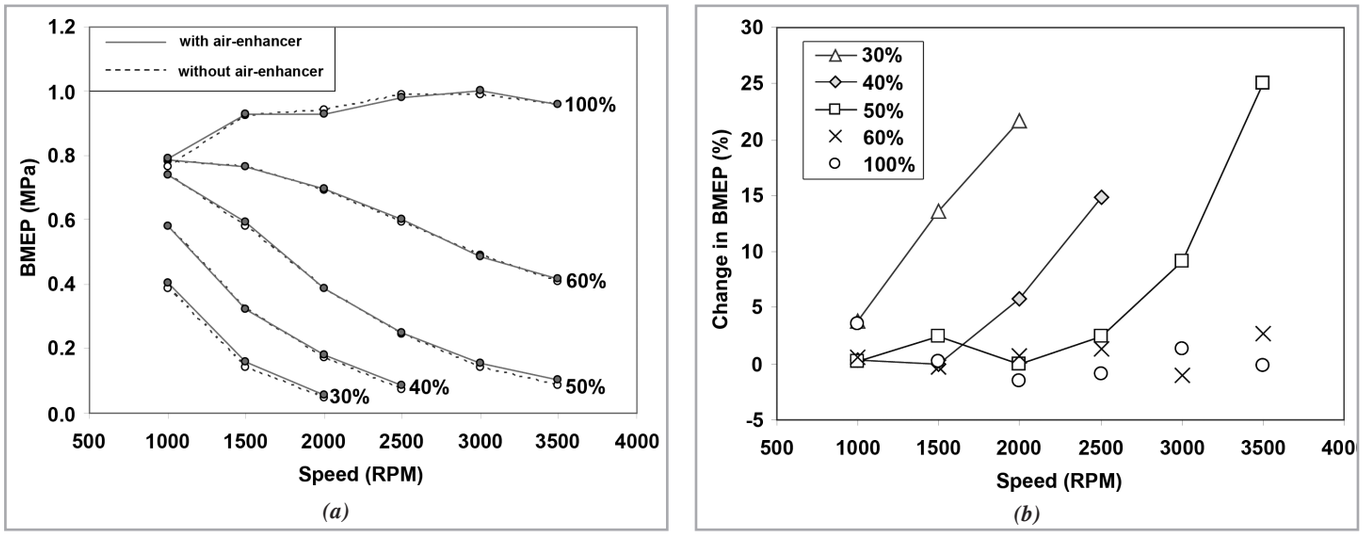

Figure 5: Variation of the measured BMEP with engine speed at different throttle opening positions with and without the airflow enhancer, (b) changes in the BMEP

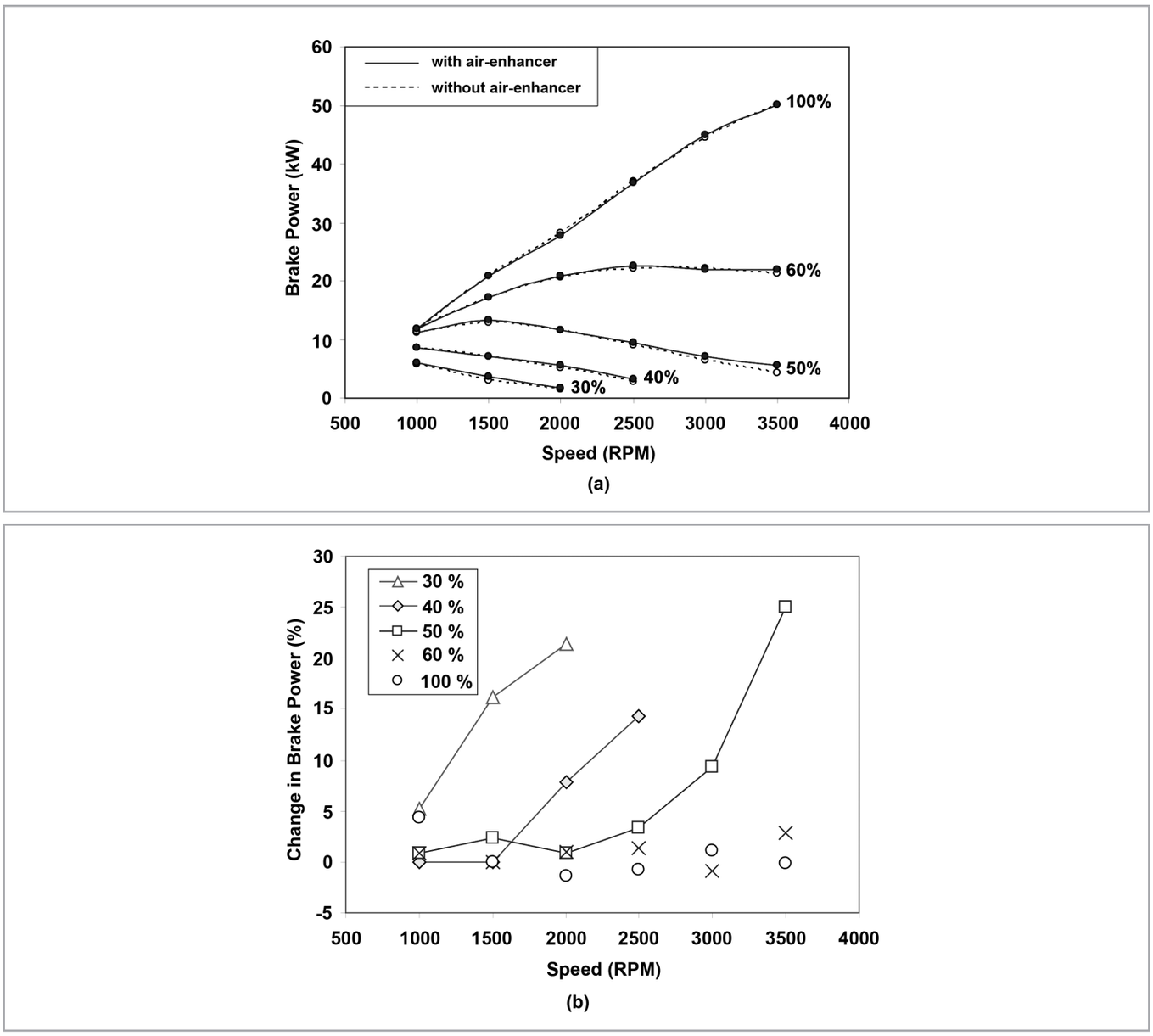

Figure 6: (a) Variation of the measured brake power with engine speed at different throttle opening positions with and without the airflow enhancer, (b) changes in the brake power

Shown in Figure 6(a) is the variation of the brake power with engine speed for the same experiment conditions as described for Figure 4 and with the same representations of symbols and lines. It is shown in Figure 6(a) that the brake power decreases with the engine speed when operated at 30% and 40% opening. The same trend is exhibited for experiments with 50% and 60% opening; however each displays an increase in brake power at lower engine speeds. For 100% opening, it is clear that the brake power increases with the engine speed. The change in the resulting brake power as a result of installing the airflow enhancer is shown in Figure 6(b). Similar to the graphs in Figures 4(b) and (b), the brake power increases significantly for experiments with low engine throttle (30%, 40% and 50%), although for 50% opening, the increase in BMEP is only demonstrated at engine speeds of higher than 2000 *RPM*. At other conditions, the effect of the airflow enhancer is shown to be negligible.

In general, the results show improvements in the torque, BMEP and brake power at some conditions when the air intake system of the engine was installed with the airflow enhancer. These are however limited to operations at 30%, 40% and 50% throttle open positions. The increases in torque, BMEP and brake power are proportional to the engine speed. The reason behind this is due to the higher number of intake stroke, which creates vacuum condition that enabled the airflow enhancer to induce more air into the combustion chamber. Obviously, the present work demonstrates that the airflow enhancer does not produce any effect when operated at 60% and 100% opening. This is probably because the volume of air induced by the normal operation (without airflow enhancer) is large and enough for the engine to reach the highest performance. During the normal operation, the volumetric efficiency is already high and no additional air can further be added.

5.0 CONCLUSIONS

The engine performance, as a result of installing an air-enhancing device at the air intake system of a spark ignition engine, was investigated in order to verify the claims made by its manufacturer. The use of such a device, which operated by mean of forced induction, was studied to determine its capability to enhance engine performances. The manufacturer claimed that by connecting the airflow enhancer to the manifold supply air inlet, extra air could be induced into the combustion chamber, which would then enhance the performance of the engine by improving its volumetric efficiency. The investigation was conducted by an experiment using a four-stroke single-cylinder engine test bed with and without the air-enhancing device. It was demonstrated that the brake power, brake mean effective pressure (BMEP) and torque increased significantly with the engine speed when operated at low load (30% to 50% of the throttle opened), although these were limited to a certain range of engine speeds. Nevertheless, at larger throttle openings, the device demonstrated insignificant effect to the engine's performance. ■

REFERENCE

[1] Crude Oil Futures Price Quotes, NYMEX, http://www.nymex.com/, 18 July 2008.

[2] W. W. Pulkrabek, *Engineering Fundamentals of the Internal Combustion Engine*, International ed, Prentice-Hall, 1997.

[3] H. Uchida, "Trend of Turbocharging Technologies," R&D Review of Toyota CRDL, vol. 41, pp. 1-8, 2006.

[4] N. S. Jackson, Future Automotive Powertrains - The End of the Internal Combustion Engine? The 91st Thomas Hawksley Lecture, Institution of Mechanical Engineers, UK, 2003.

[5] W. Crouse and D. Anglin, *Automotive Engines*, 8th ed, McGraw Hill, Glencoe, 1994.

[6] Introduction to Surbo and Twin Surbo, Surbo Engineering Singapore, http://www.surbo.net, 7 August 2006.

[7] L. Michaud, "Atmospheric Vortex Engine," *Sustainability and the Seminar Series*: IEEE London Section, London, 2007.

[8] R. B. Russell, (WO/2007/070412) Device for Enhancing Fuel Efficiency of Internal Combustion Engines, World Intellectual Property Organization, *http://www.wipo.int*, 2007.

[9] Hiclone, KPS Automotive Parts, http://www.hiclone.co.uk, 2008.

[10] W. Mitchelson, "Clear the Air," *Land Rover World*, pp. 118-119, September 2004.

[11] M. Mohd-Abidin, An Investigation on the Effects of an Intake Air-Swirl Device on Fuel Consumption of a Spark Ignition Engine, Final Year Project Dissertation, Universiti Teknologi PETRONAS, 2008.

[12] J. Westcott, Engine air inlet flow enhancement device for internal combustion engines, http://www.freepatentsonline.com/7146961.html, 2006.

[13] Engine Induction Products, Visteon Corporation, http://www.visteon.com, 4 August 2006.

[14] J. Gibboney, James W, Air intake system for an internal combustion engine, in *US Patent 5487874*.

PROFILES



EN. MIOR AZMAN MEOR SAID

En. Mior Azman Meor Said is a Lecturer at Universiti Teknologi Petronas (UTP) and a member of Board of Engineers Malaysia (BEM). He obtained his M.Sc. in Mechanical Engineering from Washington of University in St. Louis, MO, USA in 2005 and his B.Sc. in Mechanical Engineering (Hons) from Universiti Tenaga Nasional in 2002. After graduating from his undergraduate studies, he worked for a year as a Research & Development Engineer at DENSO (M) Sdn. Bhd. His research interests include computational fluid dynamics, combustion and thermal fluid system.



ENGR. DR SHAHARIN ANWAR SULAIMAN

Engr. Dr Shaharin Anwar Sulaiman is a Senior Lecturer at Universiti Teknologi Petronas (UTP). Graduated in 1993 with a B.Sc. in Mechanical Engineering from Iowa State University, he earned his M.Sc. in Thermal Power and Fluids Engineering from UMIST in 2000, and Ph.D. in Combustion from the University of Leeds in 2006. During his early years as a graduate, he worked as Mechanical and Electrical (M&E) Project Engineer in Syarikat Pembenaan Yeoh Tiong Lay (YTL) for five years prior to joining UTP as a tutor) in 1998. His research interests include combustion, sprays and atomization, HVAC and renewable energy. He is also a certified Professional Engineer with the Board of Engineers, Malaysia, and a Corporate member of the Institution of Engineers Malaysia.



ENGR. RAHMAT ISKANDAR SHAZI

Engr. Rahmat Iskandar Shazi is a Lecturer at University Teknologi PETRONAS (UTP). He graduated in 1999 with a B.Eng in Mechanical Engineering from UMIST, prior to joining UTP as a trainee lecturer. He continued his studies at University of Illinois at Urbana-Champaign, obtaining his MSc in 2003. His research interests are diesel ignition and combustion, atomisation and sprays, energy and innovation management. He is a graduate member of the Institution of Engineers Malaysia.

ROLE OF SENIOR MANAGEMENT IN TQM IMPLEMENTATION IN MALAYSIAN SMALL AND MEDIUM ENTERPRISES

(Date received: 12.3.2008)

Baba Md. Deros[1], Mohd Nizam Ab. Rahman[2], Jaharah A. Ghani[3], Dzuraidah Abd. Wahab[4], Mohd. Hazri Hashim[5] and Nor Kamaliana Khamis[6]

Advanced Manufacturing Research Group
Department of Mechanical and Materials Engineering, Faculty of Engineering
Universiti Kebangsaan Malaysia, 43600 UKM Bangi, Selangor
Email: [1]hjbaba@vlsi.eng.ukm.my

ABSTRACT

During the last two decades, quality had become a very important issue in many large organisations for both industrial and service sectors. They regard quality as a formidable weapon in addressing business competition and challenges both from local and global competitors. At present, small and medium enterprises (SMEs) had also joint the bandwagon in their effort to improve their products and services quality. One of the bold step taken by SMEs involved in the automotive components manufacturing sector to improve their product and service quality and hence their overall competitiveness in the open market is by implementing Total Quality Management (TQM). SMEs' main objectives in implementing TQM in their organisations are to ensure their products manufactured or services provided shall satisfy their customers' requirements and needs. This paper presents a survey conducted to identify the level of SMEs senior managements' awareness and their attitude towards implementing TQM activities. In this study, one important aspect of TQM that is "senior management responsibilities and involvement in providing top-down short and long term support" was used as a parameter to identify their level of awareness and attitude towards the importance of implementing TQM in SMEs.

Keywords: *Product, Quality, Service, Senior Management, SMEs, TQM*

1.0 INTRODUCTION

During the late 1990s, increasing globalisation and market competition had made it necessary for SMEs to improve their effectiveness. This new and challenging environment has motivated many senior management in manufacturing SMEs to re-evaluate their competitive strategies and management practices with the aim of improving organisational performance in the area of quality. TQM is a management philosophy that integrates strategy, management practices and organisational outcomes to create a quality organisation that continuously improves and sustain performance [1].

2.0 TQM DEFINITIONS

A review of the definitions of the TQM from literature indicates that it means differently to authors and researchers. Kanji [2] defines TQM "as a way of life an organisation committed to customer satisfaction through continuous improvement". This way of life varies from organisation to organisation and from one country to another but has certain principles, which can be implemented to secure market share, increase profits and reduce costs. Dale [3] defines TQM as "the mutual cooperation of everyone in an organisation and associated business process to produce products and services, which meet the needs and expectations of the customers". Dale [3] believes TQM is both a philosophy and a set of guiding principles for managing an organisation. Meanwhile, Juran and Gryna [4] define TQM as "a philosophy aimed at achieving business excellence through the use and application of tools and techniques, as well as management of soft aspects, such as human motivation in work". On the other hand, Berry [5] defines the TQM process as "a total corporate focus on meeting and exceeding customers' expectations and significantly reducing costs resulting from poor quality by adopting a new management system and corporate culture". This review revealed that there is no universally agreed definitions of TQM, however, as noted by Mann and Kehoe [6], basically the various and variety of TQM definitions can be classified into two types, namely: definitions which describe TQM in terms of its ultimate goal; and definitions that describe TQM in terms of activities or functions that need to be addressed to achieve its objectives.

3.0 HISTORICAL DEVELOPMENT OF TQM

The historical development of TQM has been clearly established through the quality movement for most of the twentieth century. Garvin [7] classified the historical evolution of TQM into four distinct stages: Quality inspection (1910s); Quality control (1924s); Quality assurance (1950s) and Total quality management (1980s). Table 1 describe the stages and characteristics of TQM development. As shown in Table 1, throughout this period of ongoing development (*i.e.* 1910s to 1990s), TQM had advanced and developed through the influence of many differing factors.

Table 1 : Characteristics of different stages in TQM
(Source: Dahlgaard et al. [8])

Stage	Characteristics
QI (1910s) Quality Inspection	Salvage; Sorting; Corrective action; Identify sources of non-conformance
QC (1924s) Quality Control	Quality manual; Performance data; Self-inspection; Product testing; Quality planning; Use of statistics; Paperwork control
QA (1950s) Quality Assurance	Third-party approvals; Systems audits; Quality planning; Quality manuals; Quality costs; Process control; Failure mode and effect analysis (FMEA); Non-production operation
TQM (1980s) Total Quality Management	Focused vision; Continuous improvements; Internal customer; Performance measure; Prevention; Company-wide application; Inter-departmental barriers; Management leadership

Davenport *et al*. (1996), and Wilkinson and Willmott (1994), (as quoted by McAdam [9]) cited that these influencing development factors range from the business process movement to the development of human resources and empowerment concepts had holistically transformed the TQM philosophy as shown in Figure 1. Hence, it can be summarised, that throughout this development period, TQM has moved from a predominantly narrow and mechanistic approach to a more subjective and broader organisational philosophy.

4.0 SENIOR MANAGEMENT DEFINITION

Senior management is generally a team of individuals at the highest level of organisational management who have the day-to-day responsibilities of managing a corporation [10]. There are most often higher levels of responsibility, such as a board of directors and those who own the company (shareholders), but they focus on managing the senior management instead of the day-to-day activities of the business. They are sometimes referred to, within corporations, as top management, upper management, or simply seniors.

5.0 SENIOR MANAGEMENT COMMITMENT AND LEADERSHIP

The need for senior management commitment and leadership is recognised by most prominent writers in the area of quality such as Dale [3], Juran and Gryna [4], Berry [5], Garvin [7], Dahlgaard *et al*. [8], Yusof [10], Bounds *et al*. [11], Oakland [12], Aalbregtse *et al*. [13], Kanji and Baker [14], Deming [15], Feigenbaum [16], Crosby [17], and Shewhart [18].

For example, Yusof [10] reported "management commitment and leadership represents a paradigm shift from the traditional management role and responsibilities, towards a new role, supporting and enhancing the total quality culture and environment". In other words, the leaders who have a deep understanding and thinking, who know what to do and how to lead the change process, must lead TQM.

6.0 ROLE OF SENIOR MANAGEMENT IN TQM IMPLEMENTATION

The first thing which senior management must realise from the outset is that TQM is a long-term business strategy. The senior management should start TQM implementation because they are the primary internal change agent for quality improvement.

In this situation, the senior management has two major roles; they are shaping organisational values and establishing a managerial infrastructure to actually bring about change. They have to prepare themselves with knowledge about the criteria of TQM and put in their mind the TQM agenda [19].

TQM is the management process used to make continuous improvement to all functions in organisations. The ideal continuous improvement process is the ones that begin with and have genuine senior management involvement. On the other hand, Leonard and McAdam [20] believe TQM implementation needs commitment to quality and continuously improving from all levels of staff.

7.0 MOTIVES FOR IMPLEMENTING TQM

Shea and Gobeli (1995) (as quoted by Yusof and Aspinwall [21]) cited some of the motives reported by a group of small [20] companies, which studied, about the reasons to choose TQM process, namely:

(a) Promotion of growth – it is easier to convince the company's bankers to invest in them if there is evidence that the organisation is well run;



***Figure 1 : TQM influencing development factors** [9]*

(b) Management belief in the principle of customer satisfaction and employee empowerment which reflects the management style supporting TQM;

(c) Changing customer expectations even for organisations seen to be doing well (competitive issue);

(d) Making work more enjoyable; and

(e) To improve poor company performance if the company is not doing well (survival issue).

Even though these reasons looked varied, they all are focusing on improvement. Income is an important issue especially for small businesses. They must understand and realise that improvements in their business and in other aspects such as the working environment are important for survival. For example, Yusof and Aspinwall [21] reported on a case study in a small company whose reason for adopting TQM was to develop a new culture as well as management's desire to return the company to profitability. Meanwhile, Ghobadian and Gallear [22] found in one of the companies they studied cited its prime reasons for adopting TQM are to overcome internal problems such as poor delivery performance, quality related problems caused by a narrow functional approach and poor financial returns.

8.0 SURVEY METHODOLOGY

A survey is considered the most economical among methods available for data collection due to its ability in performing quick, efficient data collection and analysis [23]. A prerequisite in designing a good questionnaire is to decide what to measure. This step seems simple and self-evident but if overlooked may result in producing low quality questionnaires [24].

The survey questionnaire in this study was developed based on previous studies found in the literature and the general rules by Fowler [25] on questions and answers basic characteristics, which are fundamental to a good measurement process. The final survey instrument was based on nine statements, believed to be critical for managing TQM implementation in an organisation.

In this survey, respondents were asked to rate two aspects on a five point Likert scale, first on the level or degree of importance placed on each statement and secondly, the extent to which they thought it is currently a practice in the organisation. For the perceived importance, the rating scales ranged from 1 = not important at all, 2 = not important, 3 = neutral, 4 = important, to 5 = very important; while for the extent or degree of practice was given as 1 = very low, 2 = low, 3 = moderate, 4 = high, 5 = very high. An additional scale (0) was provided for both aspects to allow for those respondents who did not know or unsure of the answer.

For example, 'Senior management gives an utmost attention and priority to internal and external customers and their needs. If importance = 4, this means it is an important indicator for successful TQM implementation; and if practice = 5, this means highly practiced.

9.0 POPULATION AND SAMPLE OF THE STUDY

The sample for the full survey consisted of 150 SMEs, which were randomly selected from the Malaysian automotive industry vendors' list. A questionnaire was sent by postal mail to the senior management of each SME. The authors believe that it is crucial to find out the perception of critical factors from those who have an understanding and practical experience in actual industrial environment. A reply-paid self-addressed envelope was included.

10.0 OBJECTIVES OF THE SURVEY

In this survey, the authors attempted to investigate the SMEs' senior management perceptions and practices of the nine statements that believed to be critical for managing TQM implementation in an organisation. The statements are, senior management:

(1) gives an utmost attention and priority to internal and external customers and their needs;
(2) employees are empowered to solve quality related problems within their own work areas;
(3) practice continuous improvement compared to maintenance;
(4) promotes cooperation and not competition among their employees;
(5) act as a coach and trainer to their employees;
(6) continuous commitment in providing high quality products and services;
(7) promotes teamwork effort;
(8) set realistic objectives for the company and let everyone knows about it;
(9) make decision based on facts.

11.0 SURVEY RESULTS AND ANALYSIS

In this study, 150 sets of questionnaires were distributed to the vendors for automotive manufacturers in Malaysia securing a response of 32 companies, which is equivalent to 21.3%. For comparison, a postal survey on 350 automotive manufacturers in Malaysia by Deros [1] also received a low response rate of 19.4%.

The first aspect investigated was the general background of the respondents, which includes respondent's occupation, number of years in the business, the type of products manufactured and quality system certification. Seventy percent (70%) of the respondents' comprise of senior executives, managers and engineers. Ninety percent (90%) of the companies had been in the business for more than 10 years.

The top three groups of products manufactured by the companies, which forms 87% are metal (48%), wood (29%) and plastic parts (10%). With regards to quality system certification, all of the respondents had a least one certification in place (*i.e.* ISO 9001, QS 9000, ISO 14000, TS 16949). The quality improvement activities that were performed by the respondents comprise of total productive maintenance, quality management system, quality function deployment (QFD), FMEA and *etc*.

The survey revealed some pertinent issues on the role of senior management in implementing TQM in their respective companies. Figure 2 shows the overall percentages with respect to the nine critical success factors for TQM implementation and their level of importance as perceived by the senior management. It can be seen from Figure 2, the two most critical success factors that received the highest percentage ranking (*i.e.* 41.38 percent) for very important level

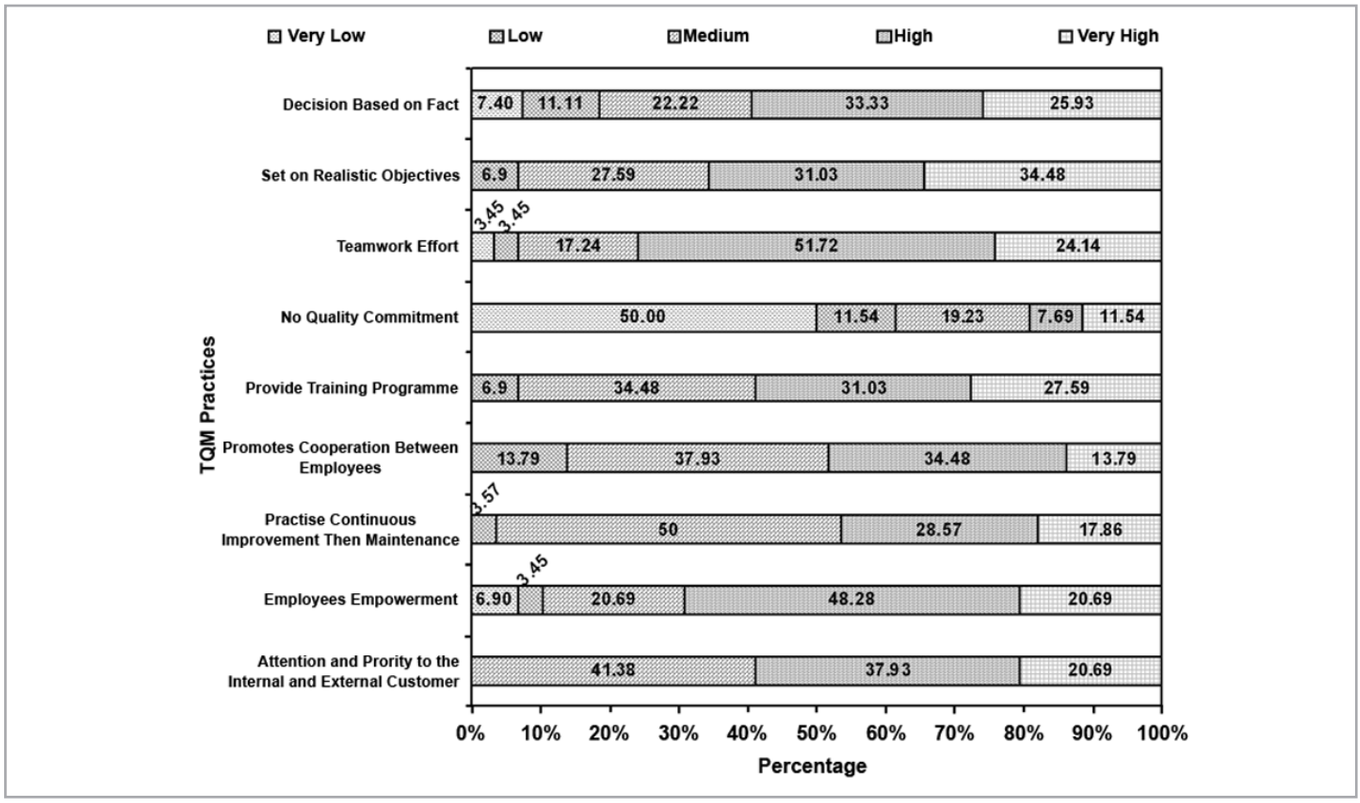

Figure 2 : Senior management's perception of importance on TQM

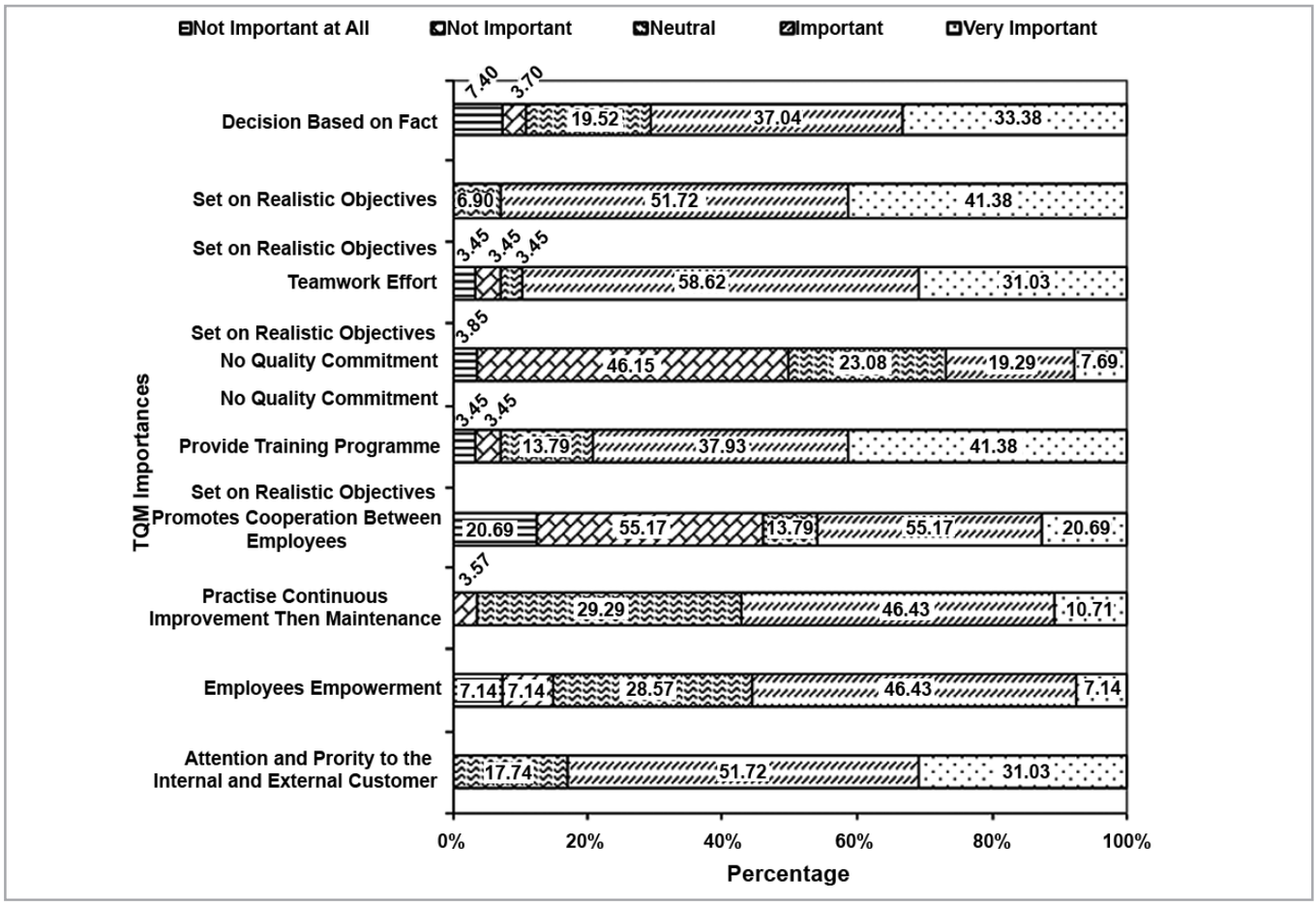

Figure 3 : Senior management's TQM practices

(*i.e.* Likert scale value 5) are senior management's ability to set realistic TQM objectives and provide TQM training programme for their employees.

The critical success factors that receive the next highest percentage ranking of 33.33 percent is to make decision based on fact. It is followed by two other factors that shared the same ranking of 31.03 percent, which comprise of teamwork effort and attention and priority to internal and external customers. Thus, it can be concluded from the survey results that in order of importance the SMEs senior managements' believes the five critical success factors must be considered in TQM implementation effort in order to ensure its success are senior management's ability to: set realistic TQM objectives; provide TQM training programme for their employees; make decision based on fact; organise teamwork effort; and give proper attention and priority to internal and external customers.

On the other hand, the two success critical factors, which receive the lowest percentage rankings in terms of senior managements' perception of importance is related to their commitment to quality (7.69 percent) and employees empowerment (7.14 percent). In other words, the survey results reveal that senior management view these two critical success factors do not have much impact on the success or failure of the TQM implementation effort.

In the authors' view, the lower rankings by senior management for these two factors may probably be due to their view on TQM as a philosophy or mindset rather than TQM as a way of life or doing things on daily practices.

Referring to Figure 3, in terms of actual practice the most critical success factors that received the highest percentage ranking (*i.e.* 34.48 percent) for very important level (*i.e.* Likert scale value 5) is senior managements' ability to set realistic TQM objectives. The critical success factor that receives the next highest percentage ranking of 27.59 percent is senior managements' ability to provide TQM training programme for their employees.

It is followed by two other critical success factors in order of practice percentage rankings, which comprise of senior management practice of making decision based on fact (25.93 percent) and teamwork effort (24.14 percent). Therefore, it can be concluded that the SMEs' senior management practices these four critical success factors in order of percentage ranking as follows: set realistic TQM objectives, provide TQM training programme for their employees, makes decision based on fact, practice teamwork effort.

On the other hand, the two success critical factors, which receive the lowest percentage rankings in terms of senior managements' practice is related to their commitment to quality (11.54 percent) and promotes cooperation between employees (13.79 percent).

12.0 CONCLUSIONS

Since the number survey respondents were rather small, the survey result is not conclusive on its own, but is useful in understanding the current situation pertaining to the beliefs of TQM's importance and attitude towards implementing TQM activities as well as the actual practices of TQM in Malaysian SMEs. The authors concluded that the five most significant TQM implementation critical success factors are the SMEs' senior management perception and practice in setting a realistic TQM objectives, providing TQM related trainings to their employees, making decision based on fact, enhancing teamwork effort, giving priority and attention to the internal and external customer. Comparing the perceptions of importance and actual practices, reveal the similarities and consistencies between what SMEs senior management's perception of importance and actual practices on TQM.

In most cases, the actual practices are much lower than the perception of importance. However, it is quite surprising to know from both Figures 2 and 3 that the SMEs senior management have the least perception of importance and practice to quality commitment. The survey methodology used in this study has several limitations. The survey analysis is conducted based on 32 companies only. However, the authors believed, it is adequate to show the trend of TQM perceptions and practices among senior management in Malaysian automotive manufacturing SMEs. ■

REFERENCES

[1] Deros, B.M. 2004. Development of a Benchmarking Implementation Framework for Small and Medium Sized Enterprises, Ph.D Thesis, Faculty of Mechanical Engineering, University Teknologi Malaysia.

[2] Kanji, G.K. (1990). "Total Quality Management: The Second Industrial Revolution", Total Quality Management, Vol. 1 No.3, pp. 3-12.

[3] Dale, B.G. (ed.) (1994). "Managing Quality", Prentice Hall, London.

[4] Juran, J.M. and Grayna, F. M. (1993). "Quality Planning and Analysis", 3rd Edition, McGraw Hill International Editions.

[5] Berry, T.H. (1991). "Managing the Total Quality Transformation", McGraw-Hill Book Company, New York.

[6] Mann, R. and Kehoe, D. (1994). "An Evaluation of the Effects of Quality Improvement Activities on Business Performance", International Journal of Quality and Reliability Management, Vol. 11, No.4, pp. 29-44.

[7] Garvin, D. A. (1988). "Managing Quality: The Strategic and Competitive Edge", The Free Press, New York, NY.

[8] Dahlgaard J. J., Kristensen K. and Kanji, G.K (1998). "Fundamentals of Total Quality Management – Process Analysis and Improvement", 1st Edition, Chapman and Hall, London.

[9] McAdam, R. (2000). "Three Leafed Clover? TQM, Organisational Excellence and Business Improvement" , The TQM Magazine, Vol. 12 No.5, pp. 314-320.

[10] Yusof, S.M. (2000). "Development of a Framework for TQM Implementation in Small Business", Ph.D Thesis, Faculty of Engineering, University of Birmingham, United Kingdom.

[11] Bounds, G., Yorks, L., Adams, M., Ranney, G. (1994). "Beyond Total Quality Management – Towards the Emerging Paradigm", McGraw-Hill Book Company, Singapore.

[12] Oakland, J.S. (1993). "Total Quality Management", Butterworth-Heinemann.

[13] Aalbregtse, R.J., Hejka, J.A. and McNeley, P.K. (1991). "Total Quality Management (TQM): How do you do it?" Automation, August, pp. 30-32.

[14] Kanji, G.K. and Baker, R.L. (1990). "Implementation of Total Quality Management", Total Quality Management, Vol. 1 No.3, pp. 375-389.

[15] Deming, W.E., (1986). "Quality, Productivity and Competitive Position", MIT Press.

[16] Feigenbaum, A.V. (1986). "Total Quality Control", 3rd Edition, McGraw-Hill Book Company, Singapore.

[17] Crosby, P.B. (1980). "Quality is Free – The Art of Making Quality Certain", McGraw-Hill Book Company, New York.

[18] Shewhart, W.A. (1931). "Economic Control of Quality of Manufactured Product", Van Nostrand, New York.

[19] Dale, B.G., and Cooper, C.L. (1994), "Introducing TQM: The Role of Senior Management", Management Decision, Vol. 32, No. 1, pp. 20-26, MCB University Press Ltd.

[20] Leonard, D., and McAdam R. (2002), "The strategic impact and implementation of TQM", The TQM Magazine, Vol. 14, No. 1, pp. 51-60, MCB University Press Ltd.

[21] Yusof, S.M. and Aspinwall, E. (2000). "A conceptual Framework for TQM Implementation for SMEs", The TQM Magazine, Vol. 12, No.1, pp. 31-36.

[22] Ghobadian, A. and Gallear, D.N. (1996). "Total Quality Management in SMEs", Omega, International Journal Management Science, Vol. 24 No. 1, pp. 83-106.

[23] Moser, C.A. and Kalton, G. (1971). "Survey Methods in Social Investigation", 2nd Edition, Heinemann Educational, London.

[24] Fowler, F.J. (1984). "Survey Research Methods", Sage Publications, London.

[25] Fowler, F.J. (1998). "Design and Evaluation of Survey Questions", in Handbook of Applied Research Methods, Bickman, L., Rog, D.J. (Editors), Sage Publications, London, pp. 229- 259.

PROFILES



BABA MD. DEROS

Baba Md. Deros is a graduate member of IEM and holds BSc (Hons) in Mechanical Engineering from University of Glamorgan, United Kingdom, Master of Science in Manufacturing Systems Engineering from University of Warwick, United Kingdom and a PhD in Mechanical Engineering from Universiti Teknologi Malaysia. He has been working as a lecturer in several Polytechnics and currently as an Associate Professor in the Department of Mechanical and Materials Engineering, Faculty of Engineering, UKM. Currently, have two major research areas, which comprise of Industrial Ergonomics focusing on developing workstation design based on Malaysian anthropometric data and Manufacturing Management focusing on benchmarking and lean techniques applications in manufacturing industry.



DR MOHD. NIZAM AB. RAHMAN

Dr Mohd. Nizam Ab. Rahman is a senior lecturer in Quality and Operations Management at the Department of Mechanical and Materials Engineering, UKM. His research interests include quality operations, modern quality management such as supply chain, BSC, Six Sigma, Production SPC etc. He graduated in Industrial Physics in 1996 and obtained an MSc in 1999 from Universiti Teknologi Malaysia and followed by an PhD from the University of Nottingham. He has been working as an R&D Engineer with Panasonic AVC Networks, and has worked in Japan for a couple of years.



A.G. JAHARAH

A.G. Jaharah is a BEng and an MSc in Manufacturing Engineering from Leeds Metro University and Warwick University, UK, respectively. She received a PhD in Manufacturing Engineering from Universiti Malaya, Malaysia. Her current research interests are machining technology of tool steels, cast iron and aerospace materials.



DZURAIDAH ABD. WAHAB

Dzuraidah Abd. Wahab is a senior lecturer at the Department of Mechanical and Materials Engineering, Universiti Kebangsaan Malaysia. Prior to joining UKM in October 2003, she was attached to the National CAD/CAM Centre, SIRIM Berhad. She received her Bachelor Degree in Chemical and Process Engineering from Universiti Kebangsaan Malaysia, and her MSc. in Design and Manufacturing and PhD in Concurrent Engineering from the Manchester Metropolitan University, United Kingdom in 1995 and 1999 respectively. Her research interests include concurrent engineering, mechanical engineering design and engineering life cycle of products.



MOHD HAZRI HASHIM

Mohd Hazri Hashim is a graduate member of IEM and holds BEng (Hons) in Manufacturing Engineering from Universiti Kebangsaan Malaysia. He has been working as project engineer in Varia Tenggara Sdn Bhd (VTSB and had handle many project including fabrication and salvaging. The holder of Insitute of Corrosion certificate also has experience in fabrication of crane and inspection mostly in painting and corrosion while working in Industrias Metalurgicas Pescarmona S.A.I.C and F(IMPSA) an Argentina company. Currently, he is pursuing his study in the technical aspect of academic sector.



NOR KAMALIANA KHAMIS

Nor Kamaliana Khamis is a tutor in the Department of Mechanical and Materials Engineering, Faculty of Engineering and Built Environment, Universiti Kebangsaan Malaysia. She graduated from UKM with a BEng in Manufacturing Engineering in 2007. She had a working experience for six months as a mechanical engineer in Research and Development Department at Motorola Technologies Sdn. Bhd. Currently; she is focusing her research in manufacturing system engineering.